NOTE TO USERS

Characterization and modeling of unsaturated water liquid transport in softwoods

Luis Miguel Candanedo Ibarra

A thesis

In

The Department

Of

Building, Civil and Environmental Engineering

Presented in Partial Fulfillment of the Requirements

for the Degree of Master of Applied Science at

Concordia University

Montréal, Québec, Canada

August 2005

Your file Votre référence
ISBN: 0-494-10217-9
Our file Notre référence
ISBN: 0-494-10217-9

ABSTRACT

Luis Miguel Candanedo
Concordia University, 2005

Wood is a construction material used for structural elements and building envelope components such as windows, and cladding. Such wooden components are exposed to wetting by rain either inevitably (cladding) or as a result of a failure (rain infiltration). As wood may come in contact with water the process of water transport in wood should be understood and quantified. Moisture may be detrimental to wood components, because when the moisture content levels are within a certain range, mold growth and rot can occur, which can later harm the health of the occupants, decrease the structural strength and destroy the aesthetic appearance of a building.

Moisture sources in the building envelope are, in order of magnitude: rain penetration, moisture brought through air movement and moisture diffusion. As rain water impinges onto the wall and runs off the surface, water may seep into cracks and accumulate within the wood frame structure. Water can move by capillary action into wood-based components and the water vapor can also be diffusing through the structure. In the hygroscopic range, the theory has evolved considerably, and by the use of sorption curves, it is possible to explain the absorption of water in the vapor phase for a range of relative humidity (from 0 to 95% RH). However, liquid mass diffusivities of water for many Canadian wood species have not yet been investigated. The main objectives of this study are to quantify averaged values of diffusivities for a specific type of wood (jack pine), and to develop a transient modeling approach for liquid-phase water transport in

wood considering the orthotropic effect of the wood structure and compare it to experimental results.

Acknowledgements

Special thanks to my thesis supervisor, Dr. Dominique Derome who has always been supportive during this period of my life. She suggested the topic of research and helped me out during my experiments and while writing this thesis and pushed me to increase the quality of the work. Merci beaucoup Dr. Derome!

I want to thank to Dr. Paul Fazio, who gave me the opportunity of working in the CRD project. I have learned a lot from his experience and from all the research team involved in the CRD project. Thank you.

I would like to thank my parents, Jose and Rosalina, who have been caring and supportive during all my life and who always have put their trust in me and encouraged me to fulfill my dreams. Thanks again.

There are a lot of people who were directly and indirectly involved in the realization of this project: Jacques Payer, Luc Demers and Joe Hrib. Without their help and advice I would have taken longer to finish this thesis and maybe even have injured myself with the equipment. Thanks for your time.

My special thanks go also to my brother José from whom I received a lot of encouragement to start graduate school, my sister-in-law Stephanie, who has helped me editing this thesis, and my dear cousin Ana who has been the best roommate-friend ever.

Finally, I want to thank my friends, Anik, Miljana, Hua, Bert, Quinru, Marianne, Evelien, Adam, Li Jun, Sergio, Pamela, Keila, Farnaz, Sami, Panagiota and Moisés, for their constant support. Thank you Guys!

Table of contents

List of Figures

List of Tables

Nomenclature

Symbol	Parameter	Units
A	Water absorption coefficient	$kg/m^2 \cdot s^{1/2}$
c	Model parameter	
D	Liquid water diffusivity / diameter of the pore	m^2/s , m
e	Thickness	m
g	Gravity	m/s^2
G	Specific gravity of wood	$kg_{\text{ovendry wood}}/kg_{\text{water}}$ $m^3_{\text{moist wood}}$
K	Permeability	m^2
k^{-1}	Capillary length	m
m_w	Water absorbed	kg/m^2
M	Moisture content of wood as a percentage of the oven dry mass	%
n	Moles of gas	Mol
P	Pressure	Pa or N/m^2
p_c	Capillary pressure	Pa
r	Radii of curvature	m
R	Gas constant	J/(K·mol)
s	Subsystem	
S	Spreading Parameter	N/m or dynes/cm
t	Time	s
T	Temperature	°C
v	Velocity	m/s

$\vec{\mathbf{v}}_o$	superficial velocity	m/s
V	Volume	m^3
w_c	Capillary saturated moisture content	kg_{water}/m^3
W	Moisture content	kg_{water}/m^3
w_g	Green or moist mass	kg
w_o	Oven dry mass	kg

Greek Alphabet Symbols

ρ	Density	kg/m^3
μ_l	Dynamic viscosity of liquid	kg/m·s
ρ_w	Normal density of water	kg/m^3
ρ_{wood}	Normal density of wood	kg/m^3
θ	Contact angle	Degrees
$\gamma_{w,a}$	Interfacial tension	N/m or dynes/cm

Subscripts

c	Capillary
a	Air
w	Water
i	ith finite element
SO	Solid
SL	Solid/liquid

Chapter 1. Introduction of the research problem and scope of the work

Wood is a construction material used for structural elements and building envelope components such as windows, and cladding. Such wooden components are exposed to wetting by rain either inevitably (cladding) or as a result of a failure (rain infiltration). As wood may come in contact with water, the process of water transport in wood should be understood and quantified. Moisture may be detrimental to wood components, because when the moisture content levels are within a certain range, mold growth and rot can occur, which can later harm the health of the occupants, decrease the structural strength and destroy the aesthetic appearance of a building.

Moisture sources in the building envelope are, in order of magnitude: rain penetration, moisture brought through air movement and moisture diffusion. As rain water impinges onto the wall and runs off the surface, water may seep into cracks and accumulate within the wood frame structure. Water can move by capillary action into wood-based components and the water vapor can also be diffusing through the structure.

Scope of the work

In the hygroscopic range, the understanding of the wetting and drying process of wood has evolved considerably, and by the use of sorption curves, it is possible to explain the absorption of water in the vapor phase for the range of relative humidity (from 0 to 95% RH). However, diffusivities of liquid water that quantify the absorption of water for many Canadian wood species have not been extensively investigated. The

main objectives of this study are to provide experimental data and properties on wood water movement for a specific type of wood (jack pine), to develop a transient modeling approach for liquid-phase water transport in wood considering the orthotropic effect of the wood structure and compare it to experimental results and to provide a further understanding of wood behavior in contact with water.

1.1 Thesis organization

Chapter one describes the research problem, the scope of the work and the thesis organization.

Chapter two presents information regarding wood macro- and microstructure. A short description about its chemical composition is done. Since jack pine, the material to be studied, belongs to the softwood group, a detailed description of softwood structure is offered. Then a discussion about the different methods employed to study moisture transport in porous material is done. Finally, an introduction about the theory that aims to describe the moisture transport in porous media is presented.

Chapter three presents the experimental work carried out to characterize unsaturated water liquid transport process in softwoods and to study the parameters that influence such process. A detailed description of each experimental methods employed and the subsequent interpretation and discussion of the results obtained are presented.

Chapter four presents the estimation of liquid diffusivities using the parameters found during the experiments. Two empirical equations for diffusivities are employed to estimate the liquid diffusivity values.

Chapter five presents numerical models describing the water absorption process in softwood using the finite element method. The modeling approach yields insight on the adequacy of the estimated liquid diffusivities obtained in chapter four. An orthotropic model is presented and compared to a point-wetting experiment.

Chapter six presents a qualitative approach to study the actual water uptake behavior in softwoods. Since for any numerical model, the boundary conditions control the results, an introduction of wetting is presented with the intention of understanding how the liquid water will spread out in wooden components. The method is used to compare the idealized model of unidirectional water transport with what really happens.

Chapter seven presents the conclusion of the present thesis. The main contributions of the research are listed and recommendations for further work in the unsaturated water liquid transport process in the softwoods are proposed.

Chapter 2. Literature review

The structural and chemical description of wood has been a topic of extensive research by botanical and wood/forest scientists. These specialists were the first who used equations such as Darcy's law to explain the movement of water in saturated wood and a diffusion type of equation, Richard's equation, for the movement of water in unsaturated wood. The theoretical background of the different equations is explained in this chapter, and the validity of the assumptions is discussed. A small summary of the means for the study of moisture transport in building materials is presented. First, a description of wood follows.

2.1. Wood as a material

Wood has many advantages when compared to other construction materials: it is available in many species, sizes, shapes and conditions; it requires far less energy to process; it is lightweight and easy to install; when dry, it has good insulating properties against heat, cold, sound and electricity. The most important advantage, however, is that it is the one of the few renewable building materials (Tsoumis, 1991).

2.1.1. Classification of woody plants

Trees are divided into two categories: hardwoods and softwoods. Botanically, trees from each category are very different from each other. Hardwoods belong to the angiospermae subdivision and softwoods to the gymnospermae subdivision.

Angiosperms have two classes: monocotylendons and dycotyledons (see table 2.1). These plants are characterized by production of seeds within ovaries, whereas gymnosperms produce seeds that lack a covering layer. The leaves of softwoods are needlelike. In contrast, hardwoods bear broad leaves (Haygreen and Bowyer, 1996).

Table 2.1. Trees in the vegetable kingdom (Haygreen and Bowyer, 1996).

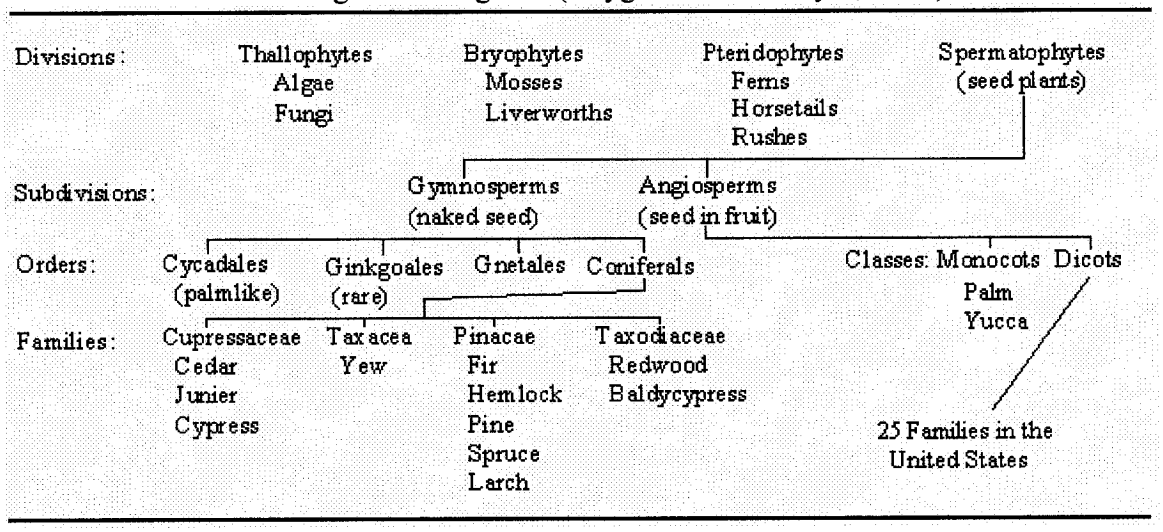

2.1.2. Wood macrostructure

Macrostructural features of wood are those visible to the naked eye or with the aid of a hand lens. Growth increments, sapwood/heartwood differences, wood rays and cell distribution patterns can be easily identified (Kollmann and Côté, 2003).

The boundaries of growth increments are usually related to annual growth in trees grown in temperate climates. When the pores in the earlywood are much larger than those formed later in the season, and when the size transition between earlywood and latewood pores is abrupt, the wood is classified as ring porous.

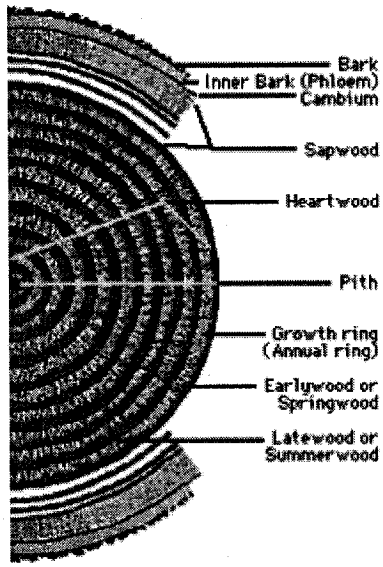

Figure 2.1. Representation of the cross section of a tree stem, showing its main parts (from Hoadley, 1990).

The outermost layer of the tree stem is called the bark. The bark is important in protecting the tender cells in and near the cambium. Without bark, these cells would be under attack from insects, animals, fungi and birds and they would be susceptible to damage from frost, wind and fire.

The woody portion of a tree is called the xylem, and includes both the sapwood and heartwood. The heartwood is composed of dead cells. Sapwood and heartwood are structurally very similar, but differ in their chemical and physical properties.

The shortest cells in the tree are the wood rays. These are oriented perpendicular to the longitudinal elements and organized into bands of tissue (Kollmann and Côté, 2003).

Figure 2.2 shows the orthotropic directions of wood.

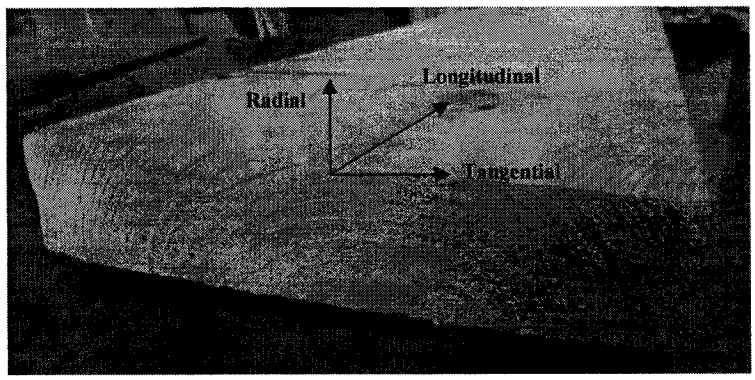

Figure 2.2. Directions according to the fiber grain and growth rings.

2.1.3. Microstructure of wood

The tree trunk is composed of millions of individual wood cells. Usually, the cells are much longer than they are broad. The majority of these cells are arranged longitudinally, in order to carry water and nutrients from the roots to the top of the tree. In addition, since there is negative pressure because of transpiration from the leaves (Zimmermann, 1983), "the vascular system must be able to support a gas invasion due to injury or cavitation. This is the role of bordered pits, or vessel-to-vessel pits" (Perré, 2003).

In hardwoods, there are two main types of cells: the fibers, which give support to the tree, and the vessels, which are the water conducting cells (Zimmerman, 1983). A vessel is an individual cell which forms a capillary for water transport. It is important to note that "the water does not leave a vessel in axial direction through the very end, but laterally along a relatively long stretch where the two vessels, the ending and the continuing one, run side by side" (Zimmerman, 1983) as shown in Figure 2.3.

In softwoods, the wood consists almost entirely of tracheid cells. These are connected on their radial walls by bordered pit pairs which allow water to "spread easily within a growth ring in tangential direction" (Zimmerman, 1983). Vessels and tracheids differ in their relative numbers and arrangement within the tree. Vessels occur in most hardwoods but very seldom in softwoods (Haygreen and Bowyer, 1996). Tracheids are generally longer and narrower than the vessels; in some species they are 7 mm or more in length (Kollmann and Côté, 2003). Since vessels and tracheids are the main water conducting cells, an extended description of them follows.

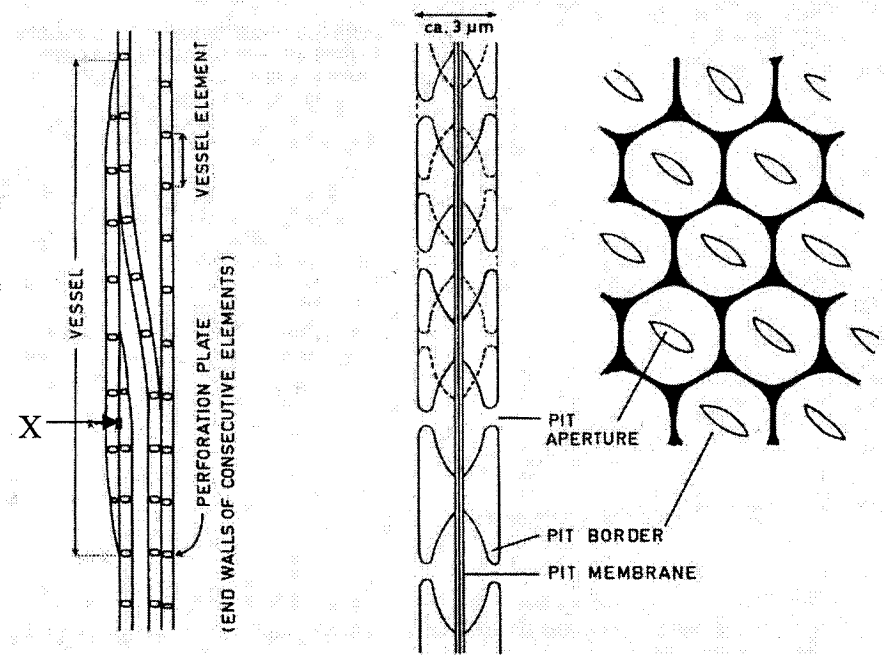

Figure 2.3. The sketch on the left shows how the vessel network is connected, and how water moves form one vessel to the other laterally through bordered pits. On the center and right side, there is a diagrammatic section through a bordered pit field as how it would look the area X from the left after making a zoom (from Zimmerman, 1983).

Vessels are not perfectly aligned, but rather twisted relative to each other, as shown in Figure 2.4. In contrast, for conifers, the tracheids are aligned nearly perfectly (Kollmann and Côté, 2003).

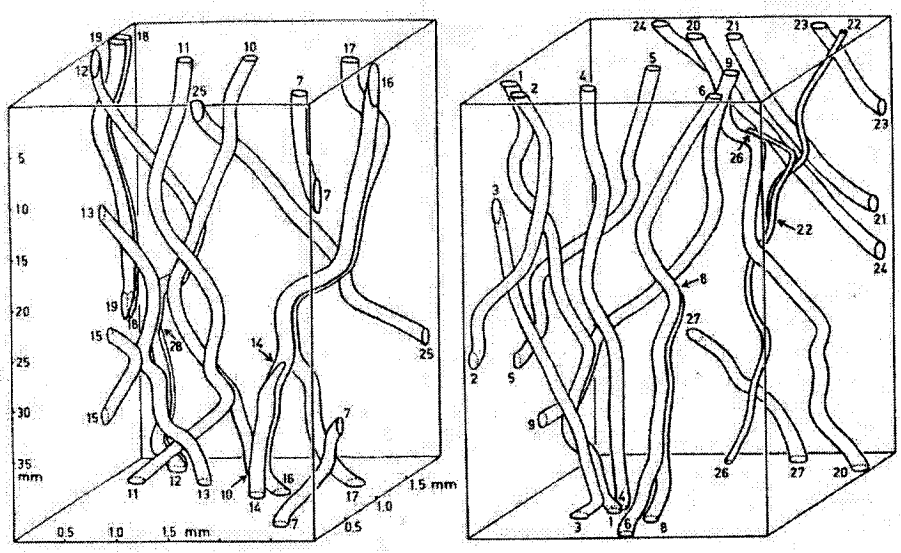

Figure 2.4. The figure shows an actual course of vessels in a piece of wood of *Cedrela fissilis*. The vessels were separated in the figure for clarity. The vessels are numbered where they exit from the box domain. The small arrows show the ending of each vessel. The axial scale is foreshortened ten times (from Zimmerman and Brown, 1971).

As mentioned above, conifers have tracheids. The cell wall of a tracheid is composed of a set of layers, as shown in Figure 2.5. The first layer is composed of cellulose microfibrils coated with hemicelluloses. The secondary wall in tracheids, fibers and vessels, is composed by three layers which are referred to as the S1, S2 and S3 layers. The S2 layer is responsible for most of the swelling and shrinkage since it constitutes between 60% to 80% of the total volume of the secondary wall.

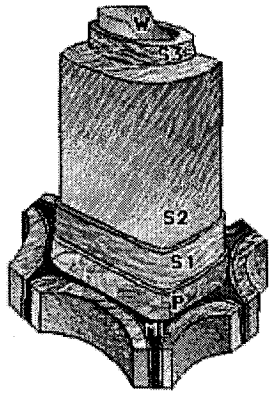

Figure 2.5. Typical model of the cell wall structure for a fiber or tracheid. The main parts of the cell wall consists of: P-primary wall; S1, S2, S3-layers of the secondary wall; W-warty layer; ML-middle lamella, the amorphous, high-lignin-content material that binds the cells together (from Koch, 1985).

In softwoods, the fluid conducting tissue consists of longitudinal and ray tracheids, also called prosenchyma. There is radial transport in the longitudinal parenchyma, which is the storage part of the tree. Longitudinal tracheids make up the majority of the wood structure. These cells are long and narrow with tapering ends. Earlywood and latewood tracheids are easily differentiable by the number of pits they contain, which varies from 50 to 300 per tracheid in earlywood, with fewer in latewood. Figure 2.6 shows a representation of earlywood and latewood tracheids (Siau, 1984). Usually the pits are classified as: simple pit pairs, bordered pit pairs and half-bordered pit pairs (Figure 2.7).

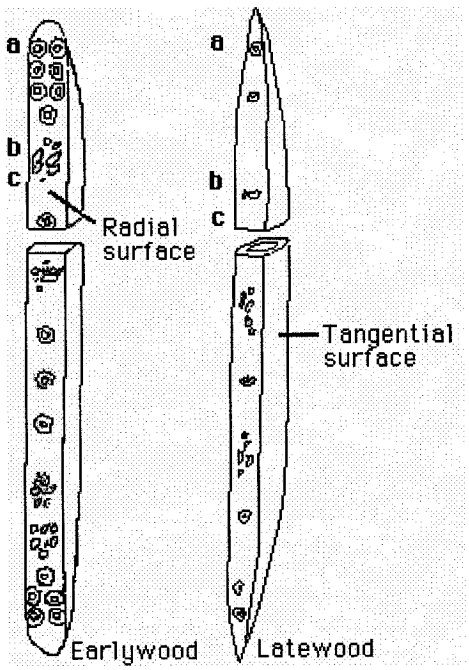

Figure 2.6. Representation earlywood (left) and latewood (right) tracheids. In each of the tracheids, the following elements can be identified: a. intertracheid bordered pits; b, bordered pits to ray tracheids; c, pinoid pits to ray parenchyma. Note that the tangential intertracheid pits have not been depicted. These pits are distributed along the length but are most frequent near the tracheid ends (from Koch, 1972).

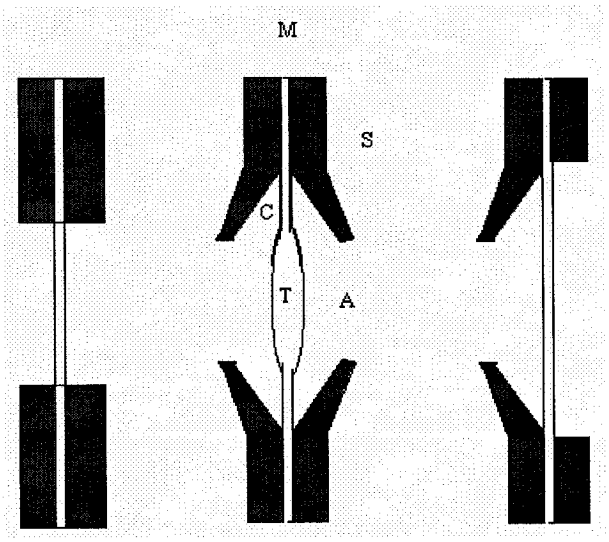

Figure 2.7. Representation of typical pit pairs. Left: Simple pit pair, Center: Bordered pit pair, Right: half-bordered pit pair. A: aperture, C, chamber, M middle lamella-primary wall; S secondary wall; T torus (after Siau, 1984).

A pit pair consists of complementary gaps or recesses in the secondary walls of two adjacent cells, together with a pit membrane that consists of a middle lamella sandwiched between two primary walls.

In softwoods, the most important pit with respect to flow properties is the bordered pit pair since nearly all of the softwood tissue consists of prosenchyma cells (tracheids).

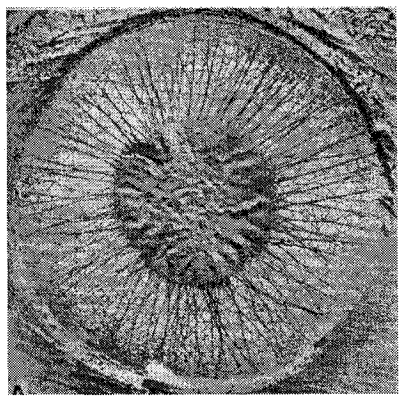

Figure 2.8. Membrane of a bordered pit in fir (Abies) taken with an electron microscope (from Tsoumis, 1991).

The torus is the thickened center portion of the pit membrane, consisting of primary wall material (Siau, 1984). For most conifers, the torus is impermeable to fluid flow. The membrane that surrounds the torus is known as the margo. Figure 2.8 shows the membrane and the margo for a bordered pit in fir (Abies).

Table 2.2. Summary of dimension of structural elements in normal softwood (Siau, 1984)

Structural element	**Dimension, μm**
Tracheid length	3,500
Tracheid diameter	35
Tracheid double cell wall thickness in latewood.	1
Tracheid lumen diameter	20-30
Thickness	
True middle lamella in latewood	0.1-4.0
Primary wall	0.1-0.2
S1 layer in latewood	1
S2 layer in latewood	3-8
S3 layer	0.1-0.2
Overall diameter of pit chambers of bordered pits	6-30
Effective diameter of pit openings	.02-4.00

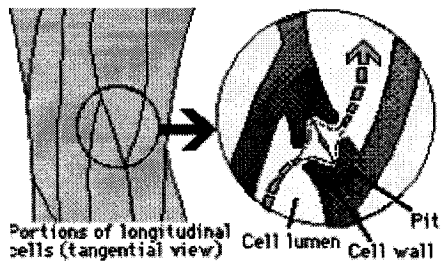

Figure 2.9 Pits are the smaller conducting elements in the lumen network for flow of water and liquids (from Haygreen and Bowyer, 1996).

Although wood vessels and tracheids form capillaries, their flow behavior is very different from that described by the Hagen-Poiseuille equation, which assumes a no-slip condition at the walls of the capillary, and a parabolic profile inside it. This is in part due to the irregularity and relative roughness of the vessels, and the bordered pits, which slow the water transport. The Hagen-Poiseuille equation uses the diameter of the capillary, so the determination of the inside diameter of the vessels/tracheids that changes with the growth rings is an issue that complicates the use of the equation.

It has been found that there is greater uniformity in properties such as permeability, capillary behavior, thermal conductivity and the diffusion of bound water, among softwoods as opposed to hardwoods (Siau, 1984). For the record, it is important to say that spruce, fir and pine (generally grouped under the abbreviation SPF used for lumber in Canada) are softwoods. In both softwoods and hardwoods, it is found that the earlywood is generally of much lower density than latewood.

2.1.4. Structure of Softwoods

Figure 2.10 shows the generalized microstructure of a typical southern pine. In the figure, it can be seen that, while the lumens (cavities) are much larger and the cell wall layers much thinner in earlywood tracheids, their width in the radial direction is almost the same as that of the latewood tracheids. The length-to-diameter ratio of the tracheids is approximately 100. (See Table 2).

2.1.5. Chemical Composition of Wood

Cellulose is the most important compound in wood. It represents 42 ± 2 % of hardwoods and softwoods (Siau, 1984). It is an organic molecule made up of carbon, hydrogen and oxygen and its structure is mainly crystalline. This crystallinity is largely responsible for the tensile strength of wood. Cellulose is also responsible for the hygroscopic properties of wood, as it also absorbs water due to its hydroxyl groups. Hemicelluloses are polysaccharides that associate with cellulose and lignin in the cell

wall. Lignin's function is to encrust the intercellular space and any openings in the cell wall. Lignins are polymerization products of aromatic alcohols.

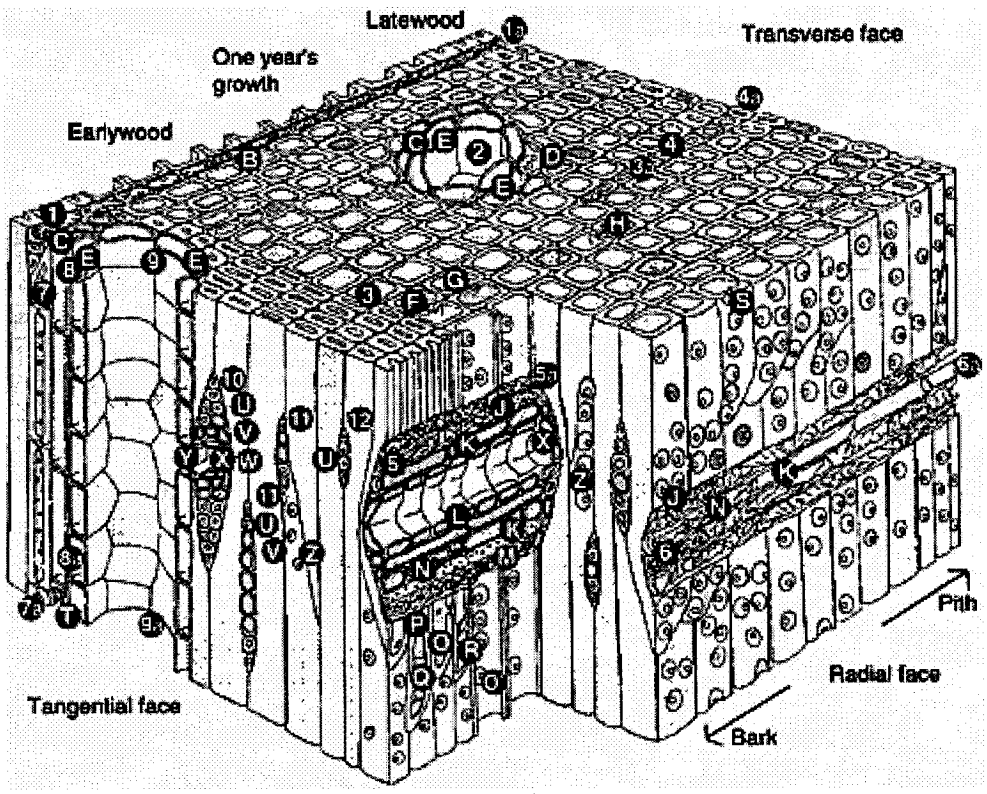

Figure 2.10. The figure depicts a general organization of a typical southern pine wood. The lumen size variation through early and latewood for the tracheids is remarked. "*Transverse view*.1-1a, ray; B, dentate ray tracheid; 2, resin canal; C, thin-walled longitudinal parenchyma; D, thick-walled longitudinal parenchyma; E, epithelial cells; 3-3a, earlywood longitudinal tracheids; F, radial bordered pit pair cut through torus and pit apertures; G, pit pair cut below pit apertures; H, tangential pit pair; 4-4a, latewood longitudinal tracheids. *Radial view*. 5-5a, sectioned fusiform ray; J, dentate ray tracheid; K, thin-walled parechyma; L, epithelial cells; M, unsectioned ray tracheid; N, thick-walled parenchyma; O, latewood radial pit; O1, earlywood radial pit; P, tangential bordered pit; Q, callitroid-like thickenings; R, spiral thickening; S, radial bordered pits; 6-6a, sectioned uniseriate heterogenous ray. *Tangential view*. 7-7a, strand tracheids; 8-8a, longitudinal parenchyma (thin-walled); T, thick-walled parenchyma; 9-9a, longitudinal resin canal; 10, fusiform ray; U, ray tracheids; V, ray parenchyma; W, horizontal epithelial cells; X, horizontal resin canal; Y, opening between horizontal and vertical resin canals; 11, uniseriate heterogenous rays; 12, uniseriate homogenous ray; Z, small tangential pits in latewood; Z1, large tangential pits in earlywood" (from Koch, 1972).

2.1.6. Moisture content, specific gravity, density and porosity of wood

In North America, it is most common to express the moisture content of wood as a percentage of the oven dry mass:

$$M = \frac{w_g - w_o}{w_o} \cdot 100\% \tag{2.1}$$

where w_g = green or moist mass, w_o = oven dry mass. It is recommended to obtain the latter after the wood has been dried in a convection oven maintained at 102 ± 3 °C (Siau, 1984).

Specific gravity G, a dimensionless number, is defined as the ratio of the oven-dry mass of a wood specimen to the mass of water displaced by the bulk specimen at a given moisture content, or alternatively the oven dry mass divided by moist volume.

$$G = \frac{w_o}{V\rho_W} \tag{2.2}$$

where V = moist volume and ρ_w = normal density of water.

The density of wood is the mass per unit volume at a given moisture content. As expected, the density of wood will increase dramatically above the fiber saturation point (FSP), since the swelling almost stops after this point.

$$\rho_{wood} = \frac{w}{V} = \frac{w_o \cdot (1 + 0.01M)}{V} \tag{2.3}$$

The density of the cell wall is generally accepted to be 1.46 g/cm^3; this value was obtained by Stamm and Hansen using helium pycnometry (Siau, 1984). However, when

using water as the displacement fluid for the density measurements, a value of 1.50 g/cm^3 has been found (Siau, 1984).

Porosity is defined as the void volume fraction of a material. Then,

$$n = \frac{V_{voidspace}}{V_{total}} = \frac{V_{voidspace}}{V_{matrix} + V_{voidspace}}, \tag{2.4}$$

where n is the porosity, $V_{void\ space}$ is the volume of the void space, V_{total} is the total volume of the material and V_{matrix} is the volume of the solid material itself. For mass transfer applications, it is better to differentiate between the total porosity and an effective porosity that takes into account the volume of the interconnected pores.

A simple formula to calculate the porosity of wood is given by Siau (1984):

$$n = 1 - G(0.667 + 0.01M) \tag{2.5}$$

This is valid for all moisture ranges if the specific gravity of wood is known.

2.2. Methods employed to study moisture transport

Before presenting equations that describe the moisture transport in porous building materials, it is useful to have an understanding of the different methods employed to study it. A good review is found in the book by Krus (1996). Testing methods can be classed as destructive or non-destructive. The main ones are described below.

The oven method is the most accurate testing method to determine moisture content. However, a determination of the moisture distribution is only possible by

destruction of the specimen (slicing technique). This method is used frequently because of its simplicity and affordability. This technique is used for experiments on the drying of wood. In the work done by Rosenkilde (2002), the moisture profile was used to determine the diffusion coefficients in all three directions relative to the grain. Despite the fact that moisture transport above the FSP is not truly a diffusion process, the diffusion coefficient was used in his work to characterize the moisture transport process.

X-ray analysis relies on the x-ray absorption of the irradiated material. Since water has a markedly lower x-ray absorption coefficient than wood, the moisture content can only be measured with very low resolution. For a complete description of how to determine moisture diffusivities from transient moisture content profiles measured by means of x-rays, refer to the work by Carmeliet *et al* (2004).

Gamma-ray attenuation is based on the absorption and dispersion of gamma rays by water. The elements used most often as emitters are ^{241}Am, ^{60}Co and ^{137}Cs, which are produced artificially. The moisture content is determined from the difference of densities of moist and dry building material. Radiation safety is an important issue pertaining to this method. Kumaran and Bomberg (1985) used this technique to determine moisture diffusivities in Portland cement and aerated concrete.

Nuclear Magnetic Resonance is based on the angular momentum of protons charged positively (spin) and the consequential magnetic moment. It uses an alternating magnetic field, at a specified frequency and at right angles to excite the hydrogen nuclei

inducing transitions between different energy levels. The high frequency energy thereby absorbed by the tested sample is dependent on the number of protons in the specimen and can serve as a measure of moisture content since hydrogen nuclei in building materials occurs most of the time only in the form of water (Krus, 1996).

In the *tracer method,* the water containing dissolved radioisotopes is used. The materials containing radioisotopes are then scanned using special equipment. Major drawbacks include the possibility of the radioisotope particles penetrating the wood to a different extent than the water because of differences in molecular size, and the need for a special radioisotope laboratory in which to undertake the experiments (Krus, 1996).

2.3. Moisture transport in porous media

After discussing the different methods of measuring the moisture content in a porous material, we now focus on the physics of moisture transport in porous materials and work previously done regarding water transport in wood.

The transport of moisture in porous media can be subdivided in two according to the level of saturation of the media. Darcy first studied moisture transport in saturated media in 1856, in his famous study "Les fontaines publiques de la ville du Dijon''(Darcy, 1856).

Pel's Ph.D. thesis (1995) presents a thorough literature review about the subject of moisture transport in porous media. A book about transport phenomena is "Introduction to modeling of transport phenomena in porous media" by Bear and Bachmant (1990) which provides the basis for the equations that describe moisture and heat transport in porous media.

The theoretical description of the movement of moisture in a porous material at the microscopic level can be done, but the resulting equations usually can not be solved since the geometry is too complex and the distribution of the phases is not known. Owing to this complexity, a macroscopic description is generally preferred.

2.3.1. Equations that describe the moisture transport in saturated porous media

The Navier-Stokes equations (continuity, energy and momentum equations) used at the macroscopic level describe the fluid flow at the microscopic level. For example let us present one of the equations (Equation 2.6).

$$\rho \frac{D}{Dt} \cdot \mathrm{v} = -\nabla p + \mu \nabla^2 \cdot \mathrm{v} + \rho \cdot \mathrm{g} \tag{2.6}$$

where t is the time, v the velocity, ρ is the density, μ the viscosity in kg/(m·s), p in N/m^2, and g the gravity in m/s^2. It is important to note that equation 2.6 assumes a constant density and viscosity (Bird *et al*, 2002).

However, the complete set of equations has no practical use for porous building material applications. For example, if one wishes to solve the former equation for the

isothermal case in vector form for the fluid in the wood structure of Figure 2.10, the boundary conditions would have to be written for every single tracheid, the velocities and pressure at the entry of each tracheid would have to be specified, and the geometry must be identical to that being studied. The complexity is prohibitive; for example, it would be extremely time consuming, not to say impossible, to represent the structure of the bordered pits, of which there are from 50 to 300 *per tracheid* in earlywood.

Nevertheless, it is interesting to mention the work at the microscopic level as presented by Valli *et al* (2002) describing the fluid flow through the margo of one bordered pit. In Figure 2.11 a 3D pressure and velocity field is presented. In order to solve the problem, Valli *et al* use the lattice-Boltzmann method since the flow is very complex at a microscopic scale. This method is not only used in porous media, but for suspension flows and multiphase flows.

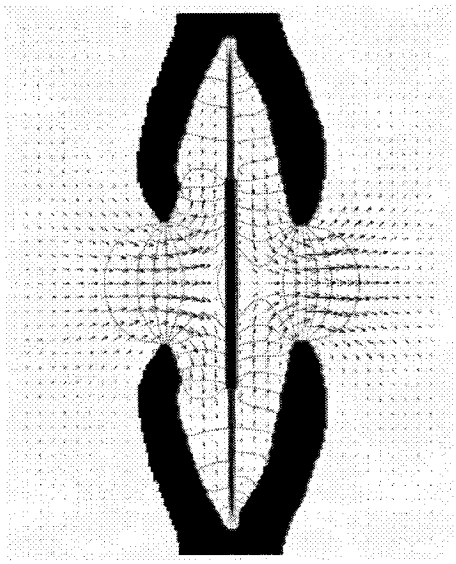

Figure 2.11 Plot of an axial view of the 3D pressure and velocity fields of fluid flow through a bordered pit. The torus has been considered to be completely impermeable to fluid flow. The arrows size represents the velocity magnitude. The results were obtained by means of the lattice-Boltzmann method (from Valli *et al*, 2002).

Equation 2.6 can be simplified in different ways. One is to neglect the acceleration term, in which case the equation described by the Hagen-Poiseuille can be obtained (Bird *et al*, 2002), but we must remember that, to use this equation, the velocity profile has to be parabolic.

Darcy's law:

The main assumptions for this law are that the matrix is rigid, macroscopically isotropic and homogeneous, the gravitational effect is negligible, and the no-slip condition at the water-solid interface is valid.

$$\vec{\mathbf{v}}_o = -\frac{k_1}{\mu_1}\nabla p \tag{2.7}$$

where $\vec{\mathbf{v}}_o$ is the superficial velocity in m/s, which is defined as the volume rate of flow through a unit cross-sectional area of the solid plus fluid, k_l is the permeability in m^2, μ_l is the dynamic viscosity of liquid water in kg/(m·s), p is the pressure in N/m^2 or Pascals and ∇ is the nabla or del operator. The same form of the equation is also used to study the permeability of a gas in a porous material.

Comstock (1969) studied the directional permeability of softwoods. He compared ratios of longitudinal to tangential permeability of gases from previous studies and developed two models of wood structure with the intention of explaining the magnitude of the difference between longitudinal and tangential permeability. Usually the studies are done with fluid in the gas phase because in the liquids phase, the "falling rate of flow

with the time and the dependence of the apparent permeability on pressure" (Comstock, 1969) present problems.

It is well known that the measured permeability at liquid saturation decreases when the sample length increases, which makes the application of Darcy's law for wood difficult (Perré, 1994). Since latewood tracheids have smaller cavities than those in earlywood, their permeability is different. This was studied by Domec and Gartner (2002). They worked with a specific conductivity (ks, m^2), which is a measure of the hydraulic efficiency of the xylem in relation to the cross-sectional area of the wood. They found that earlywood has a value of ks about 11 times compared to latewood, and also found that up to 90% of the total flow occurs through the earlywood, under saturation conditions. However, such conditions do not occur in real wood exposure situations. So, transport in non-saturated conditions should also be looked at.

2.3.2. Equations that describe the moisture transport in non-saturated porous media

The description of the flow by using the Navier Stokes equations is also possible for non-saturated microscopic porous media, but again it is extremely time-consuming to solve the equations for the complexity of the geometry of wood structure.

Generally, more assumptions are made to simplify the description of the flow in unsaturated porous media. The main assumptions are that there are two immiscible fluids, a wetting fluid (water) and a non-wetting fluid (air), and that the air is at atmospheric pressure throughout the porous material. Air is generally represented by an ideal gas mixture of water vapor and air.

A. Capillary pressure

Capillary pressure is the pressure difference between air and water that occurs at the curved interface between the two immiscible fluids. Using a constant interfacial tension or surface tension, $\gamma_{w,a}$ the capillary pressure at the microscopic level p_c is given by the Laplace formula:

$$p_c = -\gamma_{w,a}\left(\frac{1}{r'} + \frac{1}{r''}\right) \tag{2.8}$$

where r' and r'' are the principal radii of the curvature of the microscopic interface air-water surface. When the capillary pressure for water is negative, the building material will absorb water.

Macroscopic capillary pressure, which is the difference between the average pressures of air and water, is generally used in calculations. This is done because the pores in the wood all have different sizes and shapes. It is expected that the water will distribute itself within the voids of the material until an equilibrium condition is reached.

The next equation represents the macroscopic capillary pressure as a function of the liquid water content.

$$p_c(W) = p_w - p_a \tag{2.9}$$

where W is the liquid water content, p_a is the pressure of the air and p_w is the pressure of the water in the porous medium. This relationship has to be determined experimentally. The curve obtained is called the capillary pressure curve, retention curve, or sorption curve. Figure 2.12 is a diagram of capillary pressure versus moisture content.

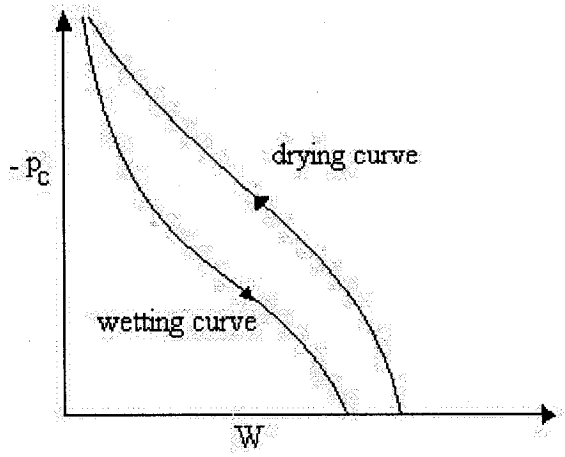

Figure 2.12. Typical diagram of a capillary pressure curve for a porous material. The main curves for drying and wetting are presented. Adapted from L. Pel (Pel, 1995)

The three main causes for the hysteresis for liquid between the two curves are the so-called ink-bottle effect, rain drop effects and air entrapment. In the hygroscopic range, hydroxyl groups play also a role in the hysteresis.

When averaging the volumetric flux of liquid water in the non-saturated porous media, the flow is described by

$$q_1 = -\frac{k_1(w_l)}{\mu_1}\nabla p_c(w_l) \tag{2.10}$$

where $k_l(w_l)$ is the permeability for liquid water as a function of the moisture content w_l.

It is worth mentioning the work done by Spolek and Plumb (1981) on capillary pressure in sofwoods. They developed a model to predict the capillary transport in softwoods and compared it with experimental results. They found that the lumen size variation within an annual growth significantly affected the local capillary pressure, indicating that separate flow paths are likely to exist in earlywood and latewood. Later, the work was further expanded to explain the heat and mass transfer in wood during

drying (Plumb *et al*, 1985). The new model included liquid transport via capillary action as well as diffusion.

B. Richard's equation

Moisture transport in unsaturated porous media is commonly simulated using the Richards equation which, with an isothermal assumption, is given by

$$\frac{\partial W}{\partial t} = \nabla \cdot (D_W(W) \cdot \nabla W) + \rho_w \frac{\partial K_W(W)}{\partial Z} \tag{2.11}$$

where W is the moisture content in kg/m^3, t *is* the time in s, D_W is the moisture diffusivity in m^2/s, K_W the hydraulic conductivity in m/s, Z is the height or depth in m and ρ_w the water density in kg/m^3. The last term in the equation is often ignored since it has to do with the gravitational forces, which are negligible compared to the capillary forces present. However, the gravity term is important when dealing with large cracks or holes (Roels, 2000).

The advantage of using the Richard's equation is that only the moisture diffusivities of the material have to be determined for each direction. These diffusities are moisture content-dependent.

The main assumptions in order to use the previous equation are a) the influence of the air can be ignored b) Darcy's law is valid, c) the solid matrix is undeformable and d) the fluid is incompressible (Roels, 2000).

When a material is absorbing moisture, there are three different stages or regions of storage. They are the region of sorption moisture or hygroscopic region, the capillary water region, and the region of supersaturation (Krus, 1996). The region of sorption moisture or hygroscopic region occurs when water is obtained from the air surrounding

the material. The capillary water region usually starts at relative humidities above 95%. Researchers have defined capillary saturation as the material moisture content which can be attained through natural absorption under normal pressure without the influence of exterior forces. This value is always below the maximum water content possible given the open pore space. The main reason that the material does not become fully saturated is because of air entrapment. The supersaturated region is often ignored because it rarely occurs under natural conditions for most building materials.

C. Percolation point of view

Since the structure of wood is of such high heterogeneity, and because pit aspiration and the presence of extractive slow down the process of water transport within the tracheids, percolation models have come into use for the description of water transport in wood. Percolation is based on the concept of statistical networks. Perré (2000) has developed models to describe the moisture transport during drying by means of percolation. The experiments that were carried out by the French team included injection of colored water in beech, and showed that only a very small part of the vessels contributes towards the liquid migration.

As we have seen in this chapter, there are many techniques to study and mathematical/statistical means to describe the moisture transport in wood. However, the most reliable techniques demand highly trained personal and expensive equipment. Due to the nature of the research problem, a procedure to study and analyze the unsaturated water liquid transport in softwood had to be developed.

Chapter 3. Water transport characterization

As we have seen, the structure of wood is of such high complexity that it is necessary to work with averaged values of the main parameters influencing the water absorption. The objectives of the performed tests were: 1. to determine variables to obtain an average value of the liquid water diffusivities for wood, 2. to evaluate the influence of the orientation of the grain on the value of the moisture diffusivity both qualitatively and quantitatively.

Researchers participating in the International Energy Agency project Annex 24 have shown that using data from water absorption tests can provide a good approximation of the average liquid water diffusivity of the material (Kumaran, 1999). In a round-robin, a chosen sample of eastern white pine was analyzed and then subjected to contact with water to determine the moisture diffusivity by γ-ray and NMR. The results varied in the shape of the diffusivity curves but were within an order of magnitude of each other. The results showed that water absorption coefficients, together with capillary saturation moisture content can be used to calculate an average value for the moisture diffusivity.

Following the conclusions of the scientists participating in the IEA, the development of a procedure for testing wood specimens was elaborated for this thesis.

First wood pieces were cut in the different orientations of the fiber grain to test their influence on the water absorption. A water absorption test was required to quantify

the absorption rate of each specimen. The test samples were not dry at the beginning because the intention was to reproduce as much as possible the wetting conditions present when there is water penetration into the building envelope. If the samples had been dried first, the rapid movement of water within the samples could have caused pit aspiration, which would have slow down the water absorption. Pit aspiration occurs when the margo is displaced in the bordered pit closing the aperture of the path for water movement (see Figure 2.7).

After the water absorption test, the samples were oven dried to obtain the moisture mass present at the end of the experiment. The porosity was determined for each sample in order to approximate the product of the porosity and the density of water to the capillary moisture content at saturation. The porosity was measured using helium pycnometry and mercury intrusion.

Mercury intrusion is not as accurate as helium pycnometry for the determination of porosity, since helium can penetrate smaller pores. Since small connecting pores cannot be reached by the mercury, the results of mercury intrusion cannot be considered accurate enough because important void volumes in the samples may not be detected. Nonetheless, mercury intrusion is a powerful tool for describing porous materials. It allows the pore size/volume distribution of the samples to be investigated. Such distributions are useful for creating moisture retention curves by using the pore size radius and the surface tension of water to determine the capillary pressure in equilibrium with the intrusion volume. These curves are useful for simulations that use capillary

pressure as driving potential. The experimental values must then be fitted to a continuous expression in order to be used in numerical simulations.

3.1 Water absorption test

A free water absorption test is one in which the bottom side of a test sample is placed in contact with water. It is important to avoid submerging the specimen, because it can result in the build-up of hydrostatic pressure which can affect the absorption rate of water.

The material selected was jack pine and the test specimens were cut in a prismatic shape with approximate dimensions w × d × h = 40 × 40 × 50 mm^3. It is important to mention that the impact of the sample size and shape parameters for water uptake was not studied. The four sides of each sample perpendicular to the water surface were covered with either varnish or adhesive tape to avoid moisture loss by evaporation through the sides. The top was left uncovered to minimize any build-up of entrapped air pressure which might slow down the absorption process. Each of the samples was hung by a string from a hook inserted at the top as shown in Figure 3.1.

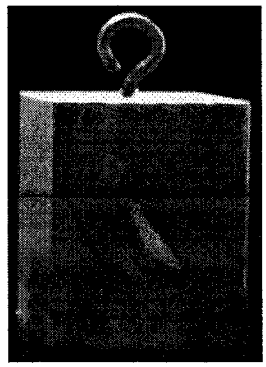

Figure 3.1. Photograph of one of the test samples.

For this experiment, a plastic tray was used as a water reservoir. Distilled water was employed to fill out the plastic tray. In order to control the depth of the samples in the water, metal strings were attached to a grooved stainless steel rod that had mobile plates. Their base was submerged only a few millimeters (~1-3).

The environmental laboratory conditions ranged from 18 to 24 °C and 50 to 70% RH for the duration of the experiments. The same digital clock was used to record the date of the weighing, including hours, minutes and seconds. The water temperature was kept constant at 20°C in order to avoid changes in water viscosity which might affect the results of the test. This was achieved by recirculation of the water using a constant temperature bath. Figure 3.2 shows the water uptake setup.

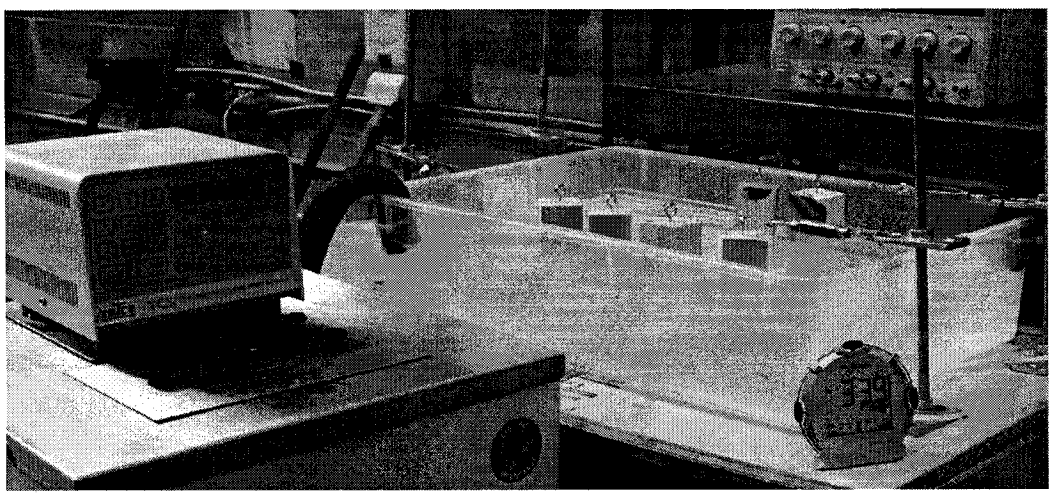

Figure 3.2. Water uptake setup. On the left: the constant temperature bath can be seen. On the right: samples in the water filled plastic tray are undergoing the test.

The samples were weighed at different time intervals. The scale used was a Voyager® Pro by OHAUS having a maximum capacity of 6100 g and with a readability

of 0.01 g grams. When the samples were removed from the water, the bottom surface was gently pressed against a layer of absorbent paper to remove drops clinging to the surface.

Figure 3.3. Weighing of the specimens. Special care was taken during the weighing to dry the droplets clinging to the bottom surface, and take the measurement as soon as possible.

The data is used to construct a graph showing the cumulative weight gained versus the square root of time where a regression curve is obtained. It is also important to measure the contact area between the samples and the water surface. The slope of this graph is the important value, i.e. the water absorption coefficient A.

The water absorption coefficient is defined by the following equation according to Schwarz (Krus, 1996)

$$m_w = A\sqrt{t} \tag{3.1}$$

where m_w is the amount of water absorbed in kg/m^2, and A is the water absorption coefficient (kg/m^{2}s$^{1/2}$). This coefficient is obtained by dividing the slope of the curve by the contact area and making the corresponding unit conversion.

Frequently a water absorption curve has the shape shown in Figure 3.4:

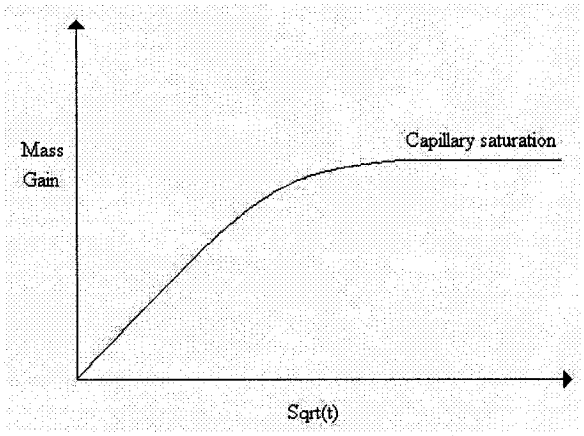

Figure 3.4. Water absorption curve for porous materials. Modified from Mukhopadhyaya *et al* (2002)

For each of the samples, the initial dimensions were taken using a Vernier caliper having a reading error of ±0.05 mm. The oven dried mass was determined at the end of the experiment by using a convection oven at 103 °C until no mass change was detectable. The contact area was computed from the measurements. These values are presented in Table 3.1.

Table 3.1. Samples dimensions, direction of the flow and their oven dried weight.

Sample	Direction of the flow	Oven dried – mass (g)	Dimensions (mm)	
			Sides	Height
A1	Longitudinal	29.43	40.6 x 40.9	50.3
B1	Longitudinal	28.04	41.0 x 41.5	50.7
C1	Longitudinal	27.80	41.1 x 40.9	48.5
D1	Longitudinal	26.23	40.8 x 40.8	48.5
E1	Longitudinal	40.00	41.0 x 40.8	50.2
F1	Longitudinal	34.70	41.3 x 41.1	50.6
E2	Longitudinal	27.63	41.3 x 40.7	48.5
F2	Longitudinal	29.23	40.7 x 41.6	50.7
G2	Longitudinal	30.89	41.0 x 41.1	48.5
H2	Longitudinal	26.84	41.3 x 40.7	50.8
A2	Radial &Tang	31.79	40.9 x 40.8	51.0
B2	Radial	28.45	41.2 x 40.0	50.7
C2	Tangential	26.69	41.1 x 40.0	51.8
D2	Tangential	36.10	40.6 x 40.8	51.0
Hooks	----------	2.04	----------	----------
Note: *Mass without hooks				

Table 3.2. Contact area and total volume of the samples

Sample	Area [mm^2]	Volume of sample [cm^3]
A1	1660.5	83.5
B1	1701.5	86.3
C1	1681.0	81.5
D1	1664.6	80.7
E1	1672.8	84.0
F1	1697.4	85.9
A2	1668.7	85.1
B2	1648.0	83.6
C2	1644.0	85.2
D2	1656.5	84.5
E2	1680.9	81.5
F2	1693.1	85.8
G2	1685.1	81.7
H2	1680.9	85.4

3.1.1. Water absorption curves

Figure 3.5 shows the water absorption curve for each of the samples during the first 5 hours. The water absorption rate at an early stage is considerably higher than the later stages when it slows down and becomes almost constant. It is also noticeable that the rate of water absorption varies for different orientations of the grain.

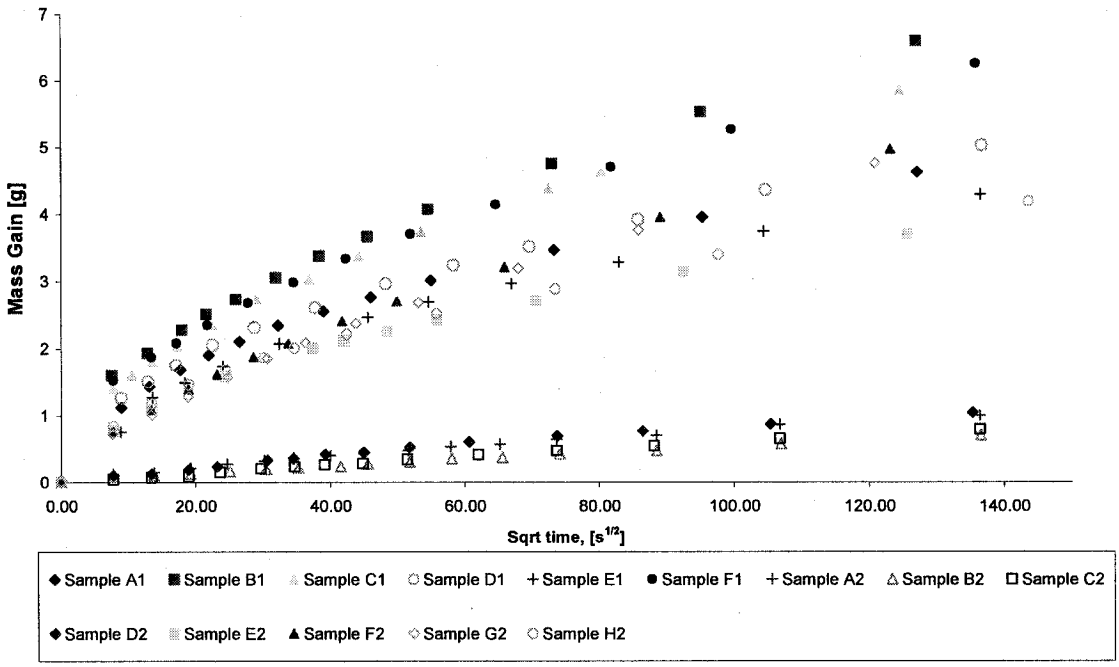

Figure 3.5. Cumulative mass as a function of square root of time for samples for the first 5 hours in order to appreciate better the higher absorption rate at the beginning.

For sample A1, if we compute different linear regressions for different time ranges, we notice the difference in the slope. The first data range goes from 0 to 54.97 $s^{1/2}$ or 0 to 0.84 hr, and the second range from 73.32 to1246.20 $s^{1/2}$ or 1.49 to 431 hr, and the last data range from 0 to 767 hr. At the beginning the slope is 0.049 [$g/s^{1/2}$], then afterwards it becomes 0.0217 [$g/s^{1/2}$] which is more than two-fold decrease. However, it

is interesting to show that if we choose the complete data range, the slope is about the same as that of the second range. The different slopes are shown in Figure 3.6.

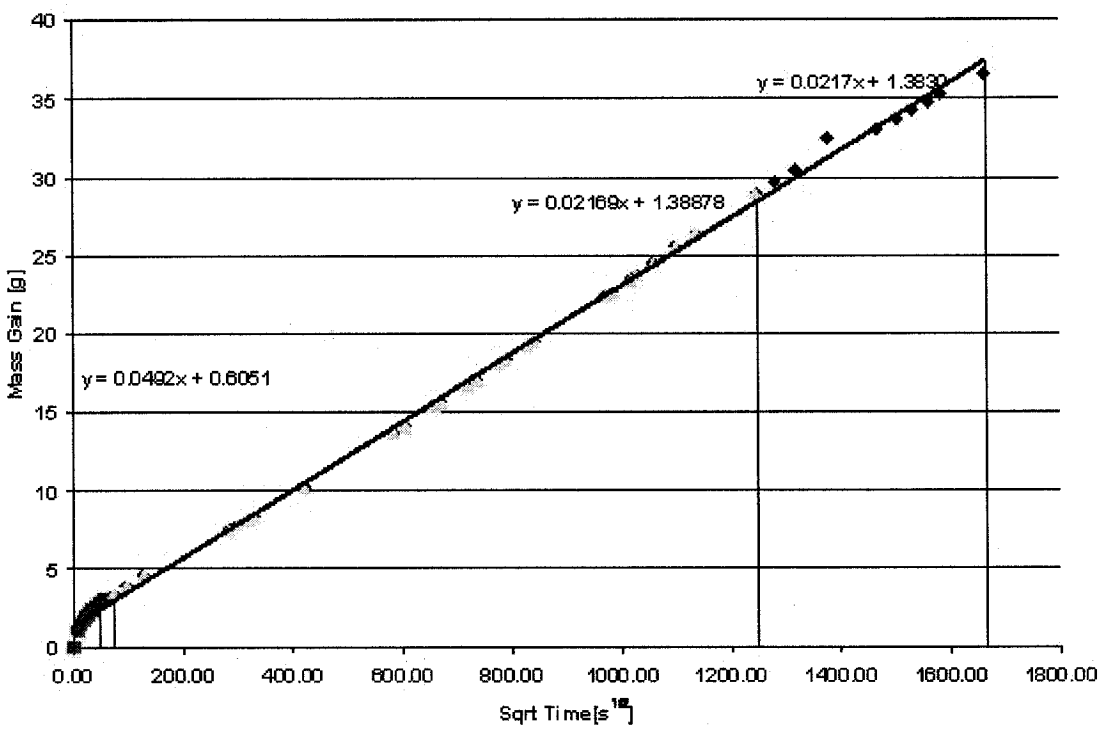

Figure 3.6. Cumulative mass as a function of square root of time for sample A1 and three linear regression curves. The vertical lines indicate each of the points employed for the linear regression.

Even though for samples A1, B1, C1, D1, E1 and F1 the water absorption experiment was run for 31 days, capillary saturation in the samples was never reached. This may be explained by the large sample size and the slow rate of diffusion in the wood.

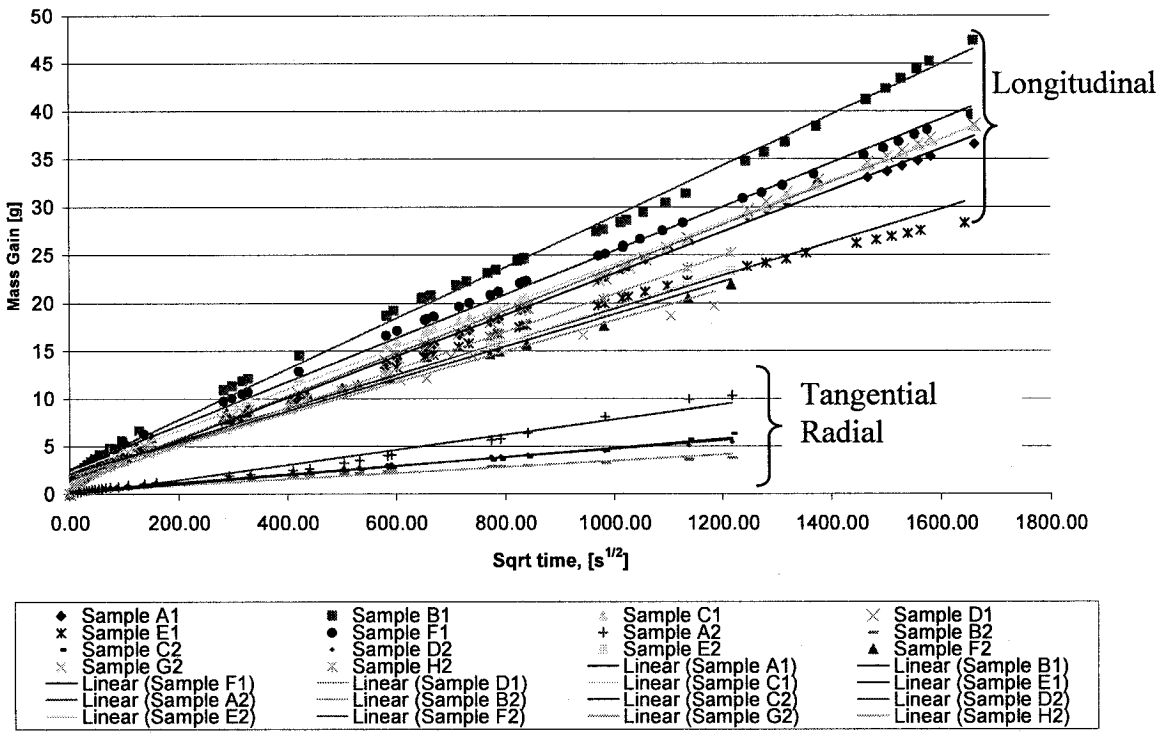

Figure 3.7. Mass gain as a function of the square root of time for all the samples. It is easy to notice the difference in water absorption rate according to orientation of the sample.

Table 3.3 summarizes the results of the regression equation for each wood sample.

Table 3.3. Regression equations, corresponding standard error in the slope coefficient and R^2 value for each sample.

Sample	Direction of Flow	Regression curve MG[g]	Std error for slope	R^2
A1	Longitudinal	MG = 0.0217 sqrt(t) + 1.3830	0.000117	0.9987
B1	Longitudinal	MG = 0.0265 sqrt(t) + 2.4378	0.000218	0.9970
C1	Longitudinal	MG = 0.0217 sqrt(t) + 2.2900	0.000172	0.9972
D1	Longitudinal	MG = 0.0223 sqrt(t) + 1.2927	0.000146	0.9981
E1	Longitudinal	MG = 0.0173 sqrt(t) + 2.0631	0.000267	0.9896
F1	Longitudinal	MG = 0.0228 sqrt(t) + 2.5912	0.000159	0.9969
E2	Longitudinal	MG = 0.0184 sqrt(t) + 1.1956	0.000169	0.9979
F2	Longitudinal	MG = 0.0169 sqrt(t) + 1.9318	0.000493	0.9791
G2	Longitudinal	MG = 0.0163 sqrt(t) + 1.9049	0.000538	0.9734
H2	Longitudinal	MG = 0.0198 sqrt(t) + 1.0779	0.000160	0.9981
A2	Radial &Tang	MG = 0.0079 sqrt(t) - 0.1373	0.000213	0.9793
B2	Radial	MG = 0.0032 sqrt(t) + 0.2017	0.000087	0.9793
C2	Tangential	MG = 0.0047 sqrt(t) + 0.0510	0.000070	0.9939
D2	Tangential	MG = 0.0044 sqrt(t) + 0.2877	0.000079	0.9912

As can be seen, the R^2 coefficients were high, ranging from 0.9987 to 0.9734, which tell us that the fitting of the experimental point to a linear equation was acceptable.

3.1.2. Computation of water absorption coefficients

Each curve is associated with a standard deviation or error for the coefficient of the slope and for the intercept. Using these values, uncertainties for the water absorption coefficient can be computed using the following formula:

$$\frac{\Delta z}{z} = \sqrt{\left(\frac{\Delta x}{x}\right)^2 + \left(\frac{\Delta y}{y}\right)^2 + \ldots} \qquad (3.2)$$

where z is the product or division of two variables. In our case, z is the division of the slope by the contact area.

Table 3.4. Water absorption coefficients, respective uncertainties and percentile error.

Sample	Direction of Flow	Water absorption coefficient - A [$kg/m^2*s^{1/2}$]	Uncertainty [$kg/m^2*s^{1/2}$]	Percentile error
A1	Longitudinal	0.01307	0.00007	0.54
B1	Longitudinal	0.0156	0.0001	0.82
C1	Longitudinal	0.0129	0.0001	0.79
D1	Longitudinal	0.01340	0.00009	0.65
E1	Longitudinal	0.0103	0.0002	1.54
F1	Longitudinal	0.01343	0.00009	0.70
E2	Longitudinal	0.0109	0.0001	0.92
F2	Longitudinal	0.0100	0.0003	2.92
G2	Longitudinal	0.0097	0.0003	3.30
H2	Longitudinal	0.0118	0.0001	0.81
A2	Radial &Tang	0.0047	0.0001	2.70
B2	Radial	0.00194	0.00005	2.72
C2	Tangential	0.00286	0.00004	1.49
D2	Tangential	0.00266	0.00005	1.80

Note: The associated uncertainties varied in order of magnitude for each sample due to the different fittings of the regression curves. As a result, the water absorption coefficients have different numbers of significant figures.

3.1.3. Discussion of the results

It is interesting to compute ratios of the longitudinal coefficients with the other two orthogonal orientations. The average of the longitudinal water absorption coefficient is 0.0121 $kg/m^2s^{1/2}$.

For the radial and tangential directions the averages are 0.0033 and 0.0027 $kg//m^2s^{1/2}$, respectively. The ratios of the A_L/A_R and A_L/A_T, are 3.66 and 4.48

respectively. This conclusively shows that the transport along the longitudinal tracheids is more important than in the other two directions by a factor of 3.7 to 4.5.

It is interesting to compare the results for the water absorption coefficient with the literature. The work by Mukhopadhyaya *et al* (2002) reported values of longitudinal water absorption coefficients ranging from 0.0109-0.0116 $kg/m^2s^{1/2}$ for eastern white pine when the temperature of the water was kept at 21°C. For our samples, the range for the longitudinal direction was 0.0097-0.0156 $kg/m^2s^{1/2}$. The range is comparable in magnitude for each wood species. Kumaran (1999) reported a longitudinal water absorption value of 0.0096 $kg/m^2s^{1/2}$ for spruce, though, in the report, it is not specified at which temperature this value was obtained.

Regarding the shape of the water absorption curves shown in Figure 3.6, it is appreciable that at the beginning of the imbibition the slope is higher and then decreases. The same behavior has been reported by several authors since the 18^{th} century for wicking (water uptake) experiments (Kornev and Neimark, 2001). When a porous material first touches water, very high wicking velocities are present (Wålinder, 2000). The theory necessary to explain such behavior may require, even the velocities are quite low, to incorporate inertial effects. However, such consideration is outside the scope of this thesis.

A question that comes to mind when analyzing the wetting stages is the duration of the wetting, for example when there is rain penetration. If there is water in contact with the wood element for less than 2 hours, it might be better to use the water absorption coefficient that corresponds to the initial period of wetting; otherwise the inertial effect might be neglected.

Another issue of the water absorption test is that it is valid for an isothermal condition. Mukhopadhyaya (Mukhopadhyaya *et al*, 2002) show that, in the case for eastern white pine, the water absorption coefficient increases for increasing temperature. They are summarized in the following table.

Table 3.5. Average water absorption coefficient for eastern white pine corresponding to different water temperatures (Mukhopadhyaya *et al*, 2002)

Temperature [°C]	Water absorption coefficient [$kg/m^2*s^{1/2}$]
3	0.0075
12	0.0094
21	0.0112
35	0.0142

The results found by the researcher can be explained because as the temperature of the fluid increases, the viscosity of the fluid diminishes, therefore there would be less dissipation of energy by viscous forces. It follows that an increase in the temperature will cause an increase in the mass transport rate.

3.2. Pycnometry test

3.2.1. Determination of porosity and density

A helium gas displacement Pycnometer is used in the test (AccuPyc 1330TC, Micromeritics, 2001). This apparatus is designed to determine the volume of solid objects. Helium is used as the testing gas since the helium molecule is the smallest

molecule in existence, composed of an individual helium atom. The atomic radius is about 49 pm or 0.49 Å. Moreover, it is not flammable because of its very low reactivity.

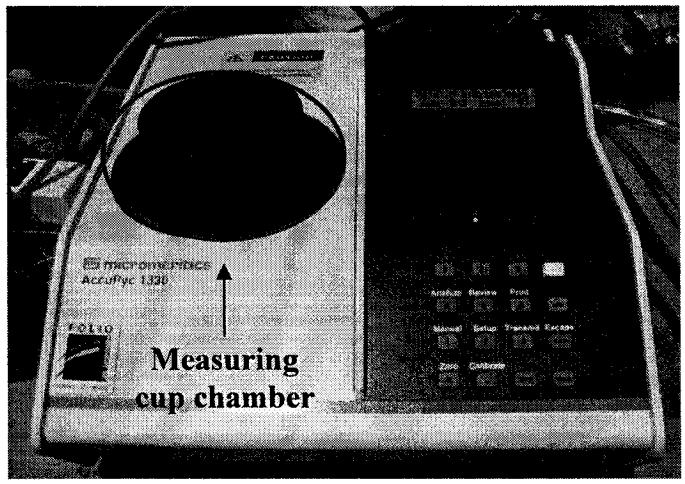

Figure 3.8. AccuPyc 1330 TC pycnometer by Micromeritics®.

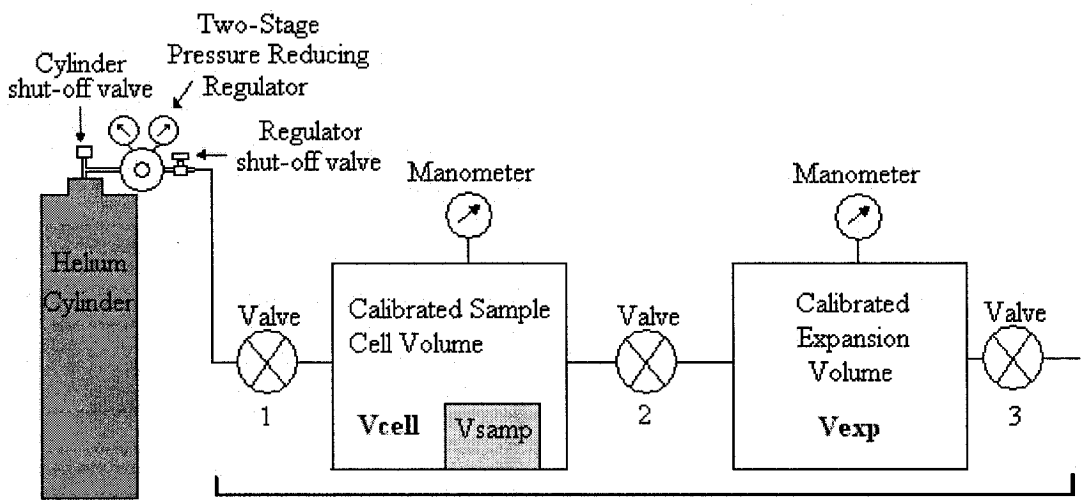

Figure 3.9. Block diagram of pycnometer.

The apparatus uses the ideal gas law for its calculations. It is assumed that both volumes, V_{cell} and V_{exp}, are at ambient temperature T_a and ambient pressure P_a, and that the valves are then closed. By opening and closing valve 1 the chamber, V_{cell}, is then changed to an elevated pressure P_1. The mass balance equation across the sample cell, V_{cell}, is

$$P_1\left(V_{cell} - V_{samp}\right) = n_c R T_a \tag{3.3}$$

where n_c is the number of moles of gas in the sample cell, R is the gas constant, and T_a is the ambient temperature.

By applying ideal gas law to the expansion volume we have:

$$P_a V_{EXP} = n_E R T_a \tag{3.4}$$

where n_E is the number of moles of gas in the expansion volume.

Then, the valve connecting V_{cell} and V_{exp} is opened while keeping valves 1 and 3 closed. The pressure will fall to an intermediate value, P_2. We now have:

$$P_2\left(V_{CELL} - V_{SAMP} + V_{EXP}\right) = n_c R T_a + n_E R T_a \tag{3.5}$$

Substituting the other equations into the last one we have:

$$P_2\left(V_{CELL} - V_{SAMP} + V_{EXP}\right) = P_1\left(V_{CELL} - V_{SAMP}\right) + P_A V_{EXP} \tag{3.6}$$

Rearranging:

$$\left(P_2 - P_1\right)\left(V_{CELL} - V_{SAMP}\right) = \left(P_A - P_2\right) \cdot V_{EXP} \tag{3.7}$$

$$V_{CELL} - V_{SAMP} = \frac{\left(P_A - P_2\right)}{\left(P_2 - P_1\right)} \cdot V_{EXP} \tag{3.8}$$

Finally the volume of our sample can be determined by using the following equation:

$$V_{SAMP} = V_{CELL} - \frac{(P_A - P_2)}{(P_2 - P_1)} \cdot V_{EXP} \tag{3.9}$$

In order to avoid errors in the determination of the volume of the material, it is necessary to keep the temperature of the pycnometer constant, this is achieved by circulating water outside the measuring chambers of the pycnometer by means of a water circulator. The set point temperature was 20 °C since that was the same temperature used in the water absorption experiments.

The minimum pressure required in the cylinders is 1.4 MPa (200 psig) according to the manufacturer of the pycnometer in order to minimize error due to low pressure during the experiments.

The samples used in the water absorption test were first dried in a convection oven set at 103°C. The weights of the samples were taken 3 times in a day for several days until no mass change was detectable.

The samples were later cut into about 32 × 32 × 40 mm^3 pieces to be placed in the measuring cup of the pycnometer and also to facilitate the computation of the total volume of each.

Since the mass of the samples changed with the cut, and as they may have absorbed some moisture from the surrounding air, the samples were dried again to ensure that they were moisture-free for the measurements. The samples were put in a cabinet with desiccant to wait for them to cool down as shown in Figure 3.10.

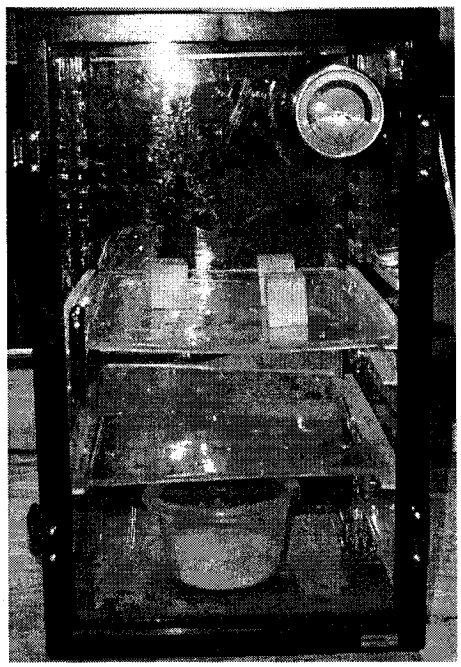

Figure 3.10. Cabinet with desiccant in order for the samples to cool down.

Then the samples were weighed using a scale having a maximum resolution of $1x10^{-2}$ grams. From the mass, the skeletal density can be calculated.

Table 3.6. Dimensions and mass of the samples cut for pycnometry.

Sample	Sides [mm]		Height [mm]	Volume [cm^3]*	Dry mass [g]
A1	31.8	31.8	39.3	39.7	13.87
B1	31.7	31.8	39.3	39.6	13.77
C1	31.6	31.8	40.2	40.3	14.25
D1	31.7	31.8	40.2	40.5	13.42
E1	31.8	31.7	39.2	39.4	18.27
F1	31.8	31.6	40.2	40.3	15.84
A2	31.7	31.8	40.2	40.5	15.61
B2	31.8	31.8	39.3	39.6	13.93
C2	31.7	31.7	40.2	40.5	13.49
D2	31.7	31.7	39.3	39.5	17.34
E2	31.8	31.8	39.3	39.6	13.51
F2	31.8	31.8	39.3	39.7	14.07
G2	31.8	31.8	39.3	39.7	14.93
H2	31.7	31.8	39.4	39.7	13.14

*Total volume of the sample, including voids and the skeletal matrix.

Finally, the samples were put into the pycnometer for the skeletal volume determination and density of the matrix. The results are summarized in Tables 3.7 and 3.8.

Table 3.7. Skeletal volume of each sample and derived porosity

Sample	Volume [cm^3]	Skeletal volume [cm^3]	Std deviation of skeletal volume [cm^3]	Porosity [%]	Estimated uncertainty in porosity [%]
A1	39.7	12.1239	0.0257	69.46	0.06
B1	39.6	10.5643	0.0205	73.32	0.05
C1	40.3	12.0018	0.0250	70.22	0.06
D1	40.5	11.0774	0.0048	72.65	0.01
E1	39.4	18.9104	0.1734	52.00	0.44
F1	40.3	13.0660	0.0187	67.58	0.05
A2	40.5	13.9769	0.0307	65.49	0.08
B2	39.6	13.9034	0.1761	64.89	0.44
C2	40.5	13.8956	0.1301	65.69	0.32
D2	39.5	13.7445	0.0389	65.20	0.10
E2	39.6	11.3467	0.0365	71.35	0.09
F2	39.7	14.5377	0.1257	63.38	0.32
G2	39.7	14.0810	0.1694	64.53	0.43
H2	39.7	10.8954	0.0239	72.56	0.06

Table 3.8. Oven dried mass, skeletal and bulk density of wood.

Sample	Oven dried mass [g]	Skeletal density [g/cm^3]	Estimated uncertainty for skeletal [g/cm^3]	Bulk density [g/cm^3]
A1	13.87	1.144	0.002	0.349
B1	13.77	1.303	0.003	0.348
C1	14.25	1.187	0.002	0.354
D1	13.42	1.211	0.001	0.331
E1	18.27	0.966	0.009	0.464
F1	15.84	1.212	0.002	0.393
A2	15.61	1.117	0.002	0.385
B2	13.93	1.002	0.013	0.352
C2	13.49	0.971	0.009	0.333
D2	17.34	1.262	0.004	0.439
E2	13.51	1.191	0.004	0.341
F2	14.07	0.968	0.008	0.354
G2	14.93	1.060	0.01	0.376
H2	13.14	1.206	0.003	0.331

3.2.2. Discussion of results

The porosity values ranged from 52 to 73.3 % for the samples measured. It does not appear that there is any correlation between porosity and density of the material as is shown in Figure 3.11.

For comparison, the heat and mass transfer simulation program WUFI (Fraunhofer Institut für Bauphysik 2005) has in its data base a value of porosity of 73% for spruce and other types of softwoods.

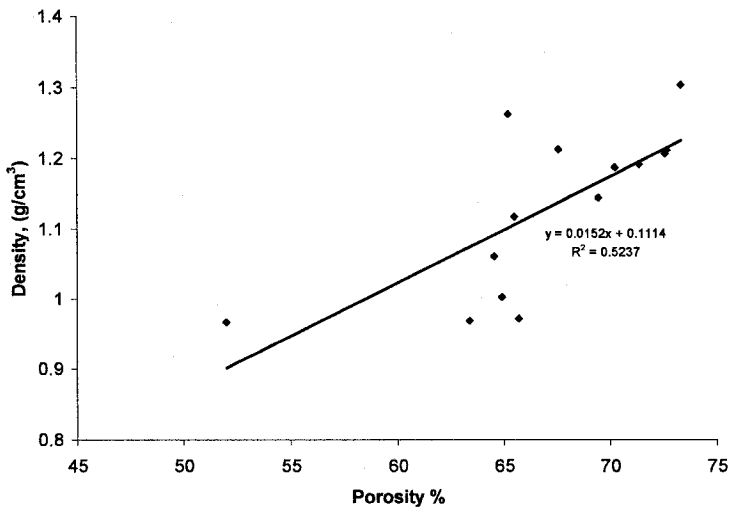

Figure 3.11 Density as function of porosity. No correlation exists between the two variables.

The porosities can be theoretically found just by using the bulk density and the density of water to determine the specific gravity, G. The equation is

$$n = 1 - G(0.667 + 0.01M) \tag{3.10}$$

Since the moisture content equals zero when the samples are oven dried, then the porosity values can be computed, the results are also compared to the results from pycnometry.

Table 3.9. Differences in porosities from the analytical and experimental method.

Sample	Porosity from pycnometry [%]	Derived porosity from specific gravity [%]	Percentile difference of porosity [%]
A1	69.46	76.70	7.24
B1	73.32	76.81	3.49
C1	70.22	76.42	6.20
D1	72.65	77.90	5.25
E1	52.00	69.07	17.07
F1	67.58	73.78	6.20
A2	65.49	74.29	8.80
B2	64.89	76.54	11.65
C2	65.69	77.78	12.09
D2	65.20	70.72	5.52
E2	71.35	77.24	5.89
F2	63.38	76.36	12.98
G2	64.53	74.92	10.39
H2	72.56	77.92	5.36

The theoretical values of the porosities tend to differ because of the low skeletal density of the wood samples. On average, the skeletal density is 1.128 g/cm^3. The lower values in the skeletal densities are due to the presence of extractives which have a lower density than the wood cell (1.5g/cm^3).

3.3. Mercury intrusion test

3.3.1. Determination of porosity and density

A Poresizer 9320 (Micromeritics©) was used. This apparatus is designed to determine the pore size distribution of samples. It is also useful for taking measurements of skeletal density and determining the breakthrough pressure or crushing pressure (Webb, 1993).

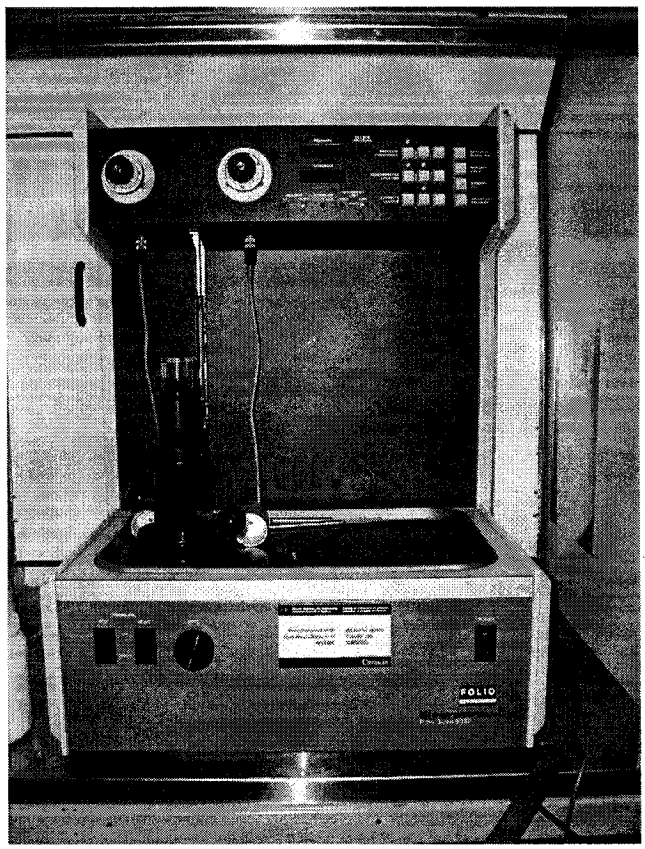

Figure 3.12. Pore sizer 9320 under exhaust hood.

Once the sample is put in place, the instrument applies a set of increasing pressures to the sample and then measures the corresponding mercury intrusion volume. This is done by measuring the change in capacitance because of the change in intrusion volume. The Pore-Sizer 9320 uses mercury because it is a non-wetting liquid to all

materials with the exception of a few noble metals (Webb, 1993). A non-wetting liquid is one for which the contact angle is more than 90 degrees, as shown in Figure 3.13.

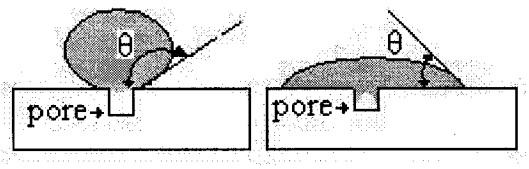

Figure 3.13. Left: a non-wetting drop of liquid will bridge the pore. Figure modified from Webb (1993). Right: a wetting drop of liquid starting to enter the pore.

As seen in the Figure 3.13, in order for the mercury to enter the pore it is necessary to apply pressure. If it is assumed that the pore has a circular cross-section with a diameter D, the area of such opening will be given by ($\pi D^2/4$). Then, if an external pressure, P is applied, the force acting on the bridged area is given by the product of P and the area. Before entering the pore, there is internal force acting on the mercury in the opposite direction to maintain equilibrium. This one is given by the product of the surface tension and the cosine of the contact angle between the capillary and the mercury acting along the perimeter of the pore (πD).

$$(\pi \cdot D^2 / 4) \cdot P = -\pi \cdot D \cdot \gamma \cdot \cos(\theta) \tag{3.11}$$

Then, solving for the diameter,

$$D = \frac{-4 \cdot \gamma \cdot \cos(\theta)}{P} \tag{3.12}$$

Equation 3.12 is known as the Washburn equation or the mechanical equilibrium equation of Young-Laplace.

Regarding mercury intrusion porosimetry for wood, this technique is employed to measure the capillary pressure of the sample. Though it is not perfect, since the pores are assumed to have a circular cross-section, and for determination of pore size for wood samples, it must be carefully employed since very thin slices of samples, less than the length of the fiber, have to be cut using a microtome to obtain the best results. This was explained in the work done by Trenard on beech, spruce, scotch pine and fir (Trenard, 1980).

In this work, the idea was not to measure the exact size of the pores, but to have an approximation between capillary pressure and moisture content. There are better methods to study the size of the micro-structure by using image analyzing techniques on scanning electron microscope (SEM) images (Roels, 2000).

Operation of the machine

First, the samples must be cut to fit the penetrometers, according to the requirements that the estimated pore volume of the sample should not exceed 90% or be less than 25% of the maximum measurable intrusion volume of the penetrometer stem. The samples also need to be dried to remove all moisture contained. Taken the previous requirements into account, some preliminary tests were done and the volume of the samples was set to be around 1.8 cm^3.

In order to measure very small pores, the sample inside the penetrometer is first put in the low pressure port where a vacuum is applied at the open end of the capillary, which helps to remove any remaining moisture. This allows us to take measurements

below atmospheric pressure, starting below 6894.75 Pa (1 psia). In the high pressure port, the maximum pressure reached was approximately 206.8 MPa (30,000 psia).

Figure 3.14. Left: Samples cut for Mercury intrusion test Right: One sample, after the mercury intrusion test, has changed completely its color due to the mercury impregnation.

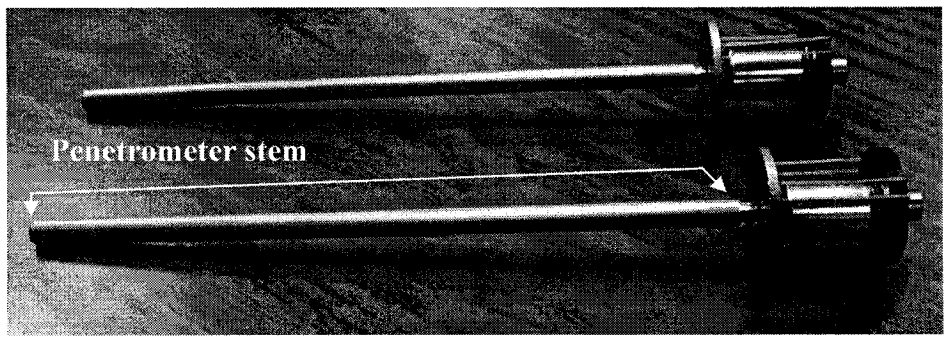

Figure 3.15. Penetrometers filled with mercury. The stem is easily identified in the picture. The volume of the stem is the one being measured by the apparatus. The outside of the glass stem which contains a capillary (empty space) is covered with a metal sleeve and together with the mercury in the capillary acts as a cylindrical capacitor because both are separated by glass which is a dielectric. A dielectric is necessary to form a capacitor. Measuring the change in capacitance, the intrusion volume can be determined.

Obtaining Results

For computing the values of diameter, the values employed in equation 3.12. where a wetting angle of 130° and a surface tension of 485 dynes/cm. This wetting angle is recommended by Micromeritics© when the contact angle is not measured. Regarding the determination of the intrusion volume, the penetrometer had a constant of 27.82

μl/pF. The machine corrects the measurements for the pressure head of the column of the fluid and assumes a constant density for mercury of 13.53 g/ml.

Results:

After running the machine, the software accompanying the equipment processes the data collected and computes the following variables:

.

Table 3.10. Total intrusion, apparent skeletal density and porosity for certain samples.

Sample	Mass [g]	Total Intrusion Volume [ml/g]	Apparent Skeletal Density [g/ml]	Porosity [%]
A1	0.6125	1.7202	1.0179	63.65
C1	0.6211	1.4589	0.9763	58.75
A2	0.6379	1.5319	0.7271	52.69
C2	0.5799	1.9450	0.7226	58.43

Comparing the porosity results with the ones obtained from the pycnometer apparatus, assuming both samples had identical porosities, we have errors of 8, 16, 19 and 11% for A1, C1, A2 and C2 respectively, for the porosity measurements using the MI machine. The errors are due in part by the fact that the samples were not cut small enough which prevented reaching important volumes of tracheids that were separated for very small pores, bordered pits, and also because the maximum pressure of 200 MPa (30,000 psia) was not reached for all the samples.

3.3.2. Moisture retention curve

From the raw data, the pore size distribution versus the intrusion volume, it is possible to convert these values to a moisture retention curve by using the water surface tension of 72.8 dynes/cm in equation 3.12.

Such curves for moisture retention curves for samples A1, C1, A2 and C2 is found in Figure 3.16.

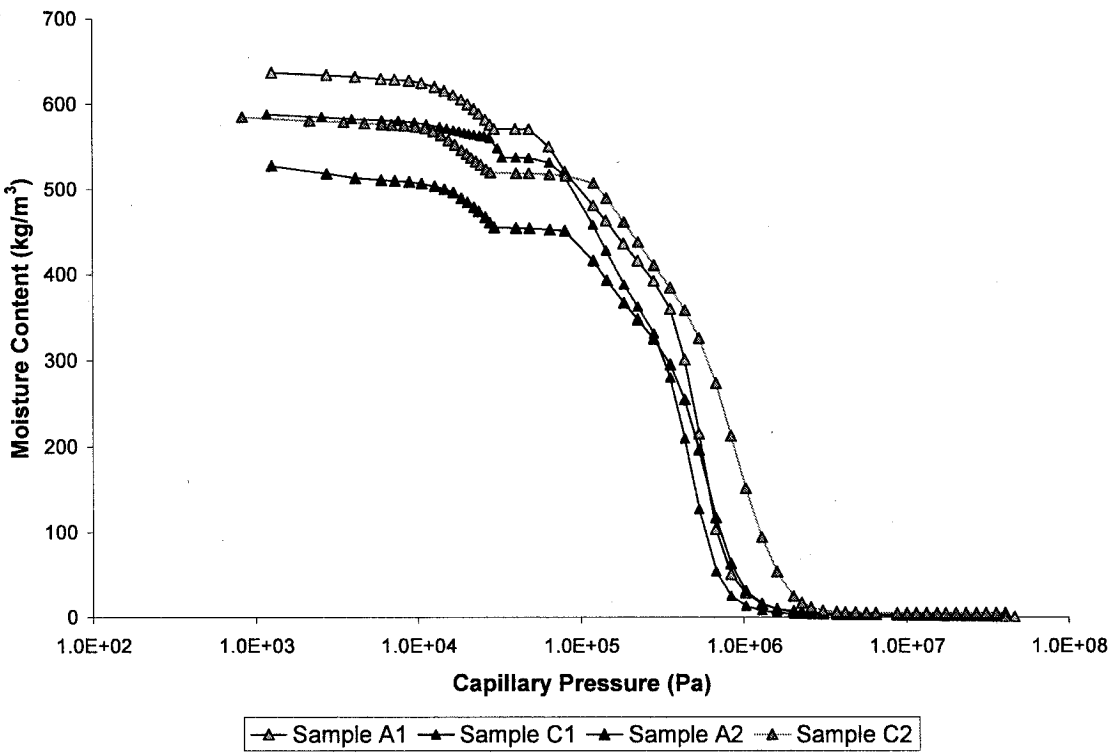

Figure 3.16. Moisture retention curve for all the samples.

For numerical simulations, it is necessary to work with a continuous expression of the moisture content. In order to do this, it is important first to see how many regions are in the distribution of the pores. By using a graph of the logarithm of the differential intrusion versus the pore diameter (m), it is possible to magnify the effect of the pore size to the intrusion volume.

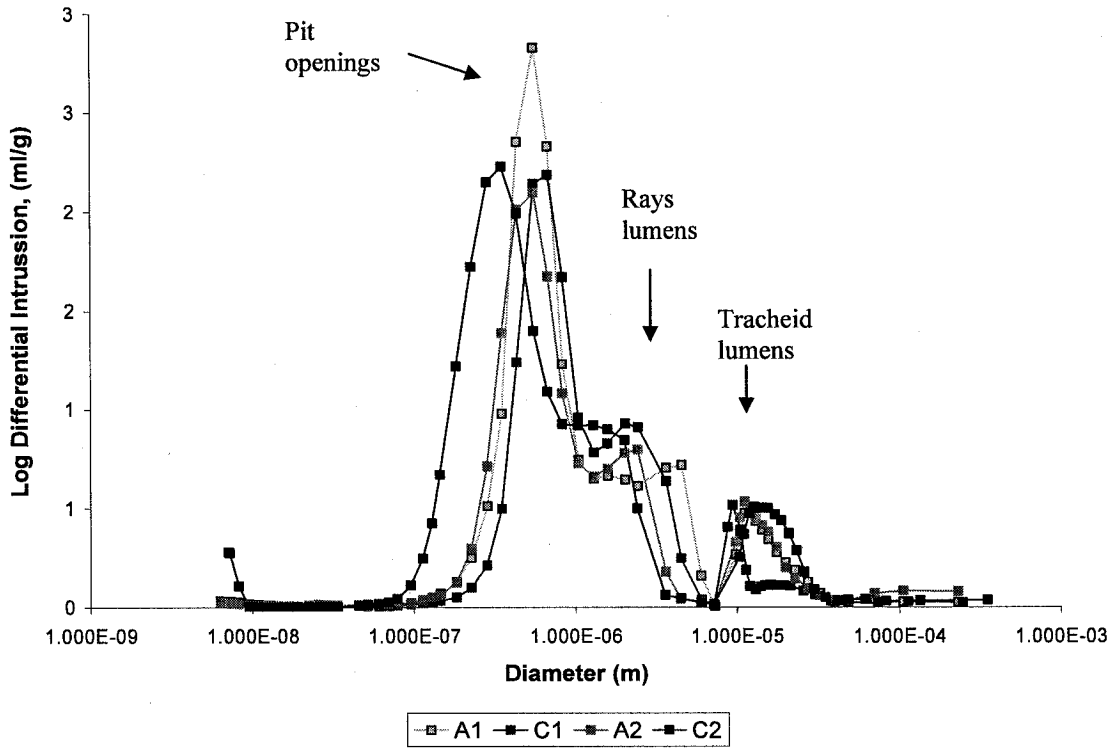

Figure 3.17. Pore volume distribution for the samples. The four curves show to have three main pore ranges which correspond to the tracheid lumens, the ray lumens and the pit openings.

3.3.3. Analytical fit of experimental data

The experimental curve obtained from the mercury intrusion test is approximated by an analytic form by a sum of power functions (Van Genuchten, 1980) (Durner, 1994)

$$W(p_c) = w_{sat} \sum_{s_i=1}^{s_n} l_1 \left(1 + (c_i p_c)^{n_i}\right)^{\left(\frac{1-n_i}{n_i}\right)} \tag{3.13}$$

where s_n is the number of subsystems, l_i weight factors ($0<l_i<1$, $\sum l_i=1$) and c_i and n_i are model parameters. In order to fit the later analytical expression for three subsystems (modality three), it is necessary to use an optimization algorithm. The method employed

was to use Solver from Microsoft Excel to minimize the error between the calculated moisture from the Van Genuchten expression and those measured.

All the curves can be fitted to the equation 3.13. In order to compare them better, the parameters c_i and n_i were kept constant. The results are found in Table 3.11.

Table 3.11. Coefficients of the analytic fit of the power function.

Parameter	Sample A1	Sample C1	Sample A2	Sample C2
c_1	8.00E-07	8.00E-07	8.00E-07	8.00E-07
c_2	7.00E-06	7.00E-06	7.00E-06	7.00E-06
c_3	1.30E-04	1.30E-04	1.30E-04	1.30E-04
Exponent n_1	4.2700	4.2700	4.2700	4.2700
Exponent n_2	1.9800	1.9800	1.9800	1.9800
Exponent n_3	1.8500	1.8500	1.8500	1.8500
Weight Factor l_1	0.0769	0.0000	0.1301	0.3878
Weight Factor l_2	0.8648	0.9717	0.7810	0.5335
Weight Factor l_3	0.0583	0.0283	0.0889	0.0787
A Coefficient	0.01307	0.01290	0.00473	0.00286

As can be easily seen, the second subsystem that has the most important weight factor, l_2, for all the samples. In case of sample C1, the weight factor l_1 was 0.

The analytical fitting against the experimental values for each of the samples is presented. From the graphs it is easily noticeable that for sample C2 the fitting was the best.

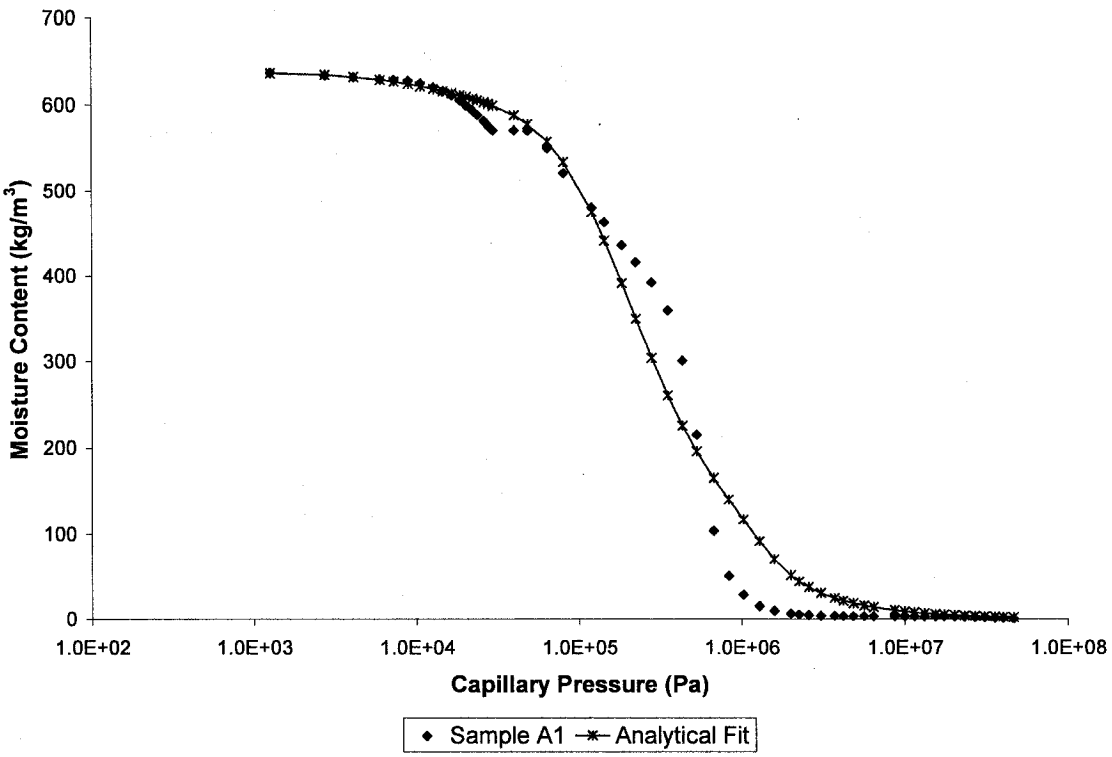

Figure 3.18. Moisture retention curve and analytical fit for sample A1.

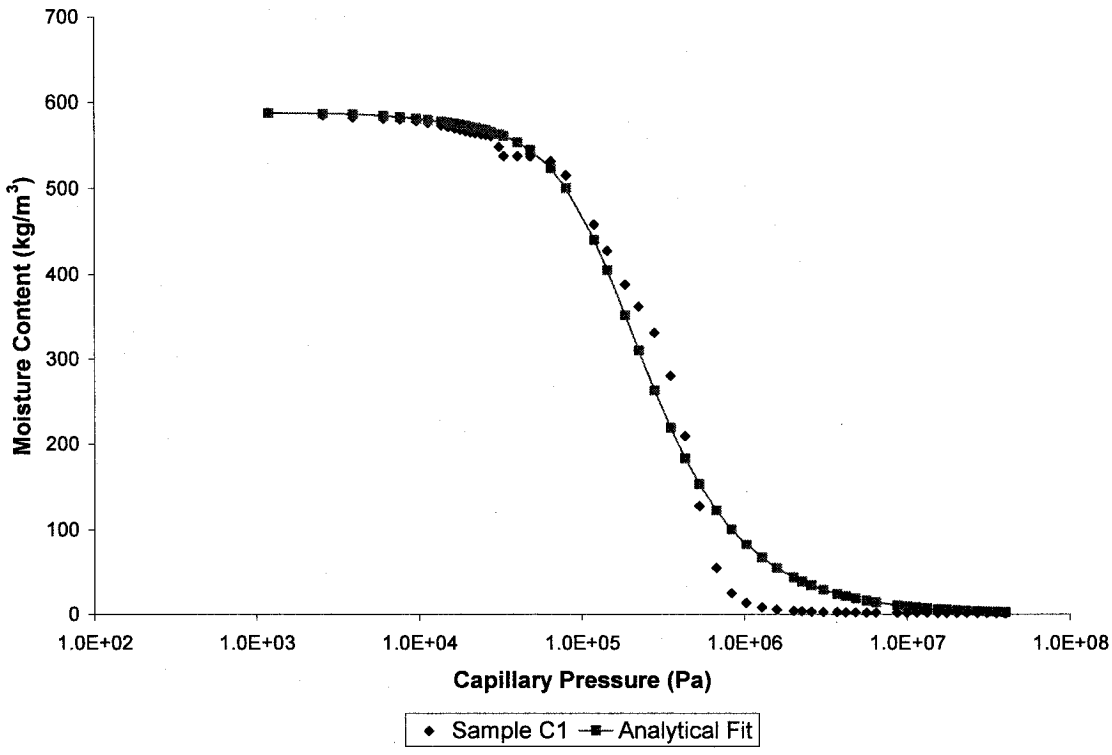

Figure 3.19. Moisture retention curve and analytical fit for sample C1.

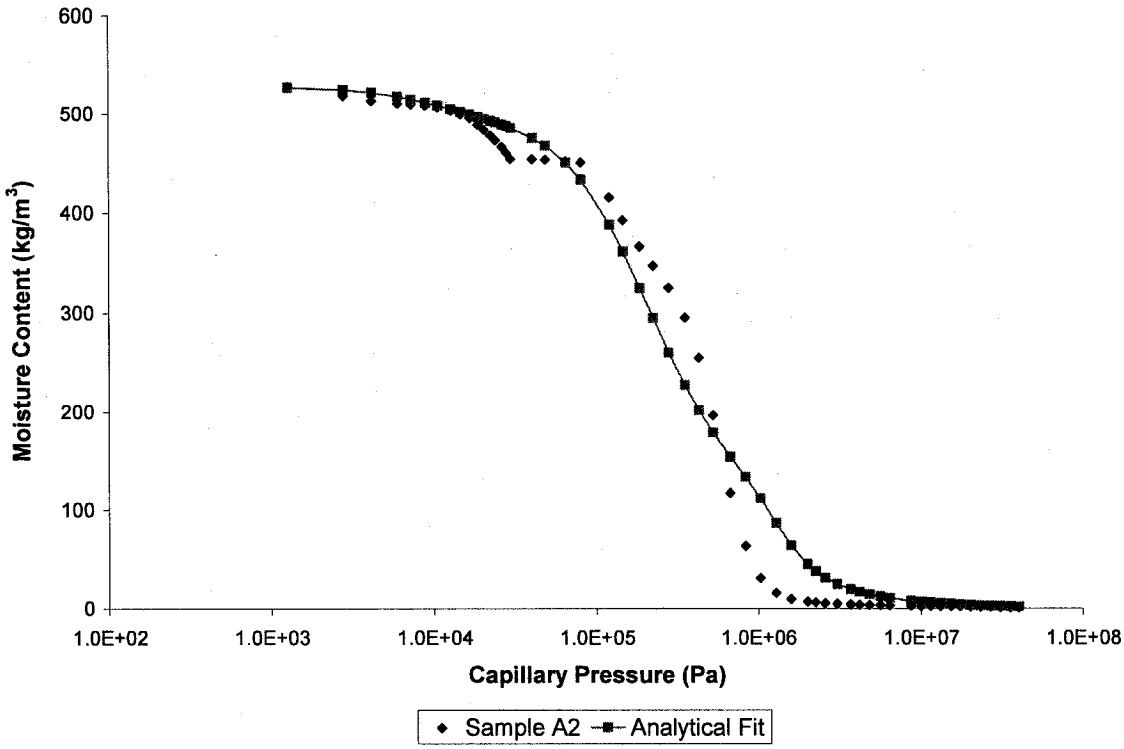

Figure 3.20. Moisture retention curve and analytical fit for sample A2

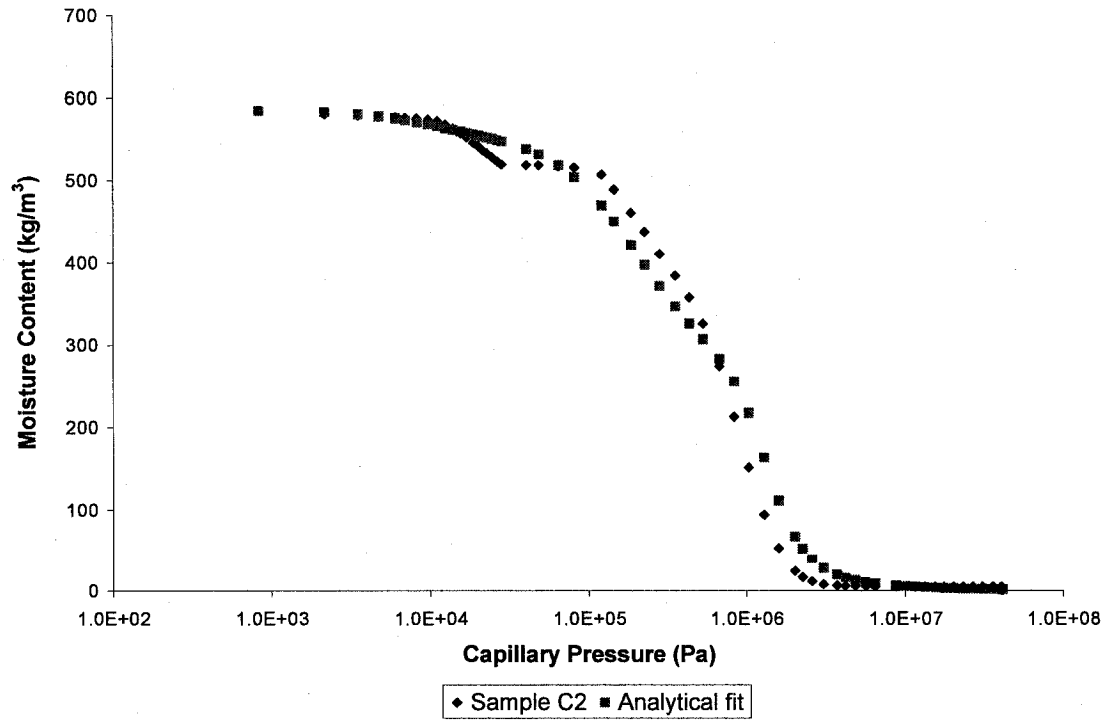

Figure 3.21. Moisture retention curve and analytical fit for sample C2.

3.3.4. Discussion of results

The method of mercury intrusion for the determination of pore size distribution constitutes a powerful tool when determining the moisture capacity of the wood sample as a function of the capillary pressure. However, the difference in porosities found by the pycnometry and mercury intrusion tests make us wonder about the reliability of using the experimental data to be fitted to the analytical Van Genuchten function to model water transport in wood.

Since the values of the porosities from the pycnometry and mercury intrusion were so different, the first recommendation would be to use a mercury intrusion machine that can reach higher intrusion pressures. Some companies have mercury intrusion machines that can reach up to 400 MPA (60,000 psia).

Another solution could be to make smaller samples so the mercury has the opportunity of filling most of the pores. However hysteresis will affect the measurements using mercury. Also, a solution could be to use scanning electron microscope (SEM) images to characterize the pore structure. Roels (2000) uses this technique by analyzing images adding to an area of 94 mm^2 to be sure the images were representative of the structure. It should be noted that the information extracted from the 2D images has to be transformed in reliable 3D information, which is not always done straight forwardly.

Regarding the analytical function employed to fit the experimental data, it is preferred over a polynomial fitting because the slope of the moisture retention curve has to be defined for the interval analyzed of capillary pressure.

The pore volume distribution was useful to appreciate the different pore subsystems that are formed by each of the different parts of the wood structure, such as tracheids, pit openings and ray lumens. The data agrees with the information regarding the structural size of the elements shown in Table 2.2 of literature review.

In Table 2.2, an expected value of tracheid lumen should be in the range of 20 to 30 μm. From the experiments, the diameters of the lumens were found to be between 7 to 35 μm approximately; the values seem to be acceptable according to the literature. Table 2.2 also gives us a range of effective diameter of pit openings to range from 0.02 to 4 μm, for the pit openings. From the curves, the diameter of pit opening is thought to be between 0.06 to 1.29 μm, which lies in the range from the literature.

Now that the main parameters related to moisture transport have been studied taking into account the water absorption coefficient for each orthogonal direction, it is important to estimate liquid diffusivities values to be used in the Richard's equation. In chapter 4, different empirical correlations will be presented correlating the water absorption coefficient and the capillary moisture content.

Chapter 4. Estimating liquid diffusivities

To model the water absorption in softwood through time is necessary to solve de Richard's equation. In order to do that, it is necessary first to compute liquid diffusivity values, which can be either constant or moisture content dependent.

Researchers participating in the International Energy Agency Annex 24 project have shown that using data from water absorption tests can provide a good approximation of the average liquid water diffusivity of the material (Kumaran, 1999). A chosen sample of eastern white pine was analyzed and then subjected to contact with water to determine the moisture diffusivity by means of γ-ray and NMR. The results varied in the shape of the diffusivity curves but were within an order of magnitude, as shown in Figure 4.1. The results showed that water absorption coefficients together with capillary saturation moisture content, can be used to calculate an average value for the moisture diffusivity as shown in Figure 4.2.

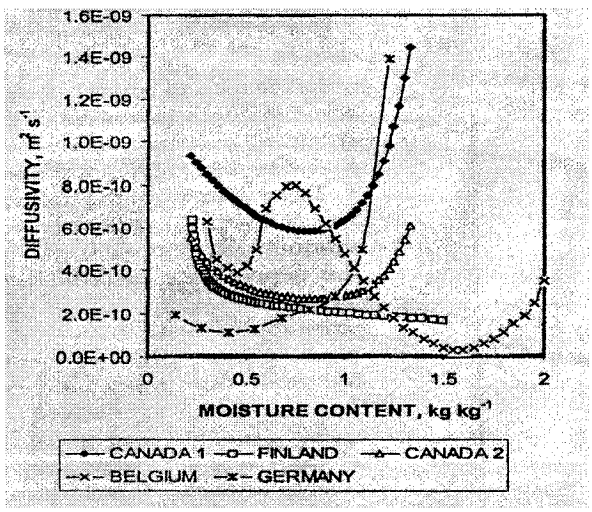

Figure 4.1. Results of the different participants for eastern white pine. The results show variability with moisture content, but fall within certain range (from Kumaran, 1999).

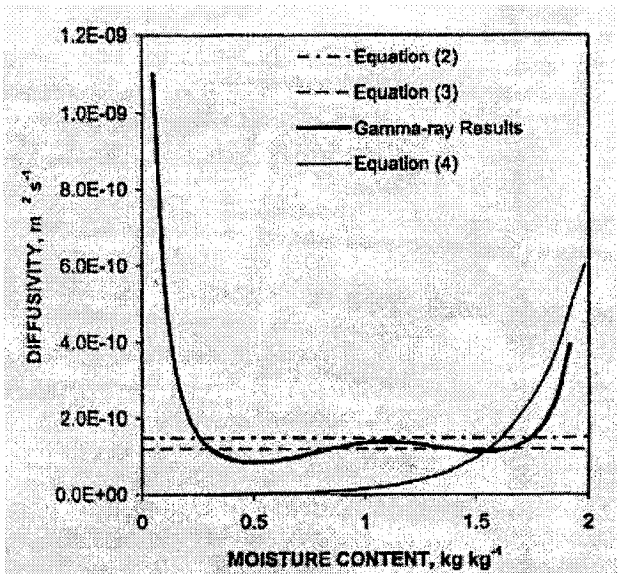

Figure 4.2. For the second exercise of the Annex 24, the spatial and temporal moisture distribution data of a piece of spruce subjected to water uptake was given to each one of the participants, so they determined the diffusivities using different analytical techniques (from Kumaran, 1999).

For Figure 4.2, equations 2, 3 and 4 are the following expressions

Equation 2: $D_w \approx \left(\frac{A}{w_c}\right)^2$

Equation 3: $D_w = \frac{\pi}{4}\left(\frac{A}{w_c}\right)^2$

Equation 4: $D_w = \left(\frac{A}{w_c}\right)^2 \frac{b^2}{2b-1} \exp b\left(\frac{w}{w_c} - 1\right)$

For equation 4, b is a fitting parameter ranging from 5 to 10. In Figure 4.2, b was assumed to be 7.5, which is typical employed for wood.

4.1 Estimation of constant liquid diffusivity

Using the equation developed by Krus and Künzel (1993) that takes into account the shape of the advancing moisture front, the average value of the liquid water diffusivity in m^2/s, D, can be calculated:

$$D = \frac{\pi}{4}\left(\frac{A}{w_c}\right)^2 \tag{4.1}$$

where w_c is the capillary saturated moisture content of the sample in kg/m^3, and A is the water absorption coefficient. Assuming that w_c is equal to the density of water (1000 kg/m^3) multiplied by the porosity of the sample, the diffusivities can be computed. It is interesting to mention that Kumaran (1999) employed a capillary moisture content for spruce approximately equal to 785 kg/m^3 that was obtained from gamma-ray measurements. In the pycnometer experiments of chapter 3, the maximum porosity found was 73.32%, which would yield a capillary moisture content of 733.2 kg/m^3, assuming that all the pores can be filled with water. Using the same logic, the following diffusivities are obtained for sample A1; 3.31×10^{-10} m^2/s from mercury intrusion and $(2.78 \pm 0.03 \times 10^{-10})$ m^2/s from pycnometry. For the rest of the samples, the diffusivities are summarized in the following Table 4.1.

Table 4.1. Diffusivities for each sample, uncertainties and percentage errors.

Sample	Direction of flow	Diffusivity (m^2/s)	Uncertainty (m^2/s)	% Error
A1	Longitudinal	2.781E-10	0.0302E-10	1.08
B1	Longitudinal	3.555E-10	0.0458E-10	1.29
C1	Longitudinal	2.651E-10	0.0413E-10	1.56
D1	Longitudinal	2.672E-10	0.0359E-10	1.34
E1	Longitudinal	3.081E-10	0.1305E-10	4.24
F1	Longitudinal	3.102E-10	0.0418E-10	1.35
E2	Longitudinal	1.833E-10	0.0339E-10	1.85
F2	Longitudinal	1.955E-10	0.1190E-10	6.08
G2	Longitudinal	1.775E-10	0.1123E-10	6.33
H2	Longitudinal	2.077E-10	0.0353E-12	1.70
A2	Radial &Tang	4.045E-11	0.1724E-11	4.26
B2	Radial	7.020E-12	0.3742E-12	5.33
C2	Tangential	1.489E-11	0.0441E-11	2.96
D2	Tangential	1.307E-11	0.0493E-11	3.77

4.2. Estimation of liquid diffusivity as a function of moisture content

The constant diffusivity yields information regarding how fast a sample will reach capillary saturation, but in reality, liquid water diffusivities are not constant, they change according to the moisture content as shown in Figure 4.2 from the gamma ray experiments.

Most of the time, exponential functions are employed to describe the moisture diffusivities for the whole moisture content range. The empirical equation proposed by Kunzel is used to calculate the liquid diffusivity as a function of the moisture content and using the water absorption coefficient.

$$D = 3.8 \cdot \left(\frac{A}{W_c} \right)^2 \cdot 1000^{\frac{W}{W_c}-1} \tag{4.2}$$

The same function is employed in WUFI-2D (Fraunhofer Institut für Bauphysik 2005) for the determination of diffusivities. Equation 4.2 has been used for several porous materials, e.g. Yu Huang (2003) used the same two expressions to estimate the diffusivities for aerated autoclaved concrete AAC from water absorption experiments.

The following graphs present the diffusivities as derived with equations 4.1 and 4.2. evaluated for averages of water absorption coefficients for each of the orthogonal directions and using an average porosity to approximate the capillary moisture content.

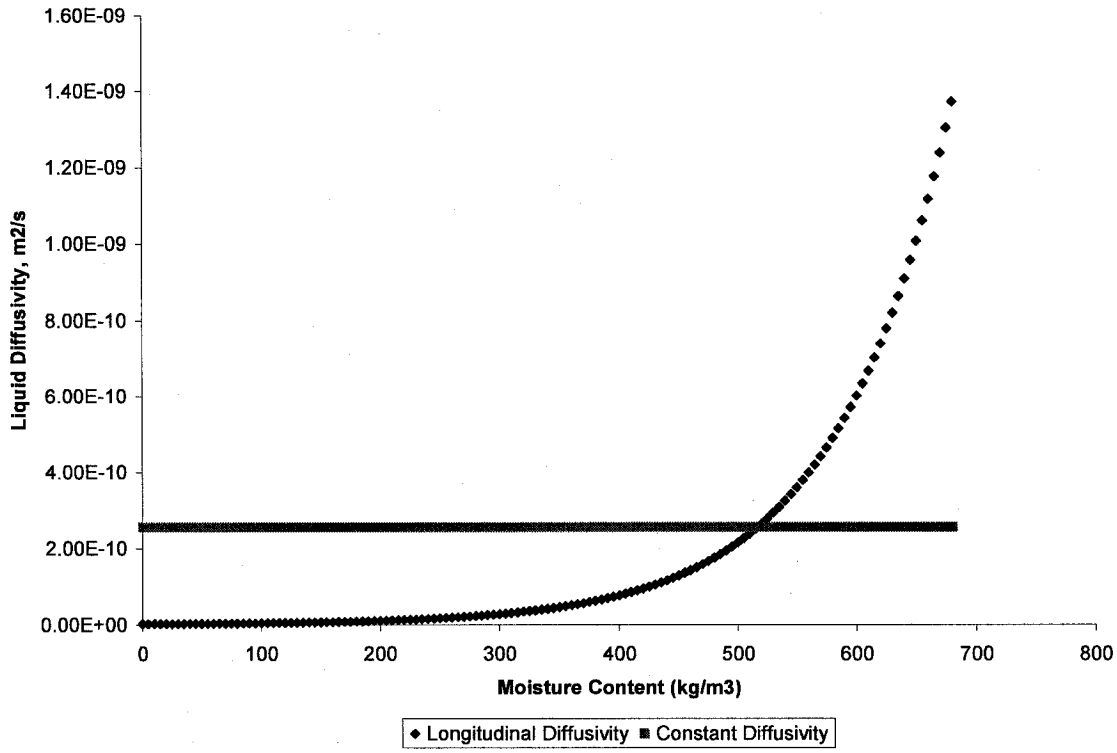

Figure 4.3. Constant average longitudinal diffusivity and moisture dependent diffusivity using equation 4.1 and 4.2 for sample A1. The variable diffusivities spans about four orders of magnitude.

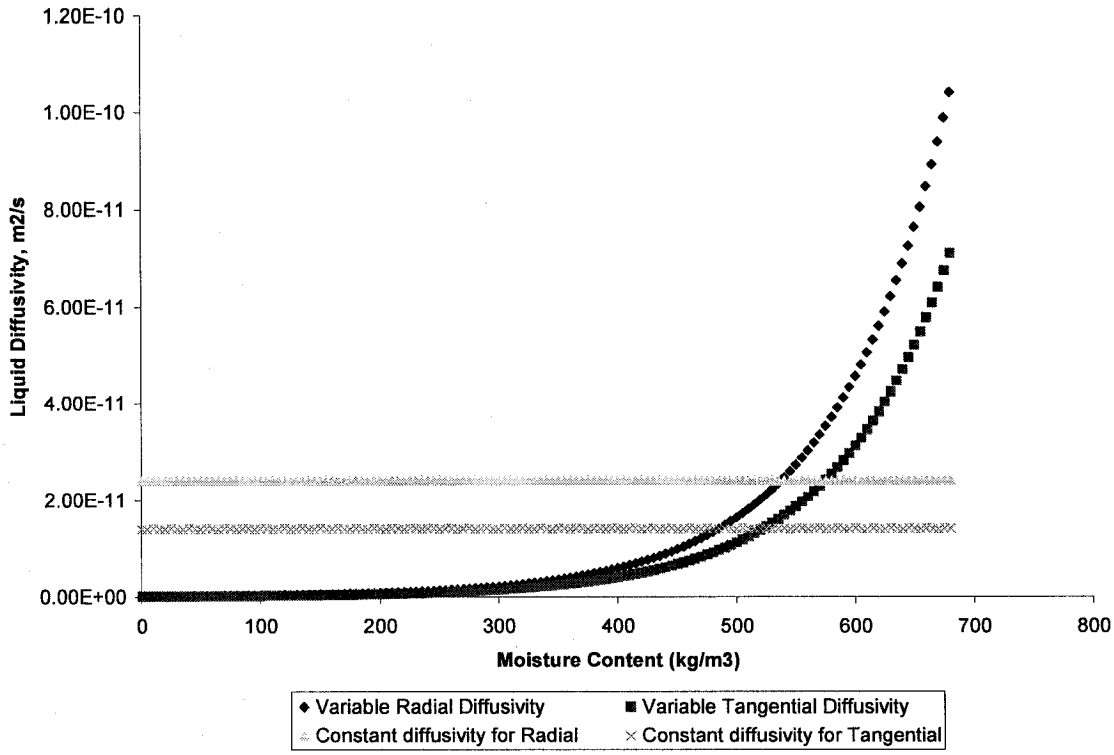

Figure 4.4. Constant average radial and tangential diffusivity and moisture dependent diffusivity for both directions using equation 4.1 and 4.2 for sample A1. The variable diffusivities spans about five powers of ten.

It is interesting to compare diffusivities obtained from water uptake experiment through gamma ray technique; the uncertainties in the data may vary from 30 to 50% according to researchers from NRC. The data is summarized in the following table:

Table 4.2. Range of moisture diffusivities for different wood species (Kumaran *et al*, 2002).

Wood Species	Lower value of diffusivity	Upper value of diffusivity
Eastern White Pine	2.51×10^{-10}	1.19×10^{-9}
Eastern White Cedar	1.23×10^{-9}	4.69×10^{-8}
Western Red Cedar	1.92×10^{-10}	3.96×10^{-9}
Spruce	1.54×10^{-10}	7.48×10^{-10}
Southern Yellow Pine	2.69×10^{-9}	1.32×10^{-8}

Comparing Table 4.2 with the estimated constant diffusivities for the longitudinal absorption, we may say that we are within the range regarding the order of magnitude for. No literature values of measured diffusivities for the other two orthogonal directions for softwoods were found.

The next task is to study which diffusivities best represent the water absorption process. In order to do this, it is necessary to solve the continuity equation by means of numerical methods, which is explained in the next chapter.

Chapter 5. Numerical simulation of water absorption in softwoods

The continuity equation for one dimensional transport, assuming the diffusivity is constant, has an analytical solution. However, when dealing with transport in two and three dimensions, it is necessary to use numerical methods to solve the partial differential equation. In this chapter, we will present how to construct 3D models that can be either linear or not to test how well the diffusivities reproduce the water uptake process.

The program chosen for the validation of our experimental diffusivity values is FEMLAB 3.0©. This program was chosen because of its well-developed user interface and user-friendliness. The software solves problems based on partial differential equations (PDEs) and it has a built-in set of common equations, such as the Fick's diffusion. Moreover, it is compatible with MATLAB, which makes it easy to write scripts. The program uses the finite element method (FEM) (FEMLAB Users guide, 2004).

A short introduction to the finite element is presented here below.

5.1. Introduction to the finite element method

The finite element method approximates a partial differential equation (PDE) by the discretization of the original problem. In this method, a continuum problem is first broken into a discrete physical representation consisting of a finite number of regions or finite elements (Dow, 1999). The finite elements are also shape functions. A shape function transforms the geometry into a set of polynomials.

Mesh

The first step in using the finite element method is to create a mesh, which is a partition of the geometry into small units of a simple shape. In 3D geometries, the method partitions subdomains into tetrahedrons (mesh elements) whose faces, edges and corners are known as mesh faces, mesh edges, and mesh vertices respectively. It partitions boundaries in the geometry into triangular boundary elements (mesh faces) (FEMLAB Users guide, 2004).

Finite Elements

After the mesh is created, it is possible to introduce approximations to the dependent variables. This is achieved by means of Lagrange elements. In the model, the Lagrange element used was quadratic.

The linear system solver

After the equations have been discretizated for each finite element of the mesh, the program solves a system of linear equations.

5.2. Sources of modeling error

Since the method subdivides the continuum, it provides the opportunity for two types of modeling error. They are called discretization errors and elemental errors. Discretization errors occur because the finite element model is by definition incapable of duplicating every one of the infinite patterns that the continuum can assume. Elemental errors most often take the form of anomalies in the representation of the equation within individual elements (Dow, 1999).

5.3. Modeling water uptake using a constant diffusivity (isotropic media)

In order to model the water uptake of the experiment we first need to establish the assumptions:

- Only the liquid migration is considered: heat and water vapor transport are not taken into account (isothermal process). Therefore the relative humidity of the air is not taken into account;
- The material is isotropic, (properties do not change with position in space);
- The flow is unidirectional;
- The diffusivity is constant and equal to the value obtained from the experiments; and
- The boundary conditions are constant.

First step: Defining the geometry of the model.

The first step is to define the geometry of the model. A prismatic model with the same size as sample A1 was constructed ($w \times d \times h = 0.0406 \times 0.0409 \times 0.0503$ m^3). The water uptake was taken to be in the longitudinal direction for this simulation.

Second step: Writing the partial differential equation

The partial differential equation (PDE) that describes the water transport must now be written.

FEMLAB incorporates a diffusion mode in which the coefficients of the equations can be input by the user.

The equation is the following:

$$\frac{\partial W}{\partial t} + \nabla \cdot (-D \cdot \nabla W) = 0 \qquad (5.1)$$

where W is the moisture content in kg/m^3, which can also be written also as $W(t,x,y,z)$, where for each coordinate t is the time. There are at least three main values of diffusivity for the direction of the unit vectors **i, j, k.** In reality, these diffusivities will be moisture-content dependent, in which case the problem becomes a non-linear one. This case will be looked at in the next section. In a non-linear model, the model properties depend on the variables solved (in this case, W).

Equation 5.1 is a modification of the Richards equation, where the term related to the gravitational effect has been neglected since it is important only in the presence of large cracks or holes (Roels, 2000). Equation 5.1 has the same form as Fick's second law of diffusion and the heat conduction equation (Bird *et al*, 2002). It expresses continuity or, in other words, conservation of mass.

Third Step: Establishing the sub-domain characteristics

The sub-domain characteristics are then established. The sub-domain is the region bounded by the edges and vertices where the phenomenon takes place.

To do this, the values of the diffusivities for each direction must be assigned. A diagonal matrix for the diffusivities will be used:

$$D = \begin{bmatrix} a & 0 & 0 \\ 0 & b & 0 \\ 0 & 0 & c \end{bmatrix} \tag{5.2}$$

Since only the diffusivity in the z-direction is taken into account, the matrix will only have a non-zero value for the constant c.

Fourth Step: Setting up boundary and initial conditions

The initial and the boundary conditions are set up.

Initial Conditions: The initial conditions describe the physical state at the start of the experiment. In this experiment, the only parameter to be used as input is the initial moisture content.

For sample A1, the volume is 83.53 cm^3 and the initial mass of moisture is 3.0 g; the initial moisture content is calculated as $W(0)$ = 3.0 g/83.53 cm^3 = 35.91 kg/m^3 in the sub-domain, assuming that the moisture is uniformly distributed in the sample volume.

The *boundary conditions* may be of two types: in the *Dirichlet type*, the solution is specified on the boundary of the region, while for the *Neumann type*, the outward normal derivative dW/dn, where n is normal to the wall, is specified on the boundary (flow). The models use the Dirichlet and Neumann boundary conditions.

5.3.1. Simulations 1 and 2

Figures 5.1 and 5.2 indicate the geometry, initial conditions and boundary conditions of simulations 1 and 2. The mass concentration at the bottom surface (z = 0) is shown in the two figures, and differences between the two correspond to the different porosities, as found using the two measurement techniques. At the other surfaces, the mass flux is set to zero.

Fifth step: Meshing the sub-domain

Meshing: The program automatically creates the mesh. In order to ensure that the grid was fine enough, the equation was solved for 5 types of meshes. The first had 127, the second 416, the third 1740, the fourth 3303 and the fifth 11327 elements. The results of the third mesh seemed not to have a significative variation, less than 0.001 g, with the second for a subdomain integration (to be explained later), so this mesh size was chosen for sample A1.

Time stepping: Since we have data for more than 2.7×10^6 seconds, a time step of 500 s for output times was used as a memory-saving measure. The time steps taken by the solver where setted up to be between 0.001 to 1.0 second. The absolute and relative tolerances were 0.0010 and 0.01 respectively. These tolerances determine the limit for the estimated error in each integration stop. This is important to avoid stability problems. Stability is said to be accomplished when the roundoff errors do not grow, regardless of the size of the time step. The errors are the residuals in the equation that are computed for all mesh elements.

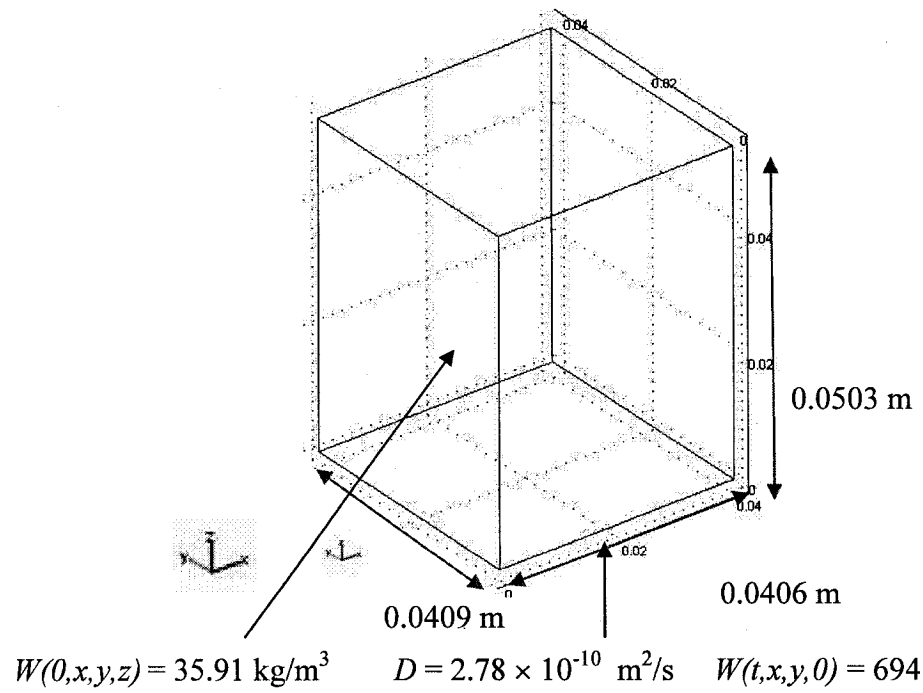

Figure 5.1. Geometry of the model and boundary and initial conditions for simulation 1.

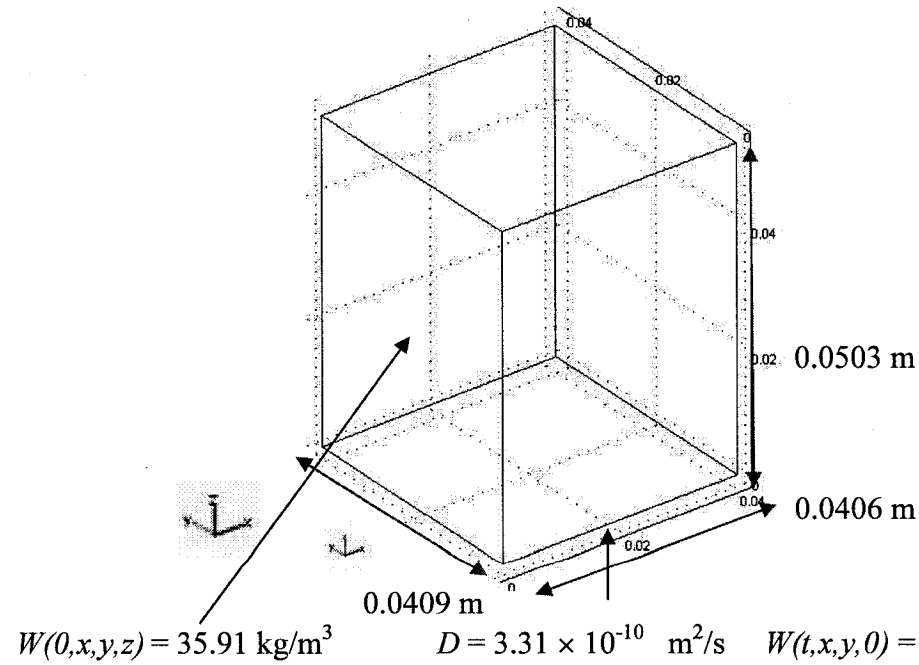

Figure 5.2 Geometry of the model and boundary and initial conditions for simulation 2.

Sixth Step: Viewing the resultts

Simulation results

After the program finds a solution for the specified times, a concentration gradient is obtained at the last requested time step (see Figure 5.3). A subdomain integration of the moisture gradient or profile provides the amount of moisture at every time step desired. This integration consists of adding up the moisture contained in each of the 3,303 elements.

In a mathematical formula, this can be expressed as

$$M(t) = \sum_{i=1}^{n} V_i \cdot W_i(t) \tag{5.3}$$

where $M(t)$ is the total moisture in the sample at a time t, V_i is the volume of the ith finite element, $W(t)$ is the moisture content of the ith element at a time t and n is the total number of elements.

A. Simulation versus measurement results

As can be seen in Figure 5.4, simulations 1 and 2 yield very similar results even though the diffusivities and boundary condition values are different. As the time increases, the error diminishes. For example, during the first 16000 seconds the error is around 26%, while for the last measurement (at approximately 32 days) the error is around 6.6%.

This disparity is in part caused by the fact that diffusivity is not a constant value; it changes with the moisture content at each point. However, the approximation of an average value yields a satisfactory agreement for increasing time. It is important to remember the high level of anisotropy in wood.

A way to reduce or minimize error is to consider two values of the water absorption coefficient: an approximate coefficient for the initial 3000 s, where the absorption of water is not linear with the square root of time and the slope of the curve is steep (see Figure 5.4), and another once the absorption process has become linear. It must be borne in mind that physically, the diffusivity is not time-dependent, but depends on factors such as temperature, material properties and moisture content.

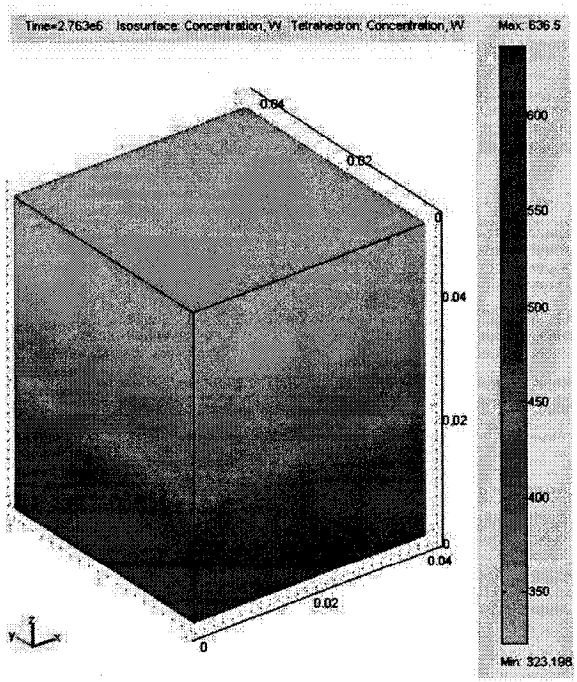

Figure 5.3 Concentration gradient for simulation 2 after 2.763×10^6 s (~32 days).

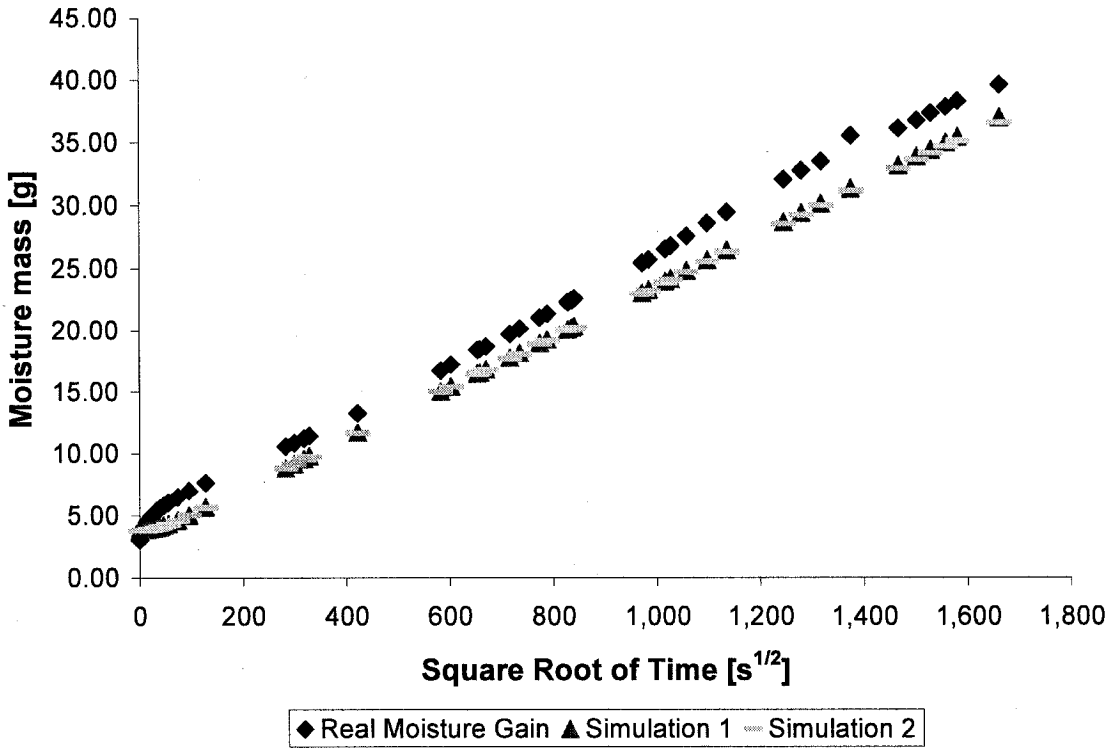

Figure 5.4. Comparison of experimental data with FEMLAB simulations for sample A1.

B. Sensitivity analysis of constant diffusivity equation

Equation (4.1) allows a sensitivity analysis to be made with respect to the effect of a change in the diffusivity on the water imbibition process.

If the value of D is changed by a factor 'x' while keeping A constant (0.01307 $kg/m^2s^{0.5}$), then it is necessary to change the capillary saturation moisture content. Rearranging equation (4.1), gives:

$$w_c' = \frac{\sqrt{\frac{\pi}{4}} * A}{\sqrt{D * x}} \tag{5.4}$$

Evaluating the last expression for two and ten times the value of the diffusivity obtained from the porosity measurement using the mercury intrusion machine, a table of the new w_c' values is presented. (Table 5.1)

Table 5.1. Capillary saturation moisture content necessary to maintain the same water absorption coefficient.

Times of D $D = 3.31x10^{-10}$ m^2/s	w_c' kg/m^3
2 D	450.18
10 D	201.32

The table shows that if we want to keep the same slope (A) at the beginning but with larger diffusivity values, it is necessary to have lower values of capillary saturation (inverse relation; see equation 5.4). In other words, the void space has to be lower so the sample reaches saturation more quickly.

Some simulation results are presented below for different diffusivity values and boundary conditions (w_c) at the bottom of the sample.

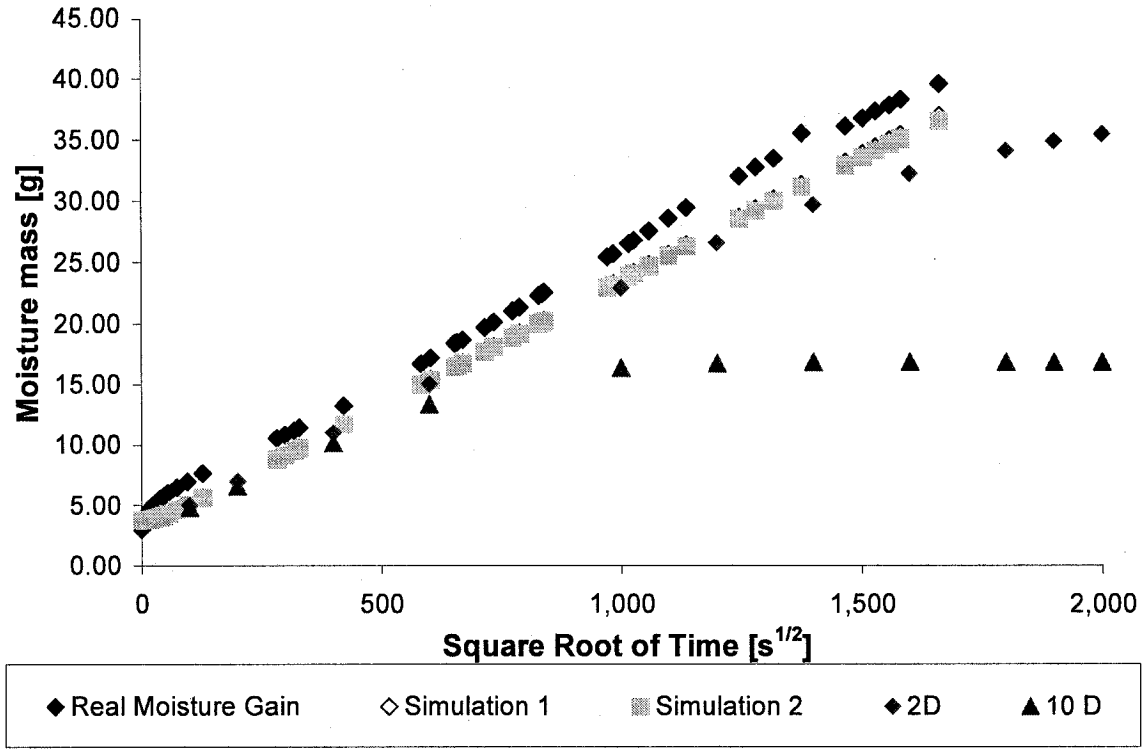

$2\ D = 6.62 \times 10^{-10}\ m^2/s \quad w_c = 450.18\ kg/m^3$

$10\ D = 3.31 \times 10^{-9}\ m^2/s \quad w_c = 201.32\ kg/m^3$

Figure 5.5. Simulation results for sample A1 for identical water absorption coefficient and different diffusivities and w_c values.

Given that the sample volume is $8.353 \times 10^{-5}\ m^3$, it is possible to obtain the amount of moisture at complete saturation; for simulation 2:

$$450.18\ kg/m^3 \times 8.353 \times 10^{-5}\ m^3 = 37.6\ grams,$$

a condition which is about to be reached in the curve of "2D" at 42 days approximately.

For the "10D" simulation, the moisture content when a stable is reached would be:

$$201.32\ kg/m^3 \times 8.353 \times 10^{-5}\ m^3 = 16.81\ grams,$$

a condition which is reached after around 1960000 s (~23 *days).*

Note that at the beginning of all the simulations, the slope is the same (A coefficient), as it should be, since the parameters were fitted to eq.4.1.

5.4 Modeling water uptake using a variable diffusivity (non linear problem)

Simulation 3

After modeling with a constant diffusivity, it is interesting to use a variable diffusivity, which will turn the model into a non linear one.

The diffusivities are expressed by the following function

$$D = 3.8 \cdot \left(\frac{0.01307}{694.9} \right)^2 \cdot 1000^{\frac{W}{694.9}-1} \tag{5.5}$$

The main assumptions are:

- The material is isotropic (material properties remain the same in all directions);
- The diffusivity is variable and moisture content dependent;
- Only the liquid migration is considered: heat and water vapor transport are not taken into account (isothermal process). Therefore the relative humidity of the air is not taken into account;
- The flow is unidirectional; and
- The boundary conditions are constant.

Simulation results

The easiest way to compare the results is comparing the moisture content through the subdomain. The following figure compares the new simulation results with the previous two.

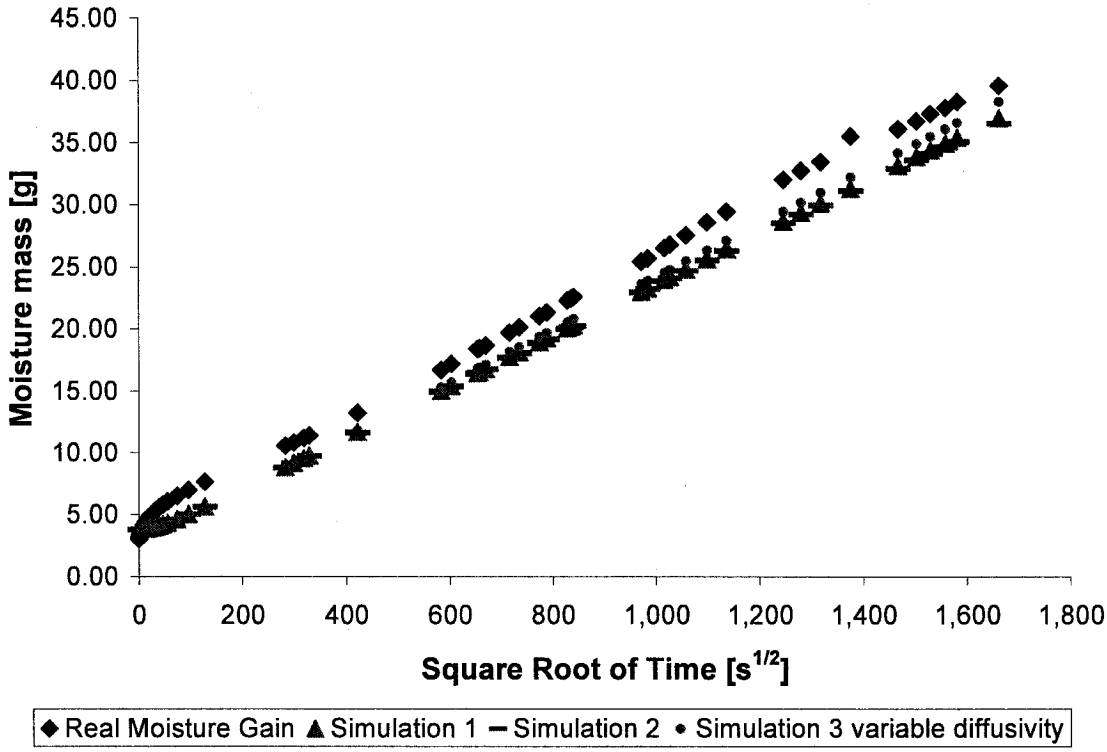

Figure 5.6. Comparison of experimental data with FEMLAB simulations for sample A1.

Comparing the three curves, it is noted that the variable diffusivity better reproduces the actual behavior of the water imbibition. The addition of the square error from the experimental to the simulation results was computed. In the case of the input derived from the pycnometry test, the addition was 237.39, sing the input derived from mercury it was 263.05 and with the variable diffusivity, the addition was 147.55 gm^2. However, the computation for the solution with the variable diffusivity took approximately thirty five times longer than the constant diffusivity approach.

5.5. Modeling the orthotropic effect in wood

Once the average diffusivities for each orthotropic direction were determined, a very simple water absorption experiment was carried out to compare the water content gradient and to study the adequacy of the experimental diffusivity values.

To achieve this, a glass cylinder was glued to the top surface of a piece of wood having a prismatic shape of approximate dimensions w × d × h = 34 × 83 × 44 mm^3, as shown in Figure 5.7.

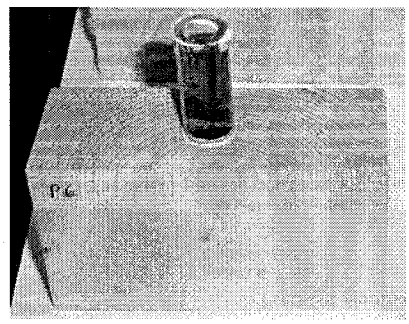

Figure 5.7. Wood sample subjected to point wetting from the top.

The glass cylinder was filled with water and care was taken to keep the cylinder at least partially filled with water until the end of the experiment. Note the direction of the fiber grain. The water was mixed with commercially available food coloring to visualize the water path within the sample. After 16 days, the sample was cut in half to observe the water penetration.

The last simulation ressembles simulations 1 and 2 with changes in the geometry of the model, boundary conditions, and more importantly the diffusivity values.

The diffusivity matrix takes the following values:

$$D = \begin{bmatrix} 2.39\text{x}10^{-11} & 0 & 0 \\ 0 & 1.39\text{x}10^{-11} & 0 \\ 0 & 0 & 2.55\text{x}10^{-10} \end{bmatrix} \quad (5.6)$$

The main assumptions are:

- The material is orthotropic;
- There is point wetting;
- From the two previous points, it follows that is the flux is multidirectional;
- The diffusivities are constant and equal to the averages values from the experiments for each corresponding wood direction;
- The boundary condition is constant at the water-wood interface and equal to the average porosity times the density of water (670.3 kg/m^3);
- The fluxes through the other faces are zero; and
- The effect of gravity in water transport is negligible.

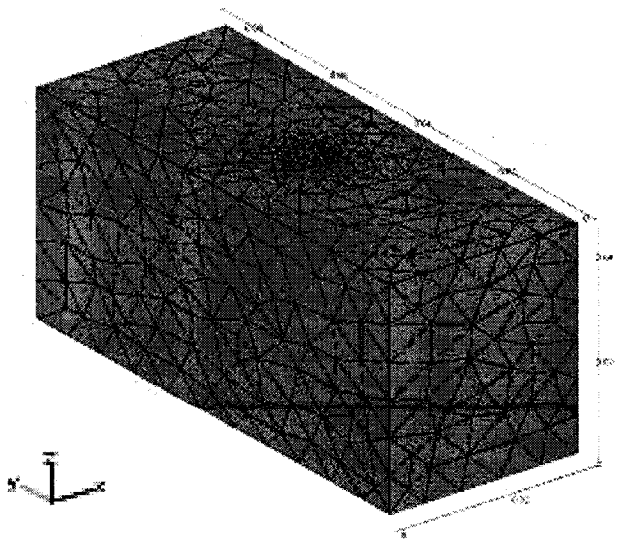

Figure 5.8 Geometry of the model and meshing for simulation of point load of orthotropic wood. The mesh is composed of 5839 tetrahedral elements.

Simulation Results:

Figure 5.9 shows the concentration gradient for two planes.

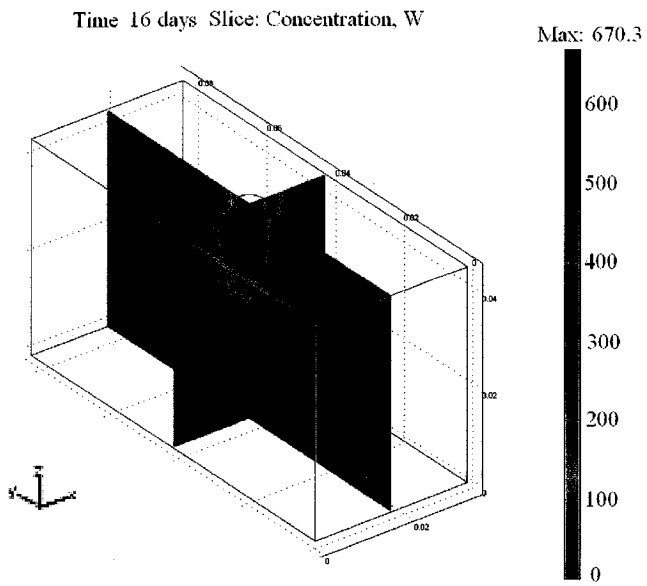

Figure 5.9. Calculated slice concentration gradient after 16 days of continuous wetting for z-x and y-z planes.

5.5.1. Qualitative comparison of the results

Figure 5.10 shows the sample cut in half with the corresponding water gradient obtained from the simulation. The simulation is incapable of reproducing the pattern of real moisture transport because the actual moisture transport occurs preferentially (more rapidly) along the latewood rings.

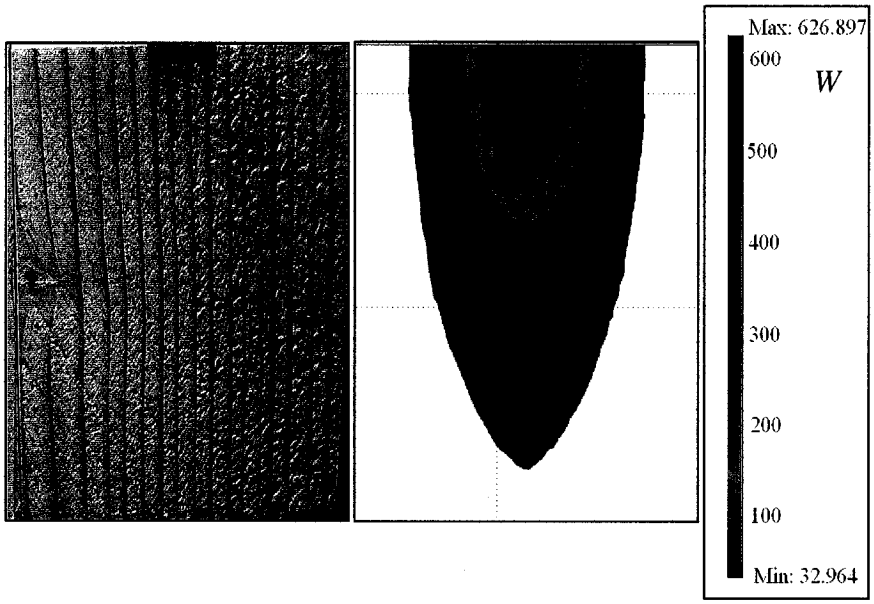

Figure 5.10. Left: The flow presents a preferential path through the latewood rings. Right: Isosurface concentration gradient.

The preferential path of the flow through the latewood rings can be explained easily. Latewood tracheids exhibit smaller lumens or cavities than the ones in earlywood. A smaller lumen would mean a higher capillary pressure; therefore, water penetrates further through this conduct. It is important to make the distinction between permeability and capillary pressure. Permeability is many times higher in earlywood than in latewood as shown in the work by Domec and Gartner for Douglas-fir (2002). The importance of the moisture profile has been recognized, since the moisture distribution in the wood can induce swelling creating strain gradients that can lead to cracking and warping (Plumb *et al*, 1985).

As we have seen, modeling of the water absorption is linked directly to the position of the wetting (boundary conditions), then it is necessary to have a better understanding of how water spreads in the surface of wood.

Chapter 6. Qualitative approach to study the actual water uptake behavior in softwoods

When a wooden element of a wood-framed house is subjected to liquid water contact because of rain penetration, modeling the process of water absorption is complex considering the boundary conditions would be dependent on the position of the wetting. When doing water uptake experiments to estimate diffusivities, the boundary conditions are very easily identifiable, since the sides are sealed to avoid any water penetration from each of the four vertical sides to force the flow to be unidirectional.

The objective of these tests was to observe the water spread in wooden elements assuming that the source of water was found at the bottom. Capillary forces are always present which makes the overall process more complex.

Before discussing the test, an introduction of the theory of wetting is presented. The main reference employed is the book of Pierre-Gilles de Gennes (de Gennes *et al*, 2004) about capillarity and wetting phenomena.

6.1. Introduction to wetting

We begin by reviewing the definition of capillarity. "Capillarity is the study of the interfaces between two immiscible liquids, or between a liquid and air. The interfaces are

deformable: they are free to change their shape in order to minimize their surface energy" (de Gennes *et al*, 2004).

Wetting refers to the study of how a liquid deposited on a solid (or liquid) substrate spreads out (de Gennes *et al*, 2004). It is useful in many industrial applications, for example, in the chemical industry for paints, ink and insecticides, in the automobile manufacturing for surface preparation prior to painting, in treatment of glass and treatment of tires to promote adhesion even on wet roads, and in construction, it is important for façade design, water proofing of concrete and protection of monuments. Regarding wood, the study of wetting phenomena on wood, i.e. the interactions of water and other liquids with wood, may add valuable information about the gluing and coating properties of wood (Wålinder, 2000).

A very important quantity in wettability is the surface tension of the liquid. The surface tension value might drop when there is contamination. It is useful to know about the wettability of materials when is required to protect building facades against graffiti and stains so they can be treated accordingly.

In the theory of wetting, a parameter called "the spreading parameter S", is used, which measures the difference in the surface energy (per unit area) of the substrate when dry and wet:

$$S = \left(E_{substrate}\right)_{dry} - \left(E_{substrate}\right)_{wet} \tag{6.1}$$

or

$$S = \gamma_{SO} - (\gamma_{SL} + \gamma) \tag{6.2}$$

where the three coefficients γ are the surface tensions at the solid/air, solid/liquid, and liquid/air interfaces, respectively.

If the parameter S is positive, the liquid will spread out completely in order to lower its surface energy, resulting in a contact angle equals to zero.

When the wetting of a surface takes place horizontally, it is important to know the contact area of the liquid and the substrate. In order to have an idea when the gravity becomes important for drops and when they are going to lose their spherical shape, it can be estimated by comparing the Laplace pressure γ / k^{-1} to the hydrostatic pressure $\rho \cdot g \cdot k^{1}$ that is suffered at a depth k^{-1} of a liquid of density ρ because of gravity. Then by equating these two pressures, it is possible to determine the capillary length (de Gennes *et al*, 2004):

$$\frac{\gamma}{k^{-1}} = \rho \cdot g \cdot k^{-1}$$
$$k^{-1} = \sqrt{\gamma / \rho \cdot g} \tag{6.3}$$

If we use this equation for the determination of the capillary length for water, we take the γ of water as 73×10^{-3}N/m, a value of 9.8 m/s^2 for the acceleration due to gravity and the density of water as 1000 kg/m^3. This results in a value of k^{-1} equal to 0.002729 m.

In the case of drops, gravity is negligible for sizes less than k^{-1}. For sizes above the capillary length, gravity effects dominate. The capillary length can also be seen as the screening length, meaning if one perturbs an initially horizontal liquid surface by placing on it a small floating object, the perturbation induced on the surface disappears in a distance k^{-1}, as shown in the figures below.

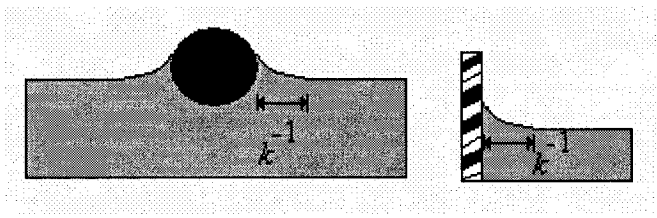

Figure 6.1. On the left a small floating object perturbs the surface of the liquid over a distance k^{-1}. On the right: the same perturbation effect is caused by the presence of a wall. Modified from de Gennes (de Gennes *et al*, 2004).

When the radius of a drop is less than the capillary radius, the capillary forces dominate and the spherical shape of the drop persists. This is explained by Laplace's equation, in which the curvature of the drop remains constant. The edges of the drops intersect the substrate at a contact angle θ_E.

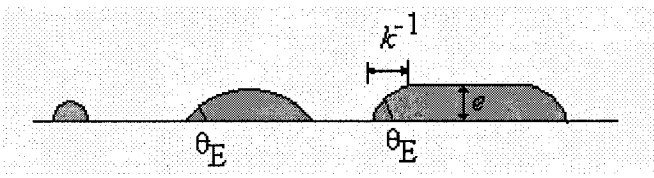

Figure 6.2. The sketch shows that when water drops increase in size on a horizontal surface, gravity cause the larger drops to flatten. Modified from de Gennes (de Gennes *et al*, 2004).

If the droplet has a radius larger than k^{-1}, gravitational effects dominates and the droplet will be flattened by its own weight. When the forces are at equilibrium, the flattened droplet will have a thickness *e*.

Using Young's law, describing the equilibrium of forces acting on the line of contact, then

$$\gamma \cdot (1 - \cos\theta_E) = \frac{1}{2}\rho \cdot g \cdot e^2 \tag{6.4}$$

Solving for *e* in the last equation, then:

$$e = 2k^{-1}\sin\left(\frac{\theta_E}{2}\right) \tag{6.5}$$

When the thickness of a drop is known on a surface, it is possible to calculate the area of wetting if a certain volume of a liquid is spilled in a surface. For example, let us say 5 liters of water is spilled and the contact angle on the edges of the puddle is 30 degrees, then

$$\begin{aligned} e &= 2 \cdot 0.002729 \sin\left(\frac{30}{2}\right) \\ e &= 0.0014126 \cdot \text{m} \end{aligned} \tag{6.6}$$

Since the volume of the puddle would be given by the wetted area and the thickness of the puddle, we have the wetted area A equal to $0.005\text{m}^3/0.0014126$ m = 3.549 m^2. The thickness of a puddle is of great importance if the volume entering building envelope components is known.

In the case in which we have a rising film with a porous medium, a contact angle θ_E can be defined at equilibrium. However, it is important to say that the definition of this contact angle remains an approximation for several reasons. The problems are that hysteresis can occur locally within the pores and air bubbles can be trapped during the capillary rise. Another situation is that porous media always have a random surface.

When a film rises in a porous medium, flow of the liquid towards the interior of the material will take place; this flow together with the weight of the film will control the height to which the fluid will rise in the walls of the porous medium.

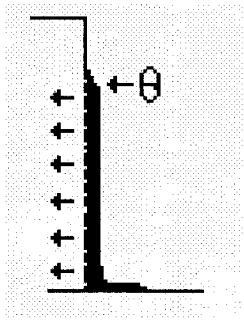

Figure 6.3. Sketch of a rising film on a porous material, the arrows indicate flux of liquid towards the inside of the porous material. Modified from de Gennes *et al* (2004).

6.1.1. Mechanisms of transport phenomena in wetting

For wetting, differences in the chemical composition of a surface will create changes in the surface tension that create forces that drag the liquid in a direction parallel to the substrate.

Even very small thermal gradients will cause drops to move. The movement will be towards the colder regions because a lower temperature increases the surface tension.

It is important to note that contamination of water by the presence of extractives at the wood-liquid interface generally results in a distinct decrease in the liquid surface tension (Wålinder, 2000).

Studies done about wetting parameters on wood such as contact angles, surface free energy and work of adhesion show that these parameters are influenced by surface roughness and heterogeneity. The capillary liquid transport may occur along tracheid channels in the surface and into the end grain cavities, pit openings and wood rays (Wålinder, 2000).

6.2. Test description and results

Wood samples having different fiber grain orientations were subjected to water uptake. The difference between this test and the water absorption tests presented in section 3.1, it is that the water flow was not forced to be unidirectional since the sides were not covered either with varnish or tape and the temperature of water was not controlled.

In addition, in order to visualize the water path, a commercially available ink was diluted in water. This has the advantage that when the wood sample dries, the water path remains visible. The drawbacks of the ink use are that it changes the surface tension of water, which will have an effect on the capillaries forming around the sample walls and change the normal viscosity of water.

Finally, the mass increase of the sample was not recorded during the test to minimize intrusion.

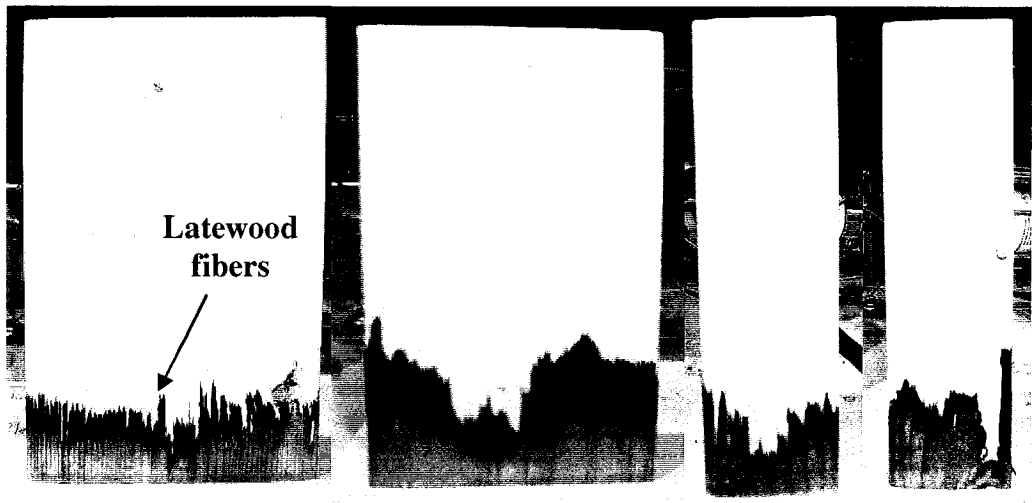

Figure 6.4. Water uptake in the longitudinal direction of the grain. The capillary height was different for each of the four vertical walls. The figure shows that the capillaries have affinities towards latewood fibers. The time of the absorption was 3 days.

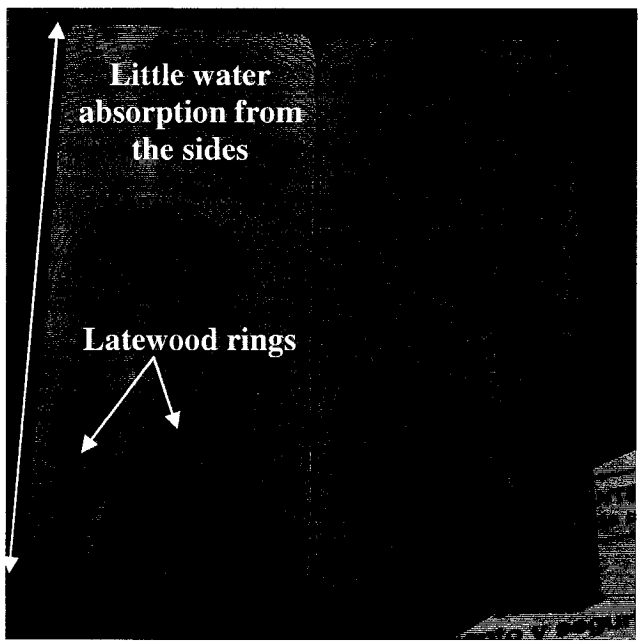

Figure 6.5. The photograph shows some slices of the specimen shown in Figure 6.3. The slice on the left corresponds to a position lower in the ground, thus closer to the water pool; the one on the right corresponds to a higher position. It is noticeable that there is little water absorption from the sides all around the edges. Again the preferential water absorption path corresponds to the latewood rings.

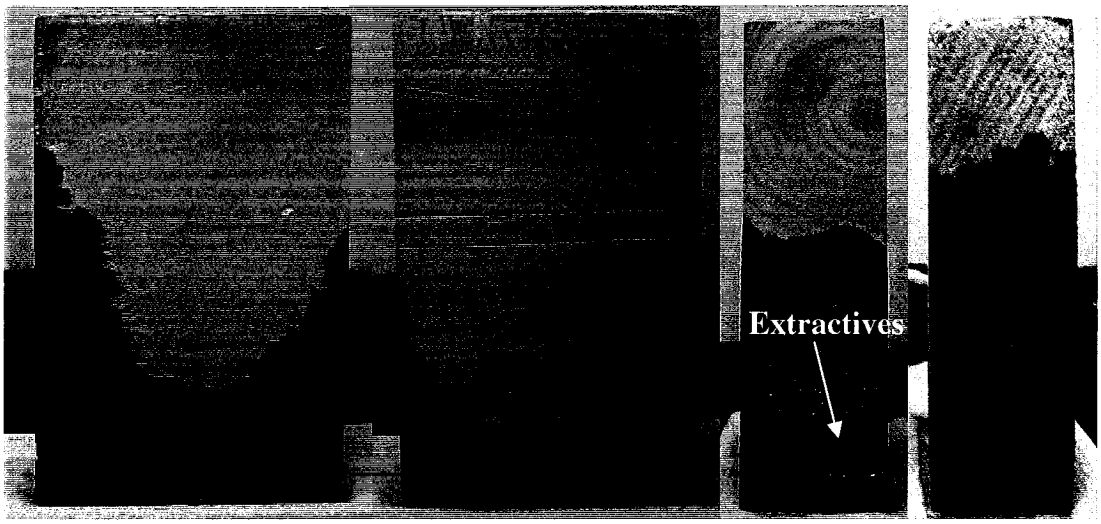

Figure 6.6. Water uptake in the radial direction of the grain. Pictures of the four vertical sides are shown. Absorption time: approximately 12 hours. It is interesting to note that the capillary rise around the walls of the samples was faster and higher than in the longitudinal case. On the figures at the right, some extractives have come out through the tracheids. Right after the water raised it started to enter through the sides as in shown in the next figure.

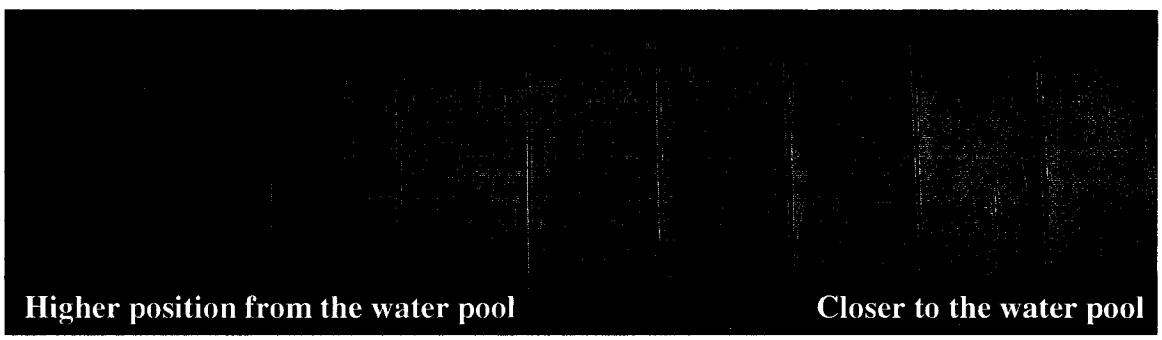

Figure 6.7. Sliced samples of the sample subjected to radial absorption. The water path was the following, first capillary rise around the walls then capillary absorption from the sides along the longitudinal fibers. It seems that the water gained is mainly due to the capillary rise from the sides instead from the water taken from the bottom boundary.

6.3 Discussion of results

The colored water test gives the opportunity of visualizing the water path taken in uncontrolled conditions of water uptake. The impact of the rising films around the walls of the specimens subjected to the water uptake is noticeable. This rise is controlled by the surface tension of the water, the contact angle of the wetting fluid, and the weight of the film itself and a portion of the risen film going towards the inside of the porous material.

Another observation is that the sample with the longitudinal orientation actually had less capillary rise from the sides than the ones along the radial direction even though the water absorption process lasted for a longer period. It is difficult to give an explanation for this when parameters such as surface roughness and surface tension are not quantified. However from touching the surfaces along the vertical sides, it seems that there was more roughness along the walls where the water rose higher.

Once again, the complexity of the wetting patterns observed clearly indicates that modeling a water uptake process considering just a constant boundary condition from the bottom of the sample represents an over simplification of the water imbibition process. However, modeling of the wetting process in its full intricacies would require more experimental work to describe all parameters involved. The ink pattern method is effective qualitatively.

Chapter 7. Conclusions

As we have seen throughout the present work, wood is a complicated building material to model for water movement and to study due to its high anisotropy and complexity of lumen network. However, good approximations of the water transport in liquid state within wood can be achieved by different means.

7.1. Contribution of the research

The contributions of this research are:

1. The measurement data of average water absorption coefficients along the three different orientations of the fibre grain for jack pine was provided. The results of water absorption coefficients are within the range for values of different species of softwoods.

2. Measurements data of the porosity of the jack pine through the use of helium pycnometry and the use of mercury intrusion to describe the poresize distributions was provided. The porosity values give an approximation of the maximum volume expected of impregnation of a fluid. The mercury intrusion data can be useful for the construction of models that use capillary pressure as a driving force. However, mercury intrusion measured data have different values for porosities compared to those given by pycnometry.

3. This thesis has shown the development of a simplified model for the simulation of the imbibition process of water in wood with constant diffusivities. The results have shown good agreement with the experimental data, particularly for long periods of water absorption. This means that taking w_c equal to the porosity multiplied by the density of water is a good approximation. It is interesting to mention that even though the diffusivities and boundary conditions were different, the results were very similar for simulations 1 and 2. The use of a variable diffusivity to simulate the water uptake process yielded slightly better results. However, the computation time was considerably longer, which reduces the practicality of this approach. It is expected as computers processors and numerical software improves this will not be a problem.

4. A qualitative method was presented. It was also use in a new point load test developed for validation of the model. The qualitative approach, although very simple, has given insight regarding the water absorption process. Wetting phenomena takes place along the four vertical sides, and it would be extremely useful for modeling to measure the thickness of the rising film, and its maximum height, wetted area, as well as to measure contact angles and the influence of the extractives on water surface tension.

Furthermore, a few observations are made on the modeling work. With respect to the sensitivity study on diffusivity using the equation of constant diffusivity, it is concluded that the only way of maintaining the same absorptivity coefficient while changing the diffusivity is to change the capillary saturation coefficient. The impact is reflected in a faster saturation time, but less water absorption since the capillary

saturation coefficient decreases inversely to an increase in the diffusivity according to equation (5.4).

While the model does not reproduce the complex anatomy of wood or the preferential moisture transport path, it may be an adequate approximation for building envelope applications.

Actual water liquid transport differed for early and latewood fibers, which makes the quantification of these diffusivities a must. By having these values, numerical models can be constructed. However, it does not seem practical from a building envelope point of view to have such specific values when the ratio of the latewood/earlywood is not known.

7.2. Recommendations for further work

Along the research work we have encountered various obstacles. Further work should be done in the following items:

1. It is known that, to model the water uptake of wood, it could be necessary to take into account the inertial effect present during the first two hours of the water absorption process. The impact of inertial effect should be studied in more detail.

2. The effect of the parameters sample size and shape on the water uptake process should be studied to see if there is a correlation between them and the water absorption coefficient.

3. Data regarding the dependency of liquid diffusivity on the water temperature should be measured thoroughly in order to use constant diffusivity models which rely on the determination of very accurate diffusivity values.

4. The pore size distribution of wood samples should be determined using a technique based on SEM together with mercury intrusion data for comparison purposes.

5. Models that use non Fickean diffusion represent an alternative to model the complex moisture transport.

In general, to study the moisture transport process in wood with a high resolution, it is necessary to use equipment such as NMR and X-ray to carry out less intrusive measurements and to have a better insight of the path water takes and to compute better diffusivity values.

References

Bear J, Bachmat Y 1990. Introduction to Modeling of Transport Phenomena in Porous Media. Kluwer Academic Publishers, Dordrecht, The Netherlands. 553 p.

Bird RB, Stewart WE, Lightfoot EN. 2002. Transport Phenomena. Second Edition. John Wiley & Sons, Inc. 895 p.

Carmeliet J, Hens H, Roels S, Adan O, Brocken H, Cerny R, Pavlik Z, Hall C, Kumaran, K, Pel L. Determination of the Liquid Water Diffusivity from Transient Moisture Transfer Experiments. Journal of Thermal Envelope and Building Science 2004, Vol. 7(4), pp. 277-306.

Celimene CC, Micales JA, Ferge L, Young RA. 1999. Efficacy of Pinosylvins against white-rot and brown-rot fungi. Holzforschung, Vol. 53, pp. 491-497.

Comstock 1969. Directional permeability of softwoods. 23rd Annual Meeting of the Forest Products Research Society at San Francisco, California, July 6-10.

de Gennes PG, Brochard-Wyart F, Quéré D. 2004. Capillarity and wetting phenomena. Drops, bubbles, pearls, waves. Springer-Verlag New York Inc. 291 p.

Darcy HPG. 1856. Les fontaines publiques de la ville de Dijon, Delmont, Paris, France.

Domec JC, Gartner BL. 2002. How do water transport and water storage differ in coniferous earlywood and latewood? Journal of Experimental Botany, Vol. 53, No. 379, pp 2369-2379.

Dow JO. 1999. A Unified Approach to the Finite Element Method and Error Analysis Procedures. University of Colorado. Academic Press, p. 533.

Durner W. 1994. Hydraulic connectivity estimation for soils with heterogeneous pore structure. Water Resources Research, Vol. 30, pp. 221-223.

Comsol 2004. Femlab 3 Users Guide.

Gerardin V. 1980. L'inventaire du capital-nature du territoire de la Baie-James: les regions écologiques et la vegetation des sols minéraux. Environment Canada, Ottawa.

Haygreen JG, Bowyer JL. 1996. Forest products and wood science. An introduction. Third Edition. Iowa State University Press/Ames, Iowa. 484 p.

Hoadley, R. B. 1990. Identifying Wood. Accurate results with simple tools. The Tauton Press. 224 p.

Huang Y. 2003. An Engineering approximation of material characteristics for input to heat, air and moisture transport model simulations. PhD thesis. Department of Building, Civil and Environmental Engineering, Concordia University, Montreal, Quebec, Canada.

Koch P. 1972. Utilization of the southern Pines. I the raw material. U.S. Department of Agriculture-Forest Service. 734 p.

Koch P. 1985. Utilization of hardwoods growing on southern pine sites. Vol. I. The raw material. USDA Agric. Handbook No. 605. U.S. Govt. Print. Off. Washington, DC.

Kollmann FFP, Côté WA. 2003. Principles of wood science and technology. Part I. Solid wood. Reprinted by CBLS, New Delhi, India (Previous copyright holder: Springer-Verlag, Berlin, Heidelberg, 1968), 592 p.

Kornev KG, Neimark AV. 2001. Spontaneous penetration of liquids in to capillaries and porous membranes revisited. Journal of Colloid and Interface Science, Vol. 235, pp. 101-113.

Krus M. 1996. Moisture Transport and Storage Coefficients of Porous Mineral Building Materials. Theoretical Principles and New Test Methods. Fraunhofer IRB Verlag, .

Krus M, Künzel HM. 1993. Determination of Dw from A-value. IEA Annex XXIV report T3-D-93/02.

Kumaran M.K. 1999. Moisture diffusivity of Building materials from water absorption measurements. Journal of Thermal Envelope and Building Science, Vol. 22, pp. 349-355.

Kumaran MK, Bomberg MT. 1985. A gamma-ray spectrometer for determination of density distribution and moisture distribution in building materials. Proceedings of the International Symposium on Moisture and Humidity, pp. 485-490.

Kumaran MK, Lackey JC, Normandin N, Tariku F, van Reenen D. 2002. A Thermal and Moisture Transport Property Database for Common Building and Insulating Materials. Final Report from ASHRAE Research Project 1018-RP

Le Goff H, Sirois L. 2004. Black spruce and jack pine dynamics simulated under varying fire cycles in the northern boreal forest of Quebec, Canada. Canadian Journal of Forest Research, Vol. 34, pp. 2399-2409. NRC Research Press.

Micromeritics. 2001. ACCUPYC 1330 TC. Operators's Manual V. 3.03

Mukhopadhyaya. P, Kumaran K, Normandin N, Goudreau P. 2002. Effect of surface temperature on water absorption coefficient of building materials. Journal of Thermal Envelope and Building Science, Vol. 26(2), pp. 179-195.

O'Brien TP, McCully ME. 1981. The study of plant structure: principles and selected methods. Termacarphi Pth, Ltd., Melbourne.

Pel L. 1995. Moisture Transport in Porous Building Materials. Doctoral Thesis; Eindhoven University of Technology, Eindhoven, The Netherlands, 127 p.

Perré P. 2000. Fundamental aspects of fluid migration in beech. Cost Action E15. Advances in Drying of wood (1999-2003) 2nd Workshop "Quality drying of hardwood" in Sopron (September 2000)

Perré P. 2003. The role of wood anatomy in the drying of wood : « great oaks from little acorns grow ». 8th International IUFRO Wood Drying Conference, pp. 11-25.

Perré. P. 1994. The importance of wood anatomy to drying behavior: Examples based on convective microwave and vacuum drying. 4th IUFRO International Conference on Wood Drying Rotorua, New Zealand, pp. 55-62.

Plumb OA, Spolek GA, Olmstead, BA. 1985. Heat and mass transfer in wood during drying. International Journal of Heat and Mass Transfer, Vol. 28, pp. 1669-1678.

Roels, S. 2000. Modelling unsaturated moisture transport in heterogeneous limestone. Ph.D. thesis. Laboratory of Building Physics, Katholieke Universiteit Leuven, Leuven, Belgium, 211 p.

Rosenkilde A. 2002. Moisture content profiles and surface phenomena during drying of wood. Doctoral Thesis, KTH-Royal Institute of Technology, Stockholm, Sweden, 36 p.

Siau JF. 1984. Transport Processes in Wood. Springer-Verlag. Springer Series in Wood Science. p. 245

Spolek and Plumb 1981. Capillary pressure in softwoods. Wood Science Technology, Vol. 15, pp. 189-199.

Trenard Y. 1980. Comparaison et interpretation de courbes obtenues par porosimétrie au Mercure. Holzforschung, Vol. 34, pp. 139-146.

Tsoumis G. 1991. Science and Technology of wood. Structure, Properties, Utilization. Van Nostrand Reinhold. New York, New York. 494 p.

Valli A, Koponen A, Vesala T, Timonen J. 2002. Simulations of Water Flow through bordered pits of Conifer Xylem. Journal of Statistical Physics, Vol. 107, Nos. 1/2. pp. 121-142.

Van Genuchten MT. 1980. A closed-form equation for predicting the hydraulic conductivity of unsaturated soils. Soil Science Society of America Journal, Vol. 44, pp. 892-898.

Webb PA. 1993. Poresizer 9320 and AutoPore II 9220. Datacollection, reduction and presentation. Micromeritics. International Sales Support Document, April 1993.

Wålinder M. 2000. Wetting Phenomena on Wood. Factors influencing measurements of wood wettability. Doctoral thesis. KTH-Royal Institute of Technology, Stockholm, Sweden, 62 p.

Fraunhofer Institut für Bauphysik. 2005. WUFI 2D help document.

Zimmerman MH. 1983. Xylem Structure and the Ascent of Sap. Springer-Verlag, 143 p.

Zimmerman MH, Brown CL. 1971. Trees. Structure and function. Springer. New York Heidelberg Berlin 336 p.

Appendix A Water absorption tables for samples

A.1. Raw Data for Sample A1

Mass [g]	Time[s] Step	Cumulative time [s]	Sqroot(t) [$s^{1/2}$]	Moisture Mass [g]	CMG [g]
34.47	0	0	0.00	0	0
35.59	80	80	8.94	1.12	1.12
35.90	92	172	13.11	0.31	1.43
36.15	144	316	17.78	0.25	1.68
36.37	169	485	22.02	0.22	1.90
36.57	222	707	26.59	0.20	2.10
36.81	335	1,042	32.28	0.24	2.34
37.02	480	1,522	39.01	0.21	2.55
37.23	600	2,122	46.07	0.21	2.76
37.48	900	3,022	54.97	0.25	3.01
37.93	2,354	5,376	73.32	0.45	3.46
38.42	3,720	9,096	95.37	0.49	3.95
39.09	7,080	16,176	127.18	0.67	4.62
42.01	63,390	79,566	282.07	2.92	7.54
42.29	9,440	89,006	298.34	0.28	7.82
42.64	11,770	100,776	317.45	0.35	8.17
42.86	6,870	107,646	328.09	0.22	8.39
44.69	69,930	177,576	421.40	1.83	10.22
48.14	162,060	339,636	582.78	3.45	13.67
48.64	23,708	363,344	602.78	0.50	14.17
49.84	63,712	427,056	653.50	1.20	15.37
49.91	5,620	432,676	657.78	0.07	15.44
50.12	16,160	448,836	669.95	0.21	15.65
51.14	64,020	512,856	716.14	1.02	16.67
51.58	26,820	539,676	734.63	0.44	17.11
52.47	59,220	598,896	773.88	0.89	18.00
52.79	22,610	621,506	788.36	0.32	18.32
53.73	64,510	686,016	828.26	0.94	19.26
53.88	11,540	697,556	835.20	0.15	19.41
54.00	8,080	705,636	840.02	0.12	19.53
56.86	238,435	944,071	971.63	2.86	22.39
57.12	24,395	968,466	984.11	0.26	22.65
57.94	64,410	1,032,876	1,016.31	0.82	23.47
58.22	22,260	1,055,136	1,027.20	0.28	23.75
58.98	64,730	1,119,866	1,058.24	0.76	24.51
60.02	87,730	1,207,596	1,098.91	1.04	25.55
60.89	83,370	1,290,966	1,136.21	0.87	26.42
63.46	262,050	1,553,016	1,246.20	2.57	28.99
64.18	87,120	1,640,136	1,280.68	0.72	29.71
64.90	97,840	1,737,976	1,318.32	0.72	30.43
66.94	156,560	1,894,536	1,376.42	2.04	32.47
67.53	258,960	2,153,496	1,467.48	0.59	33.06

68.16	105,220	2,258,716	1,502.90	0.63	33.69
68.74	81,900	2,340,616	1,529.91	0.58	34.27
69.25	89,160	2,429,776	1,558.77	0.51	34.78
69.72	73,040	2,502,816	1,582.03	0.47	35.25
71.02	260,009	2,762,825	1,662.17	1.30	36.55

A.2. Raw Data for Sample B1

Mass [g]	Time Step [s]	Cumulative time[s]	Sqroot(t)[$s^{1/2}$]	Moisture Mass [g]	CMG [g]
33.70	0	0	0.00	0.00	0.00
35.30	57	57	7.55	1.60	1.60
35.63	108	165	12.85	0.33	1.93
35.97	158	323	17.97	0.34	2.27
36.21	144	467	21.61	0.24	2.51
36.43	209	676	26.00	0.22	2.73
36.75	344	1,020	31.94	0.32	3.05
37.07	454	1,474	38.39	0.32	3.37
37.36	600	2,074	45.54	0.29	3.66
37.77	900	2,974	54.53	0.41	4.07
38.45	2,354	5,328	72.99	0.68	4.75
39.22	3,720	9,048	95.12	0.77	5.52
40.29	7,080	16,128	127.00	1.07	6.59
44.60	63,419	79,547	282.04	4.31	10.90
45.00	9,440	88,987	298.31	0.40	11.30
45.52	11,770	100,757	317.42	0.52	11.82
45.77	6,840	107,597	328.02	0.25	12.07
48.18	69,900	177,497	421.30	2.41	14.48
52.36	162,120	339,617	582.77	4.18	18.66
52.89	15,382	354,999	595.82	0.53	19.19
54.17	63,758	418,757	647.11	1.28	20.47
54.27	5,580	424,337	651.41	0.10	20.57
54.49	16,170	440,507	663.71	0.22	20.79
55.49	64,050	504,557	710.32	1.00	21.79
55.91	26,820	531,377	728.96	0.42	22.21
56.79	59,190	590,567	768.48	0.88	23.09
57.10	22,650	613,217	783.08	0.31	23.40
58.08	64,470	677,687	823.22	0.98	24.38
58.21	11,562	689,249	830.21	0.13	24.51
58.34	8,388	697,637	835.25	0.13	24.64
61.10	238,110	935,747	967.34	2.76	27.40
61.33	24,390	960,137	979.87	0.23	27.63
62.10	64,360	1,024,497	1,012.17	0.77	28.40
62.30	22,280	1,046,777	1,023.12	0.20	28.60
63.11	64,770	1,111,547	1,054.30	0.81	29.41
64.13	87,670	1,199,217	1,095.09	1.02	30.43
65.09	83,390	1,282,607	1,132.52	0.96	31.39

68.46	262,050	1,544,657	1,242.84	3.37	34.76
69.40	87,120	1,631,777	1,277.41	0.94	35.70
70.48	97,850	1,729,627	1,315.15	1.08	36.78
72.10	156,530	1,886,157	1,373.37	1.62	38.40
74.88	258,950	2,145,107	1,464.62	2.78	41.18
76.04	105,270	2,250,377	1,500.13	1.16	42.34
77.10	83,220	2,333,597	1,527.61	1.06	43.40
78.11	89,190	2,422,787	1,556.53	1.01	44.41
78.90	73,020	2,495,807	1,579.81	0.79	45.20
81.08	259,978	2,755,785	1,660.06	2.18	47.38

A.3. Raw Data for Sample C1

Mass [g]	Time Step [s]	Cumulative time[s]	Sqroot(t)[$s^{1/2}$]	Moisture Mass [g]	CMG [g]
32.88	0	0	0.00	0	0
34.28	60	60	7.75	1.40	1.40
34.48	50	110	10.49	0.20	1.60
34.68	73	183	13.53	0.20	1.80
34.92	117	300	17.32	0.24	2.04
35.23	205	505	22.47	0.31	2.35
35.61	337	842	29.02	0.38	2.73
35.90	517	1,359	36.86	0.29	3.02
36.24	600	1,959	44.26	0.34	3.36
36.61	900	2,859	53.47	0.37	3.73
37.26	2,400	5,259	72.52	0.65	4.38
37.50	1,200	6,459	80.37	0.24	4.62
38.73	9,060	15,519	124.58	1.23	5.85
42.24	63,950	79,469	281.90	3.51	9.36
42.52	9,370	88,839	298.06	0.28	9.64
42.93	11,820	100,659	317.27	0.41	10.05
43.15	6,810	107,469	327.82	0.22	10.27
45.08	69,990	177,459	421.26	1.93	12.20
48.46	161,940	339,399	582.58	3.38	15.58
48.88	23,708	363,107	602.58	0.42	16.00
49.97	63,832	426,939	653.41	1.09	17.09
50.05	5,580	432,519	657.66	0.08	17.17
50.22	16,140	448,659	669.82	0.17	17.34
51.04	64,080	512,739	716.06	0.82	18.16
51.39	26,820	539,559	734.55	0.35	18.51
52.15	59,160	598,719	773.77	0.76	19.27
52.38	22,650	621,369	788.27	0.23	19.50
53.17	64,470	685,839	828.15	0.79	20.29
53.31	11,580	697,419	835.12	0.14	20.43
53.41	8,100	705,519	839.95	0.10	20.53
55.80	238,380	943,899	971.54	2.39	22.92
55.99	24,420	968,319	984.03	0.19	23.11
56.76	64,390	1,032,709	1,016.22	0.77	23.88

56.92	22,280	1,054,989	1,027.13	0.16	24.04
57.64	64,800	1,119,789	1,058.20	0.72	24.76
58.52	87,640	1,207,429	1,098.83	0.88	25.64
59.38	83,390	1,290,819	1,136.14	0.86	26.50
62.12	262,050	1,552,869	1,246.14	2.74	29.24
62.86	87,150	1,640,019	1,280.63	0.74	29.98
63.73	97,820	1,737,839	1,318.27	0.87	30.85
65.02	156,550	1,894,389	1,376.37	1.29	32.14
67.10	258,980	2,153,369	1,467.44	2.08	34.22
67.86	105,220	2,258,589	1,502.86	0.76	34.98
68.56	83,230	2,341,819	1,530.30	0.70	35.68
69.26	89,220	2,431,039	1,559.18	0.70	36.38
69.79	72,980	2,504,019	1,582.41	0.53	36.91
71.24	259,961	2,763,980	1,662.52	1.45	38.36

A.4. Raw Data for Sample D1

Mass [g]	Time Step [s]	Cumulative time[s]	Sqroot(t)[$s^{1/2}$]	Moisture Mass [g]	CMG [g]
30.93	0	0	0.00	0.00	0.00
32.19	80	80	8.94	1.26	1.26
32.43	87	167	12.92	0.24	1.50
32.68	125	292	17.09	0.25	1.75
32.98	218	510	22.58	0.30	2.05
33.24	316	826	28.74	0.26	2.31
33.54	600	1,426	37.76	0.30	2.61
33.89	900	2,326	48.23	0.35	2.96
34.16	1,080	3,406	58.36	0.27	3.23
34.44	1,440	4,846	69.61	0.28	3.51
34.85	2,520	7,366	85.83	0.41	3.92
35.29	3,600	10,966	104.72	0.44	4.36
35.95	7,740	18,706	136.77	0.66	5.02
38.74	60,530	79,236	281.49	2.79	7.81
39.10	9,400	88,636	297.72	0.36	8.17
39.51	11,850	100,486	317.00	0.41	8.58
39.70	6,770	107,256	327.50	0.19	8.77
41.49	69,850	177,106	420.84	1.79	10.56
44.74	162,060	339,166	582.38	3.25	13.81
45.24	23,590	362,756	602.29	0.50	14.31
46.36	63,830	426,586	653.14	1.12	15.43
46.44	5,550	432,136	657.37	0.08	15.51
46.65	16,170	448,306	669.56	0.21	15.72
47.66	64,080	512,386	715.81	1.01	16.73
48.05	26,820	539,206	734.31	0.39	17.12
48.96	59,130	598,336	773.52	0.91	18.03
49.26	22,650	620,986	788.03	0.30	18.33
50.21	64,470	685,456	827.92	0.95	19.28
50.40	11,572	697,028	834.88	0.19	19.47

50.49	8,138	705,166	839.74	0.09	19.56
53.28	238,350	943,516	971.35	2.79	22.35
53.54	24,420	967,936	983.84	0.26	22.61
54.42	64,410	1,032,346	1016.04	0.88	23.49
54.67	22,260	1,054,606	1026.94	0.25	23.74
55.50	64,800	1,119,406	1058.02	0.83	24.57
56.61	87,640	1,207,046	1098.66	1.11	25.68
57.59	83,400	1,290,446	1135.98	0.98	26.66
60.65	262,040	1,552,486	1245.99	3.06	29.72
61.45	87,170	1,639,656	1280.49	0.80	30.52
62.38	97,800	1,737,456	1318.13	0.93	31.45
63.60	156,540	1,893,996	1376.23	1.22	32.67
65.50	257,880	2,151,876	1466.93	1.90	34.57
66.19	105,210	2,257,086	1502.36	0.69	35.26
66.86	83,230	2,340,316	1529.81	0.67	35.93
67.52	89,210	2,429,526	1558.69	0.66	36.59
68.05	73,000	2,502,526	1581.94	0.53	37.12
69.44	259,977	2,762,503	1662.08	1.39	38.51

A.5. Raw Data for Sample E1

Mass [g]	Time Step [s]	Cumulative time[s]	Sqroot(t)[$s^{1/2}$]	Moisture Mass [g]	CMG [g]
45.58	0	0	0.00	0.00	0.00
46.33	78	78	8.83	0.75	0.75
46.85	106	184	13.56	0.52	1.27
47.07	156	340	18.44	0.22	1.49
47.31	240	580	24.08	0.24	1.73
47.65	472	1,052	32.43	0.34	2.07
48.04	1,029	2,081	45.62	0.39	2.46
48.27	900	2,981	54.60	0.23	2.69
48.54	1,500	4,481	66.94	0.27	2.96
48.86	2,400	6,881	82.95	0.32	3.28
49.32	4,020	10,901	104.41	0.46	3.74
49.87	7,740	18,641	136.53	0.55	4.29
52.49	60,930	79,571	282.08	2.62	6.91
52.74	7,232	86,803	294.62	0.25	7.16
53.14	11,730	98,533	313.90	0.40	7.56
53.30	6,740	105,273	324.46	0.16	7.72
55.17	70,060	175,333	418.73	1.87	9.59
58.35	162,060	337,393	580.86	3.18	12.77
58.83	23,560	360,953	600.79	0.48	13.25
59.88	63,830	424,783	651.75	1.05	14.30
59.92	5,550	430,333	656.00	0.04	14.34
60.14	16,200	446,533	668.23	0.22	14.56
60.97	64,080	510,613	714.57	0.83	15.39
61.33	26,820	537,433	733.10	0.36	15.75
62.04	59,120	596,553	772.37	0.71	16.46

62.31	22,630	619,183	786.88	0.27	16.73
63.02	64,470	683,653	826.83	0.71	17.44
63.15	11,575	695,228	833.80	0.13	17.57
63.21	8,165	703,393	838.69	0.06	17.63
65.30	238,320	941,713	970.42	2.09	19.72
65.48	24,420	966,133	982.92	0.18	19.90
66.07	64,410	1,030,543	1,015.16	0.59	20.49
66.20	22,240	1,052,783	1,026.05	0.13	20.62
66.71	64,850	1,117,633	1,057.18	0.51	21.13
67.34	87,600	1,205,233	1,097.83	0.63	21.76
67.86	83,430	1,288,663	1,135.19	0.52	22.28
69.38	262,020	1,550,683	1,245.26	1.52	23.80
69.72	87,190	1,637,873	1,279.79	0.34	24.14
70.16	97,820	1,735,693	1,317.46	0.44	24.58
70.75	97,820	1,833,513	1,354.07	0.59	25.17
71.79	258,990	2,092,503	1,446.55	1.04	26.21
72.14	105,210	2,197,713	1,482.47	0.35	26.56
72.47	83,250	2,280,963	1,510.29	0.33	26.89
72.80	89,240	2,370,203	1,539.55	0.33	27.22
73.10	72,950	2,443,153	1,563.06	0.30	27.52
73.88	259,980	2,703,133	1,644.12	0.78	28.30

A.6. Raw Data for Sample F1

Mass [g]	Time Step [s]	Cumulative time[s]	Sqroot(t)[$s^{1/2}$]	Moisture Mass [g]	CWG [g]
40.31	0	0	0.00	0.00	0.00
41.83	60	60	7.75	1.52	1.52
42.18	120	180	13.42	0.35	1.87
42.39	115	295	17.18	0.21	2.08
42.66	180	475	21.79	0.27	2.35
42.99	300	775	27.84	0.33	2.68
43.29	420	1,195	34.57	0.30	2.98
43.64	600	1,795	42.37	0.35	3.33
44.01	900	2,695	51.91	0.37	3.70
44.45	1,480	4,175	64.61	0.44	4.14
45.01	2,520	6,695	81.82	0.56	4.70
45.57	3,240	9,935	99.67	0.56	5.26
46.56	8,520	18,455	135.85	0.99	6.25
50.00	60,914	79,369	281.73	3.44	9.69
50.33	9,146	88,515	297.51	0.33	10.02
50.76	11,720	100,235	316.60	0.43	10.45
50.99	6,695	106,930	327.00	0.23	10.68
53.11	70,105	177,035	420.76	2.12	12.80
56.87	162,060	339,095	582.32	3.76	16.56
57.38	23,519	362,614	602.17	0.51	17.07
58.52	63,841	426,455	653.04	1.14	18.21
58.65	5,550	432,005	657.27	0.13	18.34

58.87	16,230	448,235	669.50	0.22	18.56
59.90	64,080	512,315	715.76	1.03	19.59
60.31	26,820	539,135	734.26	0.41	20.00
61.12	59,090	598,225	773.45	0.81	20.81
61.47	22,630	620,855	787.94	0.35	21.16
62.34	64,470	685,325	827.84	0.87	22.03
62.49	11,580	696,905	834.81	0.15	22.18
62.58	8,190	705,095	839.70	0.09	22.27
65.19	238,290	943,385	971.28	2.61	24.88
65.38	24,420	967,805	983.77	0.19	25.07
66.08	64,410	1,032,215	1,015.98	0.70	25.77
66.23	2,240	1,034,455	1,017.08	0.15	25.92
66.94	64,850	1,099,305	1,048.48	0.71	26.63
67.82	87,600	1,186,905	1,089.45	0.88	27.51
68.64	83,430	1,270,335	1,127.09	0.82	28.33
71.19	262,005	1,532,340	1,237.88	2.55	30.88
71.78	87,225	1,619,565	1,272.62	0.59	31.47
72.56	97,800	1,717,365	1,310.48	0.78	32.25
73.71	156,510	1,873,875	1,368.90	1.15	33.40
75.71	259,020	2,132,895	1,460.44	2.00	35.40
76.44	105,180	2,238,075	1,496.02	0.73	36.13
77.12	83,250	2,321,325	1,523.59	0.68	36.81
77.85	89,260	2,410,585	1,552.61	0.73	37.54
78.36	72,930	2,483,515	1,575.92	0.51	38.05
79.92	259,970	2,743,485	1,656.35	1.56	39.61

A.7. Raw Data for Sample A2

Mass [g]	Time Step [s]	Cumulative time[s]	Sqroot(t)[$s^{1/2}$]	Moisture Mass [g]	CMG [g]
37.02	0	0	0.00	0.00	0
37.14	60	60	7.75	0.12	0.12
37.16	130	190	13.78	0.02	0.14
37.23	180	370	19.24	0.07	0.21
37.29	240	610	24.70	0.06	0.27
37.34	300	910	30.17	0.05	0.32
37.38	280	1,190	34.50	0.04	0.36
37.42	410	1,600	40.00	0.04	0.40
37.46	430	2,030	45.06	0.04	0.44
37.49	615	2,645	51.43	0.03	0.47
37.55	705	3,350	57.88	0.06	0.53
37.59	900	4,250	65.19	0.04	0.57
37.66	1,170	5,420	73.62	0.07	0.64
37.72	2,410	7,830	88.49	0.06	0.70
37.88	3,560	11,390	106.72	0.16	0.86
38.02	7,200	18,590	136.35	0.14	1.00
38.17	6,600	25,190	158.71	0.15	1.15
38.86	60,050	85,240	291.96	0.69	1.84

39.04	25,030	110,270	332.07	0.18	2.02
39.45	57,660	167,930	409.79	0.41	2.43
39.62	25,430	193,360	439.73	0.17	2.60
40.23	59,980	253,340	503.33	0.61	3.21
40.50	30,150	283,490	532.44	0.27	3.48
41.01	57,180	340,670	583.67	0.51	3.99
41.10	9,390	350,060	591.66	0.09	4.08
42.63	249,250	599,310	774.15	1.53	5.61
42.76	27,080	626,390	791.45	0.13	5.74
43.38	81,120	707,510	841.14	0.62	6.36
45.06	258,020	965,530	982.61	1.68	8.04
46.92	327,760	1,293,290	1,137.23	1.86	9.90
47.34	188,820	1,482,110	1,217.42	0.42	10.32

A.8. Raw Data for Sample B2

Mass [g]	Time Step [s]	Cumulative time[s]	Sqroot(t)[$s^{1/2}$]	Moisture Mass [g]	CMG [g]
33.11	0	0	0.00	0	0
33.19	60	60	7.75	0.08	0.08
33.21	130	190	13.78	0.02	0.10
33.24	180	370	19.24	0.03	0.13
33.27	260	630	25.10	0.03	0.16
33.30	298	928	30.46	0.03	0.19
33.32	310	1,238	35.19	0.02	0.21
33.34	487	1,725	41.53	0.02	0.23
33.38	353	2,078	45.59	0.04	0.27
33.41	600	2,678	51.75	0.03	0.30
33.46	690	3,368	58.03	0.05	0.35
33.48	930	4,298	65.56	0.02	0.37
33.53	1,200	5,498	74.15	0.05	0.42
33.58	2,340	7,838	88.53	0.05	0.47
33.68	3,600	11,438	106.95	0.10	0.57
33.81	7,200	18,638	136.52	0.13	0.70
33.91	6,600	25,238	158.86	0.10	0.80
34.49	60,030	85,268	292.01	0.58	1.38
34.63	25,010	110,278	332.08	0.14	1.52
34.87	57,700	167,978	409.85	0.24	1.76
34.97	25,440	193,418	439.79	0.10	1.86
35.18	59,970	253,388	503.38	0.21	2.07
35.25	30,120	283,508	532.45	0.07	2.14
35.41	57,200	340,708	583.70	0.16	2.30
35.45	9,400	350,108	591.70	0.04	2.34
35.94	249,220	599,328	774.16	0.49	2.83
35.95	27,110	626,438	791.48	0.01	2.84
36.05	81,100	707,538	841.15	0.10	2.94
36.32	259,160	966,698	983.21	0.27	3.21
36.69	326,600	1,293,298	1,137.23	0.37	3.58
36.85	188,830	1,482,128	1,217.43	0.16	3.74

A.9. Raw Data for Sample C2

Mass [g]	Time Step [s]	Cumulative time[s]	Sqroot(t)[$s^{1/2}$]	Moisture Mass [g]	CWG [g]
31.33	0	0	0.00	0	0
31.37	60	60	7.75	0.04	0.04
31.40	120	180	13.42	0.03	0.07
31.41	180	360	18.97	0.01	0.08
31.48	200	560	23.66	0.07	0.15
31.53	320	880	29.66	0.05	0.20
31.56	320	1,200	34.64	0.03	0.23
31.59	330	1,530	39.12	0.03	0.26
31.61	480	2,010	44.83	0.02	0.28
31.67	630	2,640	51.38	0.06	0.34
31.74	1,200	3,840	61.97	0.07	0.41
31.80	1,590	5,430	73.69	0.06	0.47
31.87	2,340	7,770	88.15	0.07	0.54
31.98	3,630	11,400	106.77	0.11	0.65
32.12	7,200	18,600	136.38	0.14	0.79
32.23	6,570	25,170	158.65	0.11	0.90
32.84	60,040	85,210	291.91	0.61	1.51
33.01	25,010	110,220	331.99	0.17	1.68
33.34	57,740	167,960	409.83	0.33	2.01
33.45	25,390	193,350	439.72	0.11	2.12
33.70	59,970	253,320	503.31	0.25	2.37
33.81	30,120	283,440	532.39	0.11	2.48
34.02	57,190	340,630	583.64	0.21	2.69
34.07	9,410	350,040	591.64	0.05	2.74
34.86	249,240	599,280	774.13	0.79	3.53
34.93	27,090	626,370	791.44	0.07	3.60
35.14	81,120	707,490	841.12	0.21	3.81
35.80	258,000	965,490	982.59	0.66	4.47
37.01	327,750	1,293,240	1,137.21	1.21	5.68
37.60	188,850	1,482,090	1,217.41	0.59	6.27

A.10. Raw Data for Sample D2

Mass [g]	Time Step [s]	Cumulative time[s]	Sqroot(t)[$s^{1/2}$]	Moisture Mass [g]	CMG [g]
41.56	0	0	0.00	0	0
41.66	60	60	7.75	0.10	0.10
41.68	120	180	13.42	0.02	0.12
41.75	180	360	18.97	0.07	0.19
41.79	180	540	23.24	0.04	0.23
41.89	400	940	30.66	0.10	0.33
41.91	250	1,190	34.50	0.02	0.35
41.97	350	1,540	39.24	0.06	0.41
42.00	480	2,020	44.94	0.03	0.44

42.08	660	2,680	51.77	0.08	0.52
42.16	1,000	3,680	60.66	0.08	0.60
42.25	1,760	5,440	73.76	0.09	0.69
42.32	2,040	7,480	86.49	0.07	0.76
42.43	3,630	11,110	105.40	0.11	0.87
42.60	7,200	18,310	135.31	0.17	1.04
42.70	6,570	24,880	157.73	0.10	1.14
43.33	60,050	84,930	291.43	0.63	1.77
43.50	25,000	109,930	331.56	0.17	1.94
43.80	57,750	167,680	409.49	0.30	2.24
43.93	25,380	193,060	439.39	0.13	2.37
44.18	59,970	253,030	503.02	0.25	2.62
44.29	30,150	283,180	532.15	0.11	2.73
44.54	57,180	340,360	583.40	0.25	2.98
44.60	9,390	349,750	591.40	0.06	3.04
45.40	249,240	598,990	773.94	0.80	3.84
45.45	27,090	626,080	791.25	0.05	3.89
45.62	81,120	707,200	840.95	0.17	4.06
46.04	257,990	965,190	982.44	0.42	4.48
46.62	327,760	1,292,950	1,137.08	0.58	5.06
46.96	188,820	1,481,770	1,217.28	0.34	5.40

A.11. Raw Data for Sample E2

Mass [g]	Time Step [s]	Cumulative time[s]	Sqroot(t)[$s^{1/2}$]	Moisture Mass [g]	CMG [g]
32.36	0	0	0.00	0	0
33.17	60	60	7.75	0.81	0.81
33.45	120	180	13.42	0.28	1.09
33.74	180	360	18.97	0.29	1.38
33.95	240	600	24.49	0.21	1.59
34.36	800	1,400	37.42	0.41	2.00
34.48	370	1,770	42.07	0.12	2.12
34.61	570	2,340	48.37	0.13	2.25
34.79	780	3,120	55.86	0.18	2.43
35.07	1,860	4,980	70.57	0.28	2.71
35.49	3,600	8,580	92.63	0.42	3.13
36.07	7,200	15,780	125.62	0.58	3.71
36.61	7,410	23,190	152.28	0.54	4.25
39.14	60,030	83,220	288.48	2.53	6.78
39.84	24,960	108,180	328.91	0.70	7.48
41.18	57,750	165,930	407.35	1.34	8.82
41.71	25,380	191,310	437.39	0.53	9.35
42.86	59,970	251,280	501.28	1.15	10.50
43.42	30,150	281,430	530.50	0.56	11.06
44.38	57,180	338,610	581.90	0.96	12.02
44.54	9,390	348,000	589.92	0.16	12.18
47.89	249,260	597,260	772.83	3.35	15.53

48.17	27,070	624,330	790.15	0.28	15.81
49.03	81,120	705,450	839.91	0.86	16.67
51.27	257,990	963,440	981.55	2.24	18.91
54.22	327,760	1,291,200	1,136.31	2.95	21.86
55.66	188,820	1,480,020	1,216.56	1.44	23.30

A.12. Raw Data for Sample F2

Mass [g]	Time Step [s]	Cumulative time[s]	Sqroot(t)[$s^{1/2}$]	Moisture Mass [g]	CMG [g]
34.10	0	0	0.00	0	0
34.86	60	60	7.75	0.76	0.76
35.18	120	180	13.42	0.32	1.08
35.49	180	360	18.97	0.31	1.39
35.71	180	540	23.24	0.22	1.61
35.97	280	820	28.64	0.26	1.87
36.17	320	1,140	33.76	0.20	2.07
36.50	610	1,750	41.83	0.33	2.40
36.80	740	2,490	49.90	0.30	2.70
37.30	1,860	4,350	65.95	0.50	3.20
38.05	3,600	7,950	89.16	0.75	3.95
39.06	7,230	15,180	123.21	1.01	4.96
39.97	7,380	22,560	150.20	0.91	5.87
42.62	60,020	82,580	287.37	2.65	8.52
43.16	24,970	107,550	327.95	0.54	9.06
44.05	57,750	165,300	406.57	0.89	9.95
44.51	25,380	190,680	436.67	0.46	10.41
45.19	59,980	250,660	500.66	0.68	11.09
45.51	30,170	280,830	529.93	0.32	11.41
46.15	57,140	337,970	581.35	0.64	12.05
46.24	9,400	347,370	589.38	0.09	12.14
48.70	249,270	596,640	772.42	2.46	14.60
48.97	27,060	623,700	789.75	0.27	14.87
49.68	81,125	704,825	839.54	0.71	15.58
51.65	257,995	962,820	981.23	1.97	17.55
54.58	327,750	1,290,570	1,136.03	2.93	20.48
56.00	188,820	1,479,390	1,216.30	1.42	21.90

A.13. Raw Data for Sample G2

Mass [g]	Time Step [s]	Cumulative time[s]	Sqroot(t)[$s^{1/2}$]	Moisture Mass [g]	CWG [g]
35.90	0	0	0.00	0	0
36.62	60	60	7.75	0.72	0.72
36.91	120	180	13.42	0.29	1.01
37.18	180	360	18.97	0.27	1.28
37.47	260	620	24.90	0.29	1.57
37.74	320	940	30.66	0.27	1.84

37.99	380	1,320	36.33	0.25	2.09
38.28	600	1,920	43.82	0.29	2.38
38.58	900	2,820	53.10	0.30	2.68
39.08	1,800	4,620	67.97	0.50	3.18
39.65	2,760	7,380	85.91	0.57	3.75
40.66	7,230	14,610	120.87	1.01	4.76
41.40	7,380	21,990	148.29	0.74	5.50
44.09	60,030	82,020	286.39	2.69	8.19
44.66	24,970	106,990	327.09	0.57	8.76
45.65	57,740	164,730	405.87	0.99	9.75
46.03	25,380	190,110	436.02	0.38	10.13
46.83	59,970	250,080	500.08	0.80	10.93
47.18	59,971	310,051	556.82	0.35	11.28
47.81	59,972	370,023	608.30	0.63	11.91
47.89	59,973	429,996	655.74	0.08	11.99
50.17	59,974	489,970	699.98	2.28	14.27
50.36	59,975	549,945	741.58	0.19	14.46
50.95	81,130	631,075	794.40	0.59	15.05
52.51	257,980	889,055	942.90	1.56	16.61
54.55	327,760	1,216,815	1,103.09	2.04	18.65
55.57	188,820	1,405,635	1,185.59	1.02	19.67

A.14. Raw Data for Sample H2

Mass [g]	Time Step [s]	Cumulative time[s]	Sqroot(t)[$s^{1/2}$]	Moisture Mass [g]	CMG [g]
31.59	0	0	0.00	0	0
32.43	60	60	7.75	0.84	0.84
32.77	120	180	13.42	0.34	1.18
33.05	180	360	18.97	0.28	1.46
33.27	240	600	24.49	0.22	1.68
33.45	310	910	30.17	0.18	1.86
33.59	290	1200	34.64	0.14	2.00
33.80	600	1800	42.43	0.21	2.21
34.11	1320	3120	55.86	0.31	2.52
34.47	2280	5400	73.48	0.36	2.88
34.98	4140	9540	97.67	0.51	3.39
35.78	11100	20640	143.67	0.80	4.19
38.38	60020	80660	284.01	2.60	6.79
39.12	24970	105630	325.01	0.74	7.53
40.49	57750	163380	404.20	1.37	8.90
41.07	25380	188760	434.47	0.58	9.48
42.34	60000	248760	498.76	1.27	10.75
42.92	30180	278940	528.15	0.58	11.33
44.03	57090	336030	579.68	1.11	12.44
44.19	9440	345470	587.77	0.16	12.60
48.09	249260	594730	771.19	3.90	16.50
48.40	27050	621780	788.53	0.31	16.81

49.45	81140	702920	838.40	1.05	17.86
52.03	257980	960900	980.26	2.58	20.44
55.21	327750	1288650	1135.19	3.18	23.62
56.84	188820	1477470	1215.51	1.63	25.25

Appendix B Pycnometry results

B.1. Density and Volume Report for Sample A1

Sample:	A1	Started	19/11/04	19:10:26
Sample Weight:	13.87 g	Completed	19/11/04	19:52:24
Temperature:	19.9 C			
Number of Purges:	13	Equilibration Rate	0.0200 psig/min	
Cell Volume:	109.4045 cm^3	Expansion Volume	74.6810 cm^3	

Run	Volume cm^3	Deviation cm^3	Density g/cm^3	Deviation g/cm^3	(h:m:s) Elapsed time
1	12.1002	-.0116	1.1463	0.0011	0:22:53
2	12.1054	- 0.0064	1.1458	0.0006	0:32:23
3	12.1298	0.0180	1.1434	-0.0018	0:41:49
Average Volume		12.1118 cm^3	Standard Deviation		0.0158 cm^3
Average Density		1.1452 g/cm^3	Standard Deviation		0.0015 g/cm^3

B.2. Density and Volume Report for Sample B1

Sample:	B1	Started	19/11/04	17:28:58
Sample Weight:	13.77 g	Completed	19/11/04	17:51:03
Temperature:	19.9 C			
Number of Purges:	13	Equilibration Rate	0.0200 psig/min	
Cell Volume:	109.4045 cm^3	Expansion Volume	74.6810 cm^3	

Run	Volume cm^3	Deviation cm^3	Density g/cm^3	Deviation g/cm^3	(h:m:s) Elapsed time
1	10.5877	0.0235	1.3006	- 0.0029	0:16:09
2	10.5549	-0.0093	1.3046	0.0011	0:19:03
3	10.5501	-0.0142	1.3052	0.0017	0:21:57
Average Volume		10.5643 cm^3	Standard Deviation		0.0205 cm^3
Average Density		1.3035 g/cm^3	Standard Deviation		0.0025 g/cm^3

B.3. Density and Volume Report for Sample C1

Sample:	C1	Started	18/11/04	15:06:48
Sample Weight:	14.25 g	Completed	18/11/04	15:38:39
Temperature:	19.9 C			
Number of Purges:	13	Equilibration Rate	0.0200 psig/min	
Cell Volume:	109.4045 cm^3	Expansion Volume	74.6810 cm^3	

Run	Volume cm^3	Deviation cm^3	Density g/cm^3	Deviation g/cm^3	(h:m:s) Elapsed time
1	12.0295	0.0277	1.1846	- 0.0027	0:18:50

2	11.9948	-0.0070	1.1880	0.0017	0:25:14
3	11.9810	-0.0208	1.1894	0.0021	0:31:43
Average Volume		12.0018 cm^3	Standard Deviation		0.0250 cm^3
Average Density		1.1873 g/cm^3	Standard Deviation		0.0025 g/cm^3

B.4. Density and Volume Report for Sample D1

Sample:		D1	Started	19/11/04	17:54:42
Sample Weight:		13.42 g	Completed	19/11/04	18:27:01
Temperature:		19.9 C			
Number of Purges:		13	Equilibration Rate	0.0200 psig/min	
Cell Volume:		109.4045 cm^3	Expansion Volume	74.6810 cm^3	
					(h:m:s)
Run	Volume cm^3	Deviation cm^3	Density g/cm^3	Deviation g/cm^3	Elapsed time
1	11.0830	0.0056	1.2109	- 0.0006	0:18:59
2	11.0746	-0.0028	1.2118	0.0003	0:25:35
3	11.0746	-0.0028	1.2118	0.0003	0:32:11
Average Volume		11.0774 cm^3	Standard Deviation		0.0048 cm^3
Average Density		1.2115 g/cm^3	Standard Deviation		0.0005 g/cm^3

B.5. Density and Volume Report for Sample E1

Sample:		E1	Started	19/11/04	13:05:31
Sample Weight:		18.27 g	Completed	19/11/04	14:33:34
Temperature:		19.9 C			
Number of Purges:		13	Equilibration Rate	0.0200 psig/min	
Cell Volume:		109.4045 cm^3	Expansion Volume	74.6810 cm^3	
					(h:m:s)
Run	Volume cm^3	Deviation cm^3	Density g/cm^3	Deviation g/cm^3	Elapsed time
1	19.1106	0.2001	0.9560	- 0.0102	0:44:36
2	18.8045	-0.1060	0.9716	0.0054	1:06:19
3	18.8163	-0.0941	0.9710	0.0048	1:27:55
Average Volume		18.9104 cm^3	Standard Deviation		0.1734 cm^3
Average Density		0.9662 g/cm^3	Standard Deviation		0.0088 g/cm^3

B.6. Density and Volume Report for Sample F1

Sample:	E1	Started	19/11/04	20:28:00
Sample Weight:	15.84 g	Completed	19/11/04	20:52:06
Temperature:	19.9 C			
Number of Purges:	13	Equilibration Rate	0.0200 psig/min	
Cell Volume:	109.4045 cm^3	Expansion Volume	74.6810 cm^3	

					(h:m:s)
Run	Volume cm^3	Deviation cm^3	Density g/cm^3	Deviation g/cm^3	Elapsed time
1	13.0875	0.0215	1.2103	- 0.0020	0:14:50
2	18.0546	-0.0114	1.2134	0.0011	0:19:26
3	18.0559	-0.0101	1.2132	0.0009	0:23:58
Average Volume		13.0660 cm^3	Standard Deviation		0.0187 cm^3
Average Density		1.2123 g/cm^3	Standard Deviation		0.0017 g/cm^3

B.7. Density and Volume Report for Sample A2

Sample:	A2	Started	18/11/04	17:56:43
Sample Weight:	15.61 g	Completed	18/11/04	18:42:33
Temperature:	19.9 C			
Number of Purges:	13	Equilibration Rate	0.0200 psig/min	
Cell Volume:	109.4045 cm^3	Expansion Volume	74.6810 cm^3	

					(h:m:s)
Run	Volume cm^3	Deviation cm^3	Density g/cm^3	Deviation g/cm^3	Elapsed time
1	13.9971	0.0202	1.1152	- 0.0016	0:25:22
2	13.9416	-0.0353	1.1197	0.0028	0:35:26
3	13.9920	0.0151	1.1156	- 0.0012	0:45:42
Average Volume		13.9769 cm^3	Standard Deviation		0.0307 cm^3
Average Density		1.1168 g/cm^3	Standard Deviation		0.0025 g/cm^3

B.8. Density and Volume Report for Sample B2

Sample:	B2	Started	19/11/04	11:53:52
Sample Weight:	13.93 g	Completed	19/11/04	12:51:14
Temperature:	19.8 C			
Number of Purges:	13	Equilibration Rate	0.0200 psig/min	
Cell Volume:	109.4045 cm^3	Expansion Volume	74.6810 cm^3	

					(h:m:s)
Run	Volume cm^3	Deviation cm^3	Density g/cm^3	Deviation g/cm^3	Elapsed time
1	14.1012	0.1977	0.9879	- 0.0142	0:28:58
2	13.8457	-0.0578	1.0061	0.0041	0:43:06
3	13.7635	-0.1399	1.0121	0.0101	0:57:14
Average Volume		13.9034 cm^3	Standard Deviation		0.1761 cm^3
Average Density		1.0020 g/cm^3	Standard Deviation		0.0126 g/cm^3

B.9. Density and Volume Report for Sample C2

Sample:	C2	Started	18/11/04	18:55:48
Sample Weight:	13.49 g	Completed	18/11/04	20:20:20

Temperature:		19.9 C			
Number of Purges:		13	Equilibration Rate	0.0200 psig/min	
Cell Volume:		109.4045 cm^3	Expansion Volume	74.6810 cm^3	
					(h:m:s)
Run	Volume cm^3	Deviation cm^3	Density g/cm^3	Deviation g/cm^3	Elapsed time
1	14.0287	0.1331	0.9616	- 0.0093	0:41:26
2	13.8894	-0.0062	0.9712	0.0004	1:02:45
3	13.7687	-0.1269	0.9798	0.0089	1:24:24
Average Volume		13.8956 cm^3	Standard Deviation		0.1301 cm^3
Average Density		0.9709 g/cm^3	Standard Deviation		0.0091 g/cm^3

B.10. Density and Volume Report for Sample D2

Sample:		D2	Started	19/11/04	14:36:05
Sample Weight:		17.34 g	Completed	19/11/04	15:15:53
Temperature:		19.9 C			
Number of Purges:		13	Equilibration Rate	0.0200 psig/min	
Cell Volume:		109.4045 cm^3	Expansion Volume	74.6810 cm^3	
					(h:m:s)
Run	Volume cm^3	Deviation cm^3	Density g/cm^3	Deviation g/cm^3	Elapsed time
1	13.7868	0.0423	1.2577	- 0.0039	0:21:31
2	13.7363	-0.0082	1.2623	0.0007	0:30:24
3	13.7104	-0.0341	1.2647	0.0031	0:39:40
Average Volume		13.7445 cm^3	Standard Deviation		0.0389 cm^3
Average Density		1.2616 g/cm^3	Standard Deviation		0.0036 g/cm^3

B.11. Density and Volume Report for Sample E2

Sample:		E2	Started	19/11/04	10:33:38
Sample Weight:		13.51 g	Completed	19/11/04	11:13:13
Temperature:		19.9 C			
Number of Purges:		13	Equilibration Rate	0.0200 psig/min	
Cell Volume:		109.4045 cm^3	Expansion Volume	74.6810 cm^3	
					(h:m:s)
Run	Volume cm^3	Deviation cm^3	Density g/cm^3	Deviation g/cm^3	Elapsed time
1	11.3829	0.0362	1.1869	- 0.0038	0:22:45
2	11.3474	0.0006	1.1906	- 0.0001	0:31:02
3	11.3099	-0.0368	1.1945	0.0039	0:39:27
Average Volume		11.3467 cm^3	Standard Deviation		0.0365 cm^3
Average Density		1.1907 g/cm^3	Standard Deviation		0.0038 g/cm^3

B.12. Density and Volume Report for Sample F2

Sample:		F2	Started	18/11/04	13:15:02
Sample Weight:		14.07 g	Completed	18/11/04	14:41:27
Temperature:		19.9 C			
Number of Purges:		13	Equilibration Rate	0.0200 psig/min	
Cell Volume:		109.4045 cm^3	Expansion Volume	74.6810 cm^3	
					(h:m:s)
Run	Volume cm^3	Deviation cm^3	Density g/cm^3	Deviation g/cm^3	Elapsed time
1	14.6149	0.0772	0.9627	- 0.0052	0:43:01
2	14.6055	0.0678	0.9633	- 0.0045	1:04:38
3	14.3927	-0.1450	0.9776	0.0097	1:26:17
Average Volume		14.5377 cm^3	Standard Deviation		0.1257 cm^3
Average Density		0.9679 g/cm^3	Standard Deviation		0.0084 g/cm^3

B.13. Density and Volume Report for Sample G2

Sample:		G2	Started	18/11/04	13:15:02
Sample Weight:		14.93 g	Completed	18/11/04	14:41:27
Temperature:		19.9 C			
Number of Purges:		13	Equilibration Rate	0.0200 psig/min	
Cell Volume:		109.4045 cm^3	Expansion Volume	74.6810 cm^3	
					(h:m:s)
Run	Volume cm^3	Deviation cm^3	Density g/cm^3	Deviation g/cm^3	Elapsed time
1	14.2766	0.1956	1.0458	- 0.0052	0:36:33
2	13.9831	-0.0979	1.0677	0.0073	0:55:10
3	13.9833	-0.0977	1.0677	0.0073	1:13:18
Average Volume		14.0810 cm^3	Standard Deviation		0.1694 cm^3
Average Density		1.0604 g/cm^3	Standard Deviation		0.0127 g/cm^3

B.14. Density and Volume Report for Sample H2

Sample:		H2	Started	19/11/04	18:35:34
Sample Weight:		13.14 g	Completed	19/11/04	19:07:44
Temperature:		19.9 C			
Number of Purges:		13	Equilibration Rate	0.0200 psig/min	
Cell Volume:		109.4045 cm^3	Expansion Volume	74.6810 cm^3	
					(h:m:s)
Run	Volume cm^3	Deviation cm^3	Density g/cm^3	Deviation g/cm^3	Elapsed time
1	10.9211	0.0256	1.2032	- 0.0028	0:17:56
2	10.8915	-0.0039	1.2064	0.0004	0:25:06
3	10.8736	-0.0218	1.2084	0.0024	0:32:02

Average Volume	10.8954 cm^3	Standard Deviation	0.0239 cm^3
Average Density	1.2060 g/cm^3	Standard Deviation	0.0026 g/cm^3

Appendix C Mercury intrusion results

C.1. Mercury intrusion results and derived moisture content for sample A1

Pressure Psia mercury	Diam in meters	Capillary Pressure for water (Pas)	ml_{Hg}	Kg_{water}/m^3	Drainage data Kg_{water}/m^3
0.79	2.29E-04	1268.99	0.000000	0.00	636.50
1.72	1.05E-04	2762.85	0.004839	2.92	633.58
2.58	7.02E-05	4145.89	0.003553	2.15	631.43
3.73	4.85E-05	5999.33	0.003981	2.41	629.03
4.52	4.00E-05	7284.69	0.001164	0.70	628.32
5.55	3.26E-05	8927.77	0.002021	1.22	627.10
6.61	2.74E-05	10642.45	0.004778	2.89	624.22
7.96	2.27E-05	12817.40	0.007473	4.51	619.70
9.12	1.98E-05	14677.78	0.007656	4.63	615.08
10.35	1.75E-05	16666.18	0.007901	4.77	610.30
11.62	1.56E-05	18709.96	0.009739	5.88	604.42
12.70	1.42E-05	20451.16	0.008820	5.33	599.09
13.91	1.30E-05	22401.03	0.009739	5.88	593.21
14.87	1.22E-05	23944.02	0.008269	5.00	588.22
16.30	1.11E-05	26241.09	0.011699	7.07	581.15
17.36	1.04E-05	27957.25	0.009800	5.92	575.23
18.45	9.80E-06	29708.82	0.008085	4.88	570.34
24.85	7.28E-06	40012.09	0.000000	0.00	570.34
30.18	5.99E-06	48595.69	0.000796	0.48	569.86
39.77	4.55E-06	64026.73	0.033933	20.50	549.37
49.98	3.62E-06	80477.55	0.048204	29.12	520.25
74.82	2.42E-06	120469.96	0.066518	40.18	480.06
89.59	2.02E-06	144236.96	0.029155	17.61	462.45
114.48	1.58E-06	184315.46	0.044651	26.97	435.48
139.56	1.30E-06	224708.69	0.033504	20.24	415.24
174.13	1.04E-06	280377.43	0.039384	23.79	391.45
219.17	8.25E-07	352884.14	0.053839	32.52	358.93
269.77	6.70E-07	434367.54	0.096714	58.42	300.50
328.76	5.50E-07	529358.29	0.141855	85.69	214.81
417.98	4.33E-07	672983.59	0.184301	111.33	103.48
518.27	3.49E-07	834383.95	0.087771	53.02	50.46
636.68	2.84E-07	1024991.20	0.036995	22.35	28.11
800.12	2.26E-07	1288495.57	0.021928	13.25	14.86
986.44	1.83E-07	1587786.26	0.009065	5.48	9.39
1244.59	1.45E-07	2004129.38	0.005819	3.52	5.87
1395.92	1.30E-07	2246913.58	0.001593	0.96	4.91
1595.25	1.13E-07	2567901.23	0.001164	0.70	4.21

1895.25	9.54E-08	3052410.90	0.001041	0.63	3.58
2299.58	7.87E-08	3700127.06	0.000368	0.22	3.36
2600.41	6.96E-08	4183908.04	0.000368	0.22	3.13
2999.08	6.03E-08	4829187.39	0.000000	0.00	3.13
3495.08	5.17E-08	5632495.16	0.000184	0.11	3.02
3993.25	4.53E-08	6428256.07	0.000245	0.15	2.87
5387.58	3.36E-08	8666666.66	0.000368	0.22	2.65
6185.09	2.92E-08	9972602.74	0.000000	0.00	2.65
7086.42	2.55E-08	11419607.84	0.000000	0.00	2.65
8196.42	2.21E-08	13176470.59	0.000000	0.00	2.65
9495.09	1.90E-08	15326315.79	0.000061	0.04	2.62
10793.09	1.68E-08	17333333.33	0.000184	0.11	2.50
12483.26	1.45E-08	20082758.62	0.000245	0.15	2.36
14380.27	1.26E-08	23111111.11	0.000306	0.19	2.17
16574.77	1.09E-08	26715596.33	0.000490	0.30	1.88
18969.77	9.50E-09	30652631.58	0.000429	0.26	1.62
21958.78	8.20E-09	35512195.12	0.000735	0.44	1.17
24940.95	7.30E-09	39890410.96	0.000919	0.56	0.62
28885.46	6.30E-09	46222222.22	0.001164	0.70	-0.09

C.2. Mercury intrusion results and derived moisture content for sample C1

Pressure Psia mercury	Diam in meters	Capillary Pressure for water (Pas)	ml_{Hg}	Kg_{water}/m^3	Drainage data Kg_{water}/m^3
0.74	2.45E-04	1188.22	0.000000	0.00	587.50
1.60	1.13E-04	2581.19	0.004720	3.06	584.44
2.46	7.37E-05	3953.49	0.003602	2.34	582.10
3.76	4.81E-05	6050.05	0.002298	1.49	580.61
4.77	3.79E-05	7678.90	0.001366	0.89	579.73
4.75	3.81E-05	7652.32	0.000000	0.00	579.73
5.97	3.03E-05	9619.29	0.002919	1.89	577.84
7.06	2.56E-05	11367.54	0.003292	2.13	575.70
8.52	2.12E-05	13714.44	0.004720	3.06	572.64
9.43	1.92E-05	15180.19	0.003354	2.17	570.47
10.40	1.74E-05	16743.81	0.002671	1.73	568.73
11.23	1.61E-05	18085.50	0.002112	1.37	567.37
12.13	1.49E-05	19529.99	0.002609	1.69	565.67
12.93	1.40E-05	20825.29	0.001988	1.29	564.39
13.88	1.30E-05	22347.40	0.001739	1.13	563.26
15.09	1.20E-05	24288.32	0.001801	1.17	562.09
15.99	1.13E-05	25747.58	0.000870	0.56	561.53
17.23	1.05E-05	27741.26	0.002671	1.73	559.79
19.31	9.36E-06	31097.82	0.018881	12.24	547.55
20.68	8.74E-06	33302.46	0.016894	10.95	536.60

25.09	7.21E-06	40399.56	0.000311	0.20	536.40
30.09	6.01E-06	48448.55	0.000435	0.28	536.12
40.24	4.49E-06	64784.53	0.008323	5.40	530.72
49.84	3.63E-06	80249.13	0.025341	16.43	514.29
74.46	2.43E-06	119889.66	0.087699	56.86	457.43
89.68	2.02E-06	144394.31	0.046893	30.40	427.02
115.54	1.57E-06	186022.74	0.061116	39.63	387.40
139.77	1.29E-06	225038.64	0.040061	25.97	361.42
174.66	1.04E-06	281216.80	0.047514	30.81	330.62
218.97	8.26E-07	352542.37	0.078569	50.94	279.68
269.20	6.72E-07	433397.83	0.109065	70.71	208.96
329.23	5.49E-07	530032.76	0.126208	81.83	127.13
418.95	4.32E-07	674542.51	0.113227	73.41	53.72
518.51	3.49E-07	834862.39	0.045340	29.40	24.32
639.97	2.83E-07	1030431.71	0.017515	11.36	12.97
800.12	2.26E-07	1288495.58	0.008136	5.28	7.69
986.44	1.83E-07	1588652.48	0.003851	2.50	5.20
1246.94	1.45E-07	2008275.86	0.002236	1.45	3.75
1398.43	1.29E-07	2252126.84	0.000807	0.52	3.22
1598.60	1.13E-07	2574712.64	0.000683	0.44	2.78
1896.27	9.54E-08	3052410.90	0.000745	0.48	2.30
2298.60	7.87E-08	3700127.06	0.000311	0.20	2.10
2597.93	6.96E-08	4183908.05	0.000373	0.24	1.85
2996.27	6.04E-08	4821192.05	0.000000	0.00	1.85
3492.93	5.18E-08	5621621.62	0.000248	0.16	1.69
3992.43	4.53E-08	6428256.07	0.000248	0.16	1.53
5385.27	3.36E-08	8666666.67	0.000248	0.16	1.37
6180.77	2.93E-08	9938566.55	0.000000	0.00	1.37
7080.77	2.55E-08	11419607.84	0.000000	0.00	1.37
8195.11	2.21E-08	13176470.59	0.000000	0.00	1.37
9496.61	1.90E-08	15326315.79	0.000186	0.12	1.25
10790.12	1.68E-08	17333333.33	0.000000	0.00	1.25
12486.79	1.45E-08	20082758.62	0.000000	0.00	1.25
14381.29	1.26E-08	23111111.11	0.000000	0.00	1.25
16566.46	1.09E-08	26715596.33	0.000000	0.00	1.25
18967.63	9.50E-09	30652631.58	0.000000	0.00	1.25
21894.30	8.30E-09	35084337.35	0.000870	0.56	0.69
24888.64	7.30E-09	39890410.96	0.000621	0.40	0.28

C.3. Mercury intrusion results and derived moisture content for sample A2

Pressure Psia mercury	Diam in meters	Capillary Pressure for water (Pas)	ml_{Hg}	Kg_{water}/m^3	Drainage data Kg_{water}/m^3
0.79	2.29E-04	1268.99	0.000000	0.00	526.90

1.72	1.05E-04	2762.86	0.017032	9.18	517.72
2.58	7.02E-05	4145.90	0.009377	5.06	512.66
3.73	4.85E-05	5999.34	0.004529	2.44	510.22
4.52	4.00E-05	7284.70	0.001722	0.93	509.29
5.55	3.26E-05	8927.78	0.002105	1.14	508.15
6.61	2.74E-05	10642.46	0.003891	2.10	506.05
7.96	2.27E-05	12817.41	0.005550	2.99	503.06
9.12	1.98E-05	14677.79	0.006570	3.54	499.52
10.35	1.75E-05	16666.19	0.007463	4.02	495.49
11.62	1.56E-05	18709.96	0.012630	6.81	488.68
12.70	1.42E-05	20451.16	0.009377	5.06	483.62
13.91	1.30E-05	22401.03	0.010589	5.71	477.91
14.87	1.22E-05	23944.02	0.008867	4.78	473.13
16.30	1.11E-05	26241.09	0.012567	6.78	466.36
17.36	1.04E-05	27957.26	0.011355	6.12	460.23
18.45	9.80E-06	29708.83	0.010972	5.92	454.32
25.12	7.20E-06	40447.25	0.000957	0.52	453.80
30.29	5.97E-06	48762.52	0.000829	0.45	453.35
40.45	4.47E-06	65119.19	0.003062	1.65	451.70
50.11	3.61E-06	80673.76	0.002488	1.34	450.36
74.95	2.41E-06	120669.65	0.065385	35.26	415.10
90.68	1.99E-06	146001.50	0.042229	22.77	392.33
115.06	1.57E-06	185253.51	0.048927	26.38	365.94
139.31	1.30E-06	224293.31	0.035467	19.13	346.82
174.54	1.04E-06	281026.83	0.040889	22.05	324.77
219.91	8.23E-07	354042.55	0.055434	29.89	294.87
269.06	6.72E-07	433204.40	0.075081	40.49	254.38
328.96	5.50E-07	529647.14	0.107996	58.24	196.14
418.78	4.32E-07	674230.15	0.146462	78.98	117.16
517.20	3.50E-07	832713.75	0.100724	54.32	62.84
638.05	2.84E-07	1027160.49	0.059899	32.30	30.54
798.82	2.26E-07	1286219.08	0.028068	15.14	15.41
989.63	1.83E-07	1592997.81	0.011036	5.95	9.46
1247.45	1.45E-07	2008275.86	0.004912	2.65	6.81
1397.44	1.29E-07	2250386.40	0.001659	0.89	5.91
1594.94	1.13E-07	2567901.23	0.001595	0.86	5.05
1894.61	9.55E-08	3049214.66	0.001148	0.62	4.43
2298.27	7.87E-08	3700127.06	0.001021	0.55	3.88
2597.94	6.96E-08	4183908.05	0.000574	0.31	3.57
2995.77	6.04E-08	4821192.05	0.000447	0.24	3.33
3494.94	5.18E-08	5621621.62	0.000510	0.28	3.06
3993.77	4.53E-08	6428256.07	0.000383	0.21	2.85
5387.77	3.36E-08	8666666.67	0.000638	0.34	2.51
6185.94	2.92E-08	9972602.74	0.000319	0.17	2.33
7086.27	2.55E-08	11419607.84	0.000383	0.21	2.13

8195.77	2.21E-08	13176470.59	0.000638	0.34	1.78
9491.44	1.91E-08	15246073.30	0.000000	0.00	1.78
10787.61	1.68E-08	17333333.33	0.000064	0.03	1.75
12487.78	1.45E-08	20082758.62	0.000255	0.14	1.61
14376.45	1.26E-08	23111111.11	0.000255	0.14	1.47
16572.96	1.09E-08	26715596.33	0.000255	0.14	1.34
18964.12	9.50E-09	30652631.58	0.000447	0.24	1.10
21943.13	8.20E-09	35512195.12	0.000510	0.28	0.82
24924.47	7.30E-09	39890410.96	0.000638	0.34	0.48
28891.64	6.30E-09	46222222.22	0.001021	0.55	-0.07

C.4. Mercury intrusion results and derived moisture content for sample C2

Pressure Psia mercury	Diam in meters	Capillary Pressure for water (Pas)	ml_{Hg}	Kg_{water}/m^3	Drainage data Kg_{water}/m^3
0.52	3.494E-04	833.47	0.000000	0.00	584.30
1.35	1.342E-04	2170.09	0.008351	4.33	579.97
2.19	8.260E-05	3525.49	0.002957	1.53	578.44
2.95	6.130E-05	4750.21	0.002610	1.35	577.09
3.76	4.810E-05	6054.36	0.002436	1.26	575.83
4.34	4.169E-05	6985.51	0.001276	0.66	575.17
5.15	3.514E-05	8287.23	0.001276	0.66	574.51
6.05	2.990E-05	9739.23	0.002842	1.47	573.04
6.94	2.607E-05	11170.06	0.003479	1.80	571.23
7.78	2.324E-05	12528.66	0.007133	3.69	567.54
8.68	2.084E-05	13971.52	0.009104	4.72	562.82
9.68	1.868E-05	15587.78	0.011482	5.95	556.87
10.59	1.709E-05	17044.09	0.009858	5.11	551.77
11.63	1.555E-05	18730.06	0.012700	6.58	545.19
12.56	1.440E-05	20222.08	0.008119	4.21	540.98
13.31	1.359E-05	21432.25	0.009336	4.84	536.15
14.27	1.267E-05	22976.53	0.007713	4.00	532.15
15.27	1.184E-05	24591.69	0.008351	4.33	527.82
16.45	1.099E-05	26488.14	0.010090	5.23	522.60
17.54	1.031E-05	28242.23	0.007191	3.72	518.87
25.14	7.194E-06	40478.18	0.001276	0.66	518.21
30.14	6.001E-06	48526.05	0.000638	0.33	517.88
40.3	4.488E-06	64885.58	0.002436	1.26	516.62
50.63	3.573E-06	81511.55	0.003015	1.56	515.06
75.25	2.403E-06	121161.69	0.016527	8.56	506.50
90.34	2.002E-06	145447.28	0.034330	17.78	488.71
115.2	1.570E-06	185489.52	0.054569	28.27	460.45
140.43	1.288E-06	226104.51	0.045058	23.34	437.10
175.3	1.032E-06	282252.59	0.052249	27.07	410.04
220.18	8.214E-07	354516.68	0.051263	26.56	383.48

270.72	6.681E-07	435862.89	0.050799	26.32	357.17
330.24	5.477E-07	531677.93	0.061469	31.84	325.33
419.66	4.310E-07	675638.05	0.100613	52.12	273.21
519.54	3.481E-07	836541.22	0.117372	60.80	212.40
639.93	2.826E-07	1030431.71	0.118010	61.13	151.27
800.32	2.260E-07	1288495.58	0.110935	57.47	93.81
990.13	1.827E-07	1593869.73	0.078287	40.55	53.25
1248.33	1.449E-07	2009661.84	0.056250	29.14	24.11
1398.46	1.293E-07	2252126.84	0.014440	7.48	16.63
1597.61	1.132E-07	2572438.16	0.010322	5.35	11.29
1896.59	9.540E-08	3052410.90	0.007075	3.66	7.62
2300.58	7.860E-08	3704834.61	0.002900	1.50	6.12
2599.91	6.960E-08	4183908.05	0.000928	0.48	5.64
3000.75	6.030E-08	4829187.40	0.000580	0.30	5.34
3497.25	5.170E-08	5632495.16	0.000580	0.30	5.04
3997.25	4.520E-08	6442477.88	0.000406	0.21	4.83
5395.92	3.350E-08	8692537.31	0.000174	0.09	4.74
6194.75	2.920E-08	9972602.74	0.000000	0.00	4.74
7094.59	2.550E-08	11419607.84	0.000000	0.00	4.74
8197.59	2.210E-08	13176470.59	0.000000	0.00	4.74
9495.59	1.900E-08	15326315.79	0.000000	0.00	4.74
10791.43	1.680E-08	17333333.33	0.000000	0.00	4.74
12492.93	1.450E-08	20082758.62	0.000000	0.00	4.74
14393.77	1.260E-08	23111111.11	0.000000	0.00	4.74
16587.94	1.090E-08	26715596.33	0.000000	0.00	4.74
18989.11	9.500E-09	30652631.58	0.000000	0.00	4.74
21979.95	8.200E-09	35512195.12	0.000000	0.00	4.74
24977.12	7.200E-09	40444444.44	0.000290	0.15	4.59
25572.77	7.100E-09	41014084.51	0.008872	4.60	-0.01

Appendix D Regression statistics

D.1. Regression statistics for sample A1

Regression	Slope	Intercept
coefficients	0.021667	1.383001
s error	0.000117	0.102232
r2	0.998689	0.423664
F	34271.4164	45.000000
Ssreg	6151.40929	8.07709301

D.2. Regression statistics for sample B1

Regression	Slope	Intercept
coefficients	0.026536	2.437810
s error	0.000218	0.189950
r2	0.996968	0.787999
F	14795.591764	45.000000
Ssreg	9187.209687	27.94240626

D.3. Regression statistics for sample C1

Regression	Slope	Intercept
coefficients	0.021747	2.290027
s error	0.000172	0.150364
r2	0.997188	0.624576
F	15957.839129	45.000000
Ssreg	6225.076041	17.55428285

D.4. Regression statistics for sample D1

Regression	Slope	Intercept
coefficients	0.022349	1.292671
s error	0.000146	0.127097
r2	0.998096	0.524823
F	23588.511791	45.000000
Ssreg	6497.207793	12.39477731

D.5. Regression statistics for sample E1

Regression	Slope	Intercept
coefficients	0.017302	2.063127
s error	0.000267	0.234220
r2	0.989628	0.938458
F	4198.100788	44.000000

Ssreg	3697.281291	38.75094597

D.6. Regression statistics for sample F1

Regression	Slope	Intercept
coefficients	0.022689	2.752427
s error	0.000159	0.140259
r2	0.997830	0.562298
F	20236.798930	44.000000
Ssreg	6398.449798	13.91187371

D.7. Regression statistics for sample A2

Regression	Slope	Intercept
coefficients	0.007904	-0.137287
s error	0.000213	0.105158
r2	0.979340	0.429890
F	1374.679816	29.000000
Ssreg	254.0479466	5.359350133

D.8. Regression statistics for sample B2

Regression	Slope	Intercept
coefficients	0.003235	0.201689
s error	0.000087	0.043142
r2	0.979252	0.176296
F	1368.746645	29.000000
Ssreg	42.54122262	0.901332223

D.9. Regression statistics for sample C2

Regression	Slope	Intercept
coefficients	0.004734	0.050974
s error	0.000070	0.035192
r2	0.993880	0.140247
F	4547.524097	28.000000
Ssreg	89.44633135	0.550738649

D.10. Regression statistics for sample D1

Regression	Slope	Intercept
coefficients	0.004421	0.287742
s error	0.000079	0.039538
r2	0.991163	0.157635
F	3140.641173	28.000000
Ssreg	78.04106449	0.69576551

D.11. Regression statistics for sample E2

Regression	Slope	Intercept
coefficients	0.018376	1.195552
s error	0.000169	0.088962
r2	0.997893	0.325707
F	11839.592462	25.000000
ssreg	1256.005537	2.652130005

D.12. Regression statistics for sample F2

Regression	Slope	Intercept
coefficients	0.016862	1.931847
s error	0.000493	0.259582
r2	0.979056	0.954383
F	1168.648576	25.000000
ssreg	1064.460729	22.77118953

D.13. Regression statistics for sample G2

Regression	Slope	Intercept
coefficients	0.016267	1.904913
s error	0.000538	0.276705
r2	0.973387	1.008777
F	914.379614	25.000000
ssreg	930.5017681	25.44079488

D.14. Regression statistics for sample H2

Regression	Slope	Intercept
coefficients	0.019831	1.073379
s error	0.000160	0.085684
r2	0.998436	0.306389
F	15324.616435	24.000000
ssreg	1438.588466	2.252984492

Appendix E Identification of wood

In Canada, the wood species used for the frames are the Spruce, Pine and Fir. The two most dominant species in the continental boreal forest of northern Quebec are black spruce (Picea mariana) BSP and jack pine (Pinus banksiana Lamb.)(Gerardin 1980), (Le Goff and Sirois, 2004).

The presence of phenolic compounds can be determined by using Fast Blue BB salt (O'Brien and McCully 1981), to give a characteristic reddish-brown reaction product. Phenolic compounds are widely present in plants, and their presence often is associated with decay resistance (Celimene *et al*, 1999)

Fast Blue BB was mixed with distilled water. The proportions were 1 liter of distilled water with 10 grams of fast blue. When the solution was ready, it was only necessary to spray some of the liquid to the wood samples. After a few minutes, they will start turning into a wine-red/reddish-brown color that identify them as jack pine. The procedure of identification and the salts were obtained from researchers from FORINTEK.

Figures A and B, show the samples before the application of the solution. The same procure was applied to all the samples and the results of the tests were positive for jack pine.

Bromophenol Blue was used to guarantee that the samples were not Fir. Bromophenol Blue when is mixed with ethanol or methanol would turn blue when the wood is Fir (see Figure C).

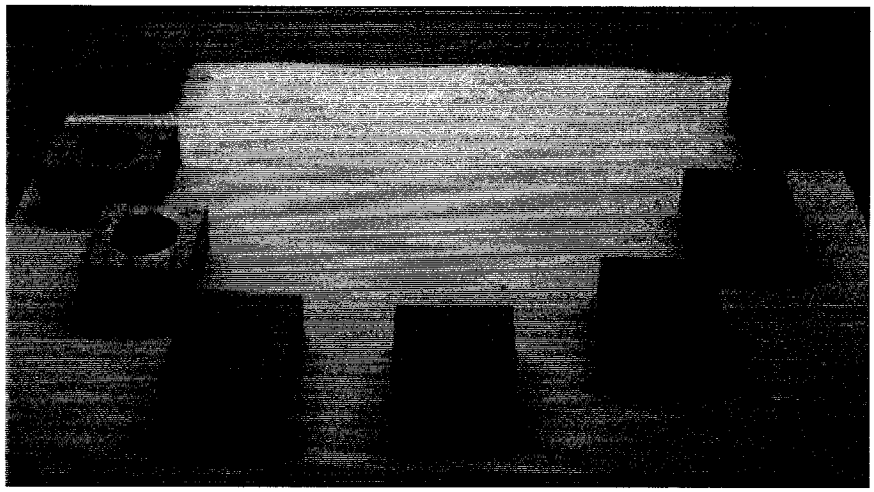

Figure A. Samples before the application of the fast blue B solution,

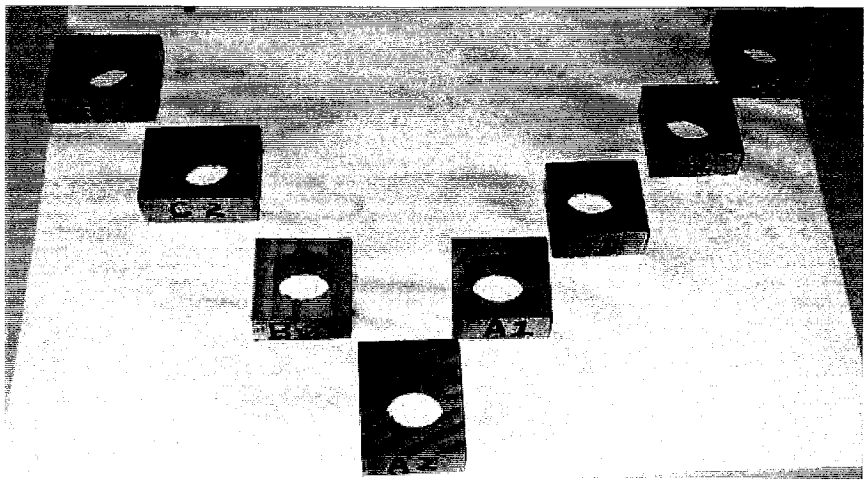

Figure B. Samples after, the wine-red color is easy noticeable.

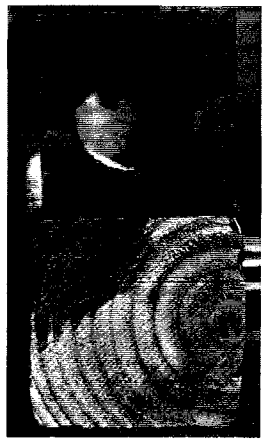

Figure C. Two different species sprayed with Bromophenol blue. The one on top is jack pine, as it can be seen the color is not really blue, but rather a greenish one. The one in the bottom is positive for Fir.